INFORMATION TO USERS

This manuscript has been reproduced from the microfilm master. UMI films the text directly from the original or copy submitted. Thus, some thesis and dissertation copies are in typewriter face, while others may be from any type of computer printer.

The quality of this reproduction is dependent upon the quality of the copy submitted. Broken or indistinct print, colored or poor quality illustrations and photographs, print bleedthrough, substandard margins, and improper alignment can adversely affect reproduction.

In the unlikely event that the author did not send UMI a complete manuscript and there are missing pages, these will be noted. Also, if unauthorized copyright material had to be removed, a note will indicate the deletion.

Oversize materials (e.g., maps, drawings, charts) are reproduced by sectioning the original, beginning at the upper left-hand corner and continuing from left to right in equal sections with small overlaps.

Photographs included in the original manuscript have been reproduced xerographically in this copy. Higher quality 6" x 9" black and white photographic prints are available for any photographs or illustrations appearing in this copy for an additional charge. Contact UMI directly to order.

ProQuest Information and Learning
300 North Zeeb Road, Ann Arbor, MI 48106-1346 USA
800-521-0600

A NOVEL APPROACH TO THE REDUCTION OF A DISTRIBUTED FEEDBACK LASER'S INTENSITY PROFILE NON-UNIFORMITY USING GLOBAL OPTIMIZATION

by

Glenn David Isenor

Submitted
in partial fulfilment of the requirements
for the degree of

DOCTOR OF PHILOSOPHY

Major Subject: Electrical and Computer Engineering

at

DALHOUSIE UNIVERSITY

Halifax, Nova Scotia July, 2001

Dalhousie University

Faculty of Engineering

The undersigned hereby certify that they have examined, and recommended to the Faculty of Graduate Studies for acceptance, the thesis entitled "A Novel Approach to the Reduction of a Distributed Feedback Laser's Intensity Profile Non-Uniformity Using Global Optimization" by Glenn David Isenor in partial fulfillment of the requirements for the degree of Doctor of Philosophy.

Dated: 17.09.2001

Supervisor: [redacted]
Dr. Michael Cada

External Examiner: [redacted]
Dr. Romain Maciejko
École Polytechnique, Montreal

Examiners: [redacted]
Dr. Z. David Chen

[redacted]
Dr. Guy Kember

Dalhousie University

Faculty of Engineering

DATE: August 30/2001

AUTHOR: Glenn David Isenor

TITLE: A Novel Approach to the Reduction of a Distributed Feedback Laser's Intensity Profile Non-Uniformity Using Global Optimization

MAJOR SUBJECT: Electrical and Computer Engineering

DEGREE: Doctor of Philosophy

CONVOCATION: October, 2001

Permission is herewith granted to Dalhousie University to circulate and to have copied for non-commercial purposes, at its discretion, the above thesis upon the request of individuals or institutions.

[redacted]
Signature of Author

DEDICATIONS

To my beautiful wife Dawn, for her unwavering support and encouragement, and to my children Lauren and Leah who have had too little of my attention for too long. None of this would have been possible without their love.

To my parents Ross and Helen, who taught me patience and perseverance.

In loving memory of my Grandfather George, a self taught individual who always wanted to know how things worked and who had the wisdom to influence a very young student to appreciate the value of an education.

In loving memory of my Grandmother Wilhelmina, for always being there.

TABLE OF CONTENTS

LIST OF TABLES vii

LIST OF FIGURES viii

LIST OF SYMBOLS AND ABBREVIATIONS x

ACKNOWLEDGEMENTS xiii

ABSTRACT xiv

1. INTRODUCTION

1.1 Thesis Objectives and Methodology 1

1.2 Layout and Scope of Thesis 3

1.3 Background and Laser Basics 4

1.4 DFB Lasers 8

1.5 Longitudinal Spatial Hole-burning 10

2. COUPLED WAVE THEORY

2.1 The Scalar Wave Equation 13

2.2 The Coupled Wave Equations 15

2.3 Threshold Oscillation Condition 17

3. TRANSFER MATRIX METHOD

3.1 Transfer Matrix Method and Global Optimization 18

3.2 Transfer Matrix Method Theory 19

3.3 Laser Threshold Condition Using the TMM 22

4. ABOVE-THRESHOLD OPTIMIZATION

4.1 Theory and Methodology 24

4.2 Numerical Examples 32

4.2.1 Coupling Coefficient Optimization 35

4.2.2 Phase Optimization 46

4.2.3 Combined Coupling Coefficient and Phase Optimization..... 49
4.3 Summary of Optimization Effects.....53

5. FURTHER ANALYSIS OF OPTIMIZED PROFILES
5.1 Optimized Profile Flatness Behavior.....55
5.2 Optimized Profile Wavelength Behavior..... 59
5.3 Threshold Current..... 61
5.4 Single Longitudinal Mode Stability..... 62

6. DISCUSSION AND CONCLUSIONS
6.1 Results Summary..... 67
6.2 Sensitivity Considerations..... 70
6.3 Non-linear Considerations.....71
6.4 Suggestion for Future Research..... 72
6.3 Concluding Comments..... 73

BIBLIOGRAPHY..... 76

APPENDIX A Solution Methodology..... 79
APPENDIX B Objective Function Visualizations..... 86
APPENDIX C Phase Optimization Graphs..... 95
APPENDIX D Coupling Coefficient Plus Phase Optimization Graphs.....101
APPENDIX E Optimization Code Listing..... 107
APPENDIX F Threshold Modes Code Listing..... 126

LIST OF TABLES

Table 4.1 Model Parameters

Table 4.2a Optimized *KL* Parameters (10,000 iterations)

Table 4.2b Optimized *KL* Parameters (20,000 iterations)

Table 4.3a Optimized *PS* Parameters (10,000 iterations)

Table 4.3b Optimized *PS* Parameters (20,000 iterations)

Table 4.4a Optimized Combined *KL* and *PS* Parameters (10,000 iterations)

Table 4.4b Optimized Combined *KL* and *PS* Parameters (20,000 iterations)

Table 5.1a Normalized Gain Margin at Threshold – *KL* Optimized Profiles

Table 5.1b Normalized Gain Margin at Threshold – *PS* Optimized Profiles

Table 5.1c Normalized Gain Margin at Threshold – *KL* plus *PS* Optimized Profiles

LIST OF FIGURES

Figure 1.1 Semiconductor Laser Diode

Figure 1.2 Index Coupled Distributed Feedback Laser

Figure 3.1 DFB Section of a Semiconductor Laser Diode

Figure 4.1 Schematic of DFB Laser Structure

Figure 4.2 Flow Chart of Numerical Procedure

Figure 4.3 Coupling Coefficient Optimization versus Un-optimized QWS Structure: Normalized Longitudinal Field Intensities (10,000 Iterations)

Figure 4.4 Field Intensity (*KL* Optimization at 3 x i_{th})

Figure 4.5 Carrier Density (*KL* Optimization at 3 x i_{th})

Figure 4.6 Refractive Index (*KL* Optimization at 3 x i_{th})

Figure 4.7 Photon Density (*KL* Optimization at 3 x i_{th})

Figure 4.8 Field Intensity Flatness (*KL* Optimization)

Figure 4.9 Average *KL* (*KL* Optimization)

Figure 4.10 Wavelength (*KL* Optimization)

Figure 4.11 Average Refractive Index (*KL* Optimization)

Figure 4.12 Average Normalized Detuning (*KL* Optimization)

Figure 4.13 Average Normalized Amplitude Gain (*KL* Optimization)

Figure 4.14 Objective Function versus *KL1*, *KL2* (*KL* Optimization at 3 x i_{th})

Figure 4.15 Coupling Coefficient Optimization versus Un-optimized QWS Structure: Normalized Longitudinal Field Intensities (10,000 Iterations)

Figure 4.16 Coupling Coefficient Plus Phase Optimization versus Un-optimized QWS Structure: Normalized Longitudinal Field Intensities (10,000 Iterations)

Figure 5.1 Field Flatness – Fixed Solution Profiles (1.1 x i_{th} and 3 x i_{th})

Figure 5.2 Lasing Wavelength – Fixed Solution Profiles (1.1 x i_{th} and 3 x i_{th})

Figure 5.3 Threshold Current – Optimized Solutions

Figure B1 Objective Function versus *KL1*, *KL2* (*KL* Optimization at 3 x i_{th})

Figure B2 Objective Function versus *KL1*, *KL3* (*KL* Optimization at 3 x i_{th})

Figure B3 Objective Function versus *KL2*, *KL3* (*KL* Optimization at 3 x i_{th})
Figure B4 Objective Function versus *KL1*, Wavelength (*KL* Optimization at 3 x i_{th})
Figure B5 Objective Function versus *KL2*, Wavelength (*KL* Optimization at 3 x i_{th})
Figure B6 Objective Function versus *KL3*, Wavelength (*KL* Optimization at 3 x i_{th})
Figure B7 Objective Function versus *KL1*, *KL3* with maximum function value = 20 (*KL* Optimization at 3 x i_{th})
Figure B8 Objective Function versus *KL2*, Wavelength with maximum function value = 20 (*KL* Optimization at 3 x i_{th})
Figure C1 Field Intensity (*PS* Optimization at 3 x i_{th})
Figure C2 Carrier Density (*PS* Optimization at 3 x i_{th})
Figure C3 Refractive Index (*PS* Optimization at 3 x i_{th})
Figure C4 Photon Density (*PS* Optimization at 3 x i_{th})
Figure C5 Field Intensity Flatness (*PS* Optimization)
Figure C6 Wavelength (*PS* Optimization)
Figure C7 Average Refractive Index (*PS* Optimization)
Figure C8 Average Normalized Detuning (*PS* Optimization)
Figure C9 Average Normalized Amplitude Gain (*PS* Optimization)
Figure D1 Field Intensity (*KL* plus *PS* Optimization at 3 x i_{th})
Figure D2 Carrier Density (*KL* plus *PS* Optimization at 3 x i_{th})
Figure D3 Refractive Index (*KL* plus *PS* Optimization at 3 x i_{th})
Figure D4 Photon Density (*KL* plus *PS* Optimization at 3 x i_{th})
Figure D5 Field Intensity Flatness (*KL* plus *PS* Optimization)
Figure D6 Wavelength (*KL* plus *PS* Optimization)
Figure D7 Average Refractive Index (*KL* plus *PS* Optimization)
Figure D8 Average Normalized Detuning (*KL* plus *PS* Optimization)
Figure D9 Average Normalized Amplitude Gain (*KL* plus *PS* Optimization)

LIST OF SYMBOLS AND ABBREVIATIONS

A_t	transmission gain
A_0	differential gain
A_1	gain curvature
A_2	differential peak wavelength
B	bimolecular recombination coefficient
c	speed of light in vacuum
C	Auger recombination coefficient
DCC	distributed coupling coefficient
DFB	distributed feedback
$E(z)$	complex amplitude of a time-harmonic field
$\tilde{E}$	actual total electric field
E	normalized total electric field
E_1	energy level
E_2	energy level
E_r	right-traveling electric field
E_s	left-traveling electric field
F	field flatness function
g	net (material) gain
GO	global optimization
h	Planck's constant (6.63×10^{-34} J s)
i	injection current
i_{th}	threshold current
InGaAsP	indium gallium arsenide phosphide
InP	indium phosphide
j	$\sqrt{-1}$
K	coupling coefficient
KL	*Kappa-L* product, length-normalized coupling coefficient
k_o	free space propagation constant
k	wave propagation constant
LSHB	longitudinal spatial hole-burning
$I(z)$	sectional field intensity

I_{avg}	average field intensity over the laser length
M	total number of laser sections
m	non-zero integer
N	carrier density
N_0	carrier density at transparency
N_{th}	carrier density at threshold
n	refractive index
n_e	effective refractive index
n_g	group refractive index
n(z)	index profile
Objf	objective function
PS	phase shift profile parameter
q	electronic charge
QWS	quarter-wave phase shift
R	Rate of non-coherent carrier recombination
R(z)	complex amplitude term: right-traveling field
R_1, R_2	complex coefficients that depend on the boundary conditions that the field encounters at the left and right-hand facets
RBCerror	right-hand boundary condition error
scal	suitable scaling (penalty) parameter
S	stimulated photon density
S(z)	complex amplitude term: left-traveling field
S_1, S_2	complex coefficients that depend on the boundary conditions that the field encounters at the left and right-hand facets
SLM	single longitudinal mode
TMM	transfer matrix method
T	forward transfer matrix
t_{ij}	matrix elements (for i,j =1,2) of the matrix T
V	volume
W	active layer width
v_g	group velocity at the Bragg wavelength.
ω	longitudinal mode frequency
ω_o	Bragg frequency
Y	overall transfer matrix

α	amplitude gain coefficient
α_{loss}	internal cavity loss
$\alpha(z)$	gain profile
β	actual propagation constant
β_o	Bragg propagation constant
$\partial n / \partial N$	differential index.
ε_o	permittivity of free space
ν	frequency
Γ	optical confinement coefficient
Λ	grating period
τ	linear recombination lifetime
τ^{-1}	spontaneous emission rate
σ	non-linear gain coefficient
λ	lasing wavelength
λ_0	peak gain wavelength at transparency
λ_{th}	lasing wavelength at threshold
λ_B	Bragg wavelength
δ	detuning coefficient
γ	complex propagation constant
ρ	self-explained parameter, $\rho = jK(\alpha - j\delta + \gamma)$

ACKNOWLEDGEMENTS

I would like to thank my thesis supervisor, Dr. Michael Cada for his support and guidance throughout this work. I would also like to thank Dr. B.S.K. Lo for his efforts in answering my questions and for our insightful discussions.

I wish to gratefully acknowledge the financial support provided to me by the Natural Sciences and Engineering Research Council of Canada (NSERC).

Finally, I want to extend my sincerest appreciation to Dr. János D. Pintér, who not only provided inspiration and encouragement, but also generously shared his valuable time and knowledge, making this work possible.

ABSTRACT

The objective of this thesis was to develop a novel methodology capable of modeling, optimizing, and analyzing the steady-state characteristics of a distributed feedback laser operating in a region above its threshold injection current. Considerations that include the existence of non-linear behaviors such as gain margin reduction at higher injection currents, wavelength stability with changes in injection current, and maximizing the flatness of light energy along the laser's cavity provided the general motivation for this work.

This new approach involved integration of the transfer matrix method with global optimization strategies to address the difficult numerical challenges associated with modeling the behavioral characteristics of a distributed feedback laser operating in the non-linear above-threshold region. The standard practice has been to first design for a desired steady-state characteristic at the threshold injection current, then to conduct an above-threshold validation to ensure that the characteristic remains. The principle advantage of this new methodology is that it offers the potential of allowing one to directly design for, and model a desired characteristic at the injection current of interest. This capability and the general nature of the methodology offer the potential to form the basis of a flexible and robust laser design tool.

A successful validation of the methodology's basic principles was carried out using a quarter-wave shifted, distributed coupling coefficient, index-coupled, distributed feedback laser. The problem was formulated in terms of an objective function whose value considered both the boundary condition error of the laser's internal light field solution, and the "flatness" of the internal light field. Global optimization was then used to iteratively select optimized values of sectional coupling coefficient and/or inter-sectional phase shift structural parameters so that the laser's internal light field approached a state of maximum flatness within the given problem's parameter constraints. Throughout the range of injection currents considered, optimized light field flatness values were more than 90% reduced over the light field flatness value of an un-optimized reference quarter-wave shifted distributed feedback laser. This was a successful result, verifying the effectiveness of the methodology and opening the way for other types of above-threshold design optimizations. Further analysis of the data revealed evidence that multiple near-optimal light field flatness solutions existed over the range of injection currents evaluated. This was a new and unexpected result.

In summary, the original contribution of this work consisted of the development and validation of a new methodology to solve and optimize the steady-state characteristics of a distributed feedback laser structure at the injection current of interest. The fundamental difference in this new methodology over the classical approach is that it is not limited to threshold design considerations. Finally, the evidence of multiple near-optimal solutions observed during the validation process is a new result and is also considered an original contribution.

1. INTRODUCTION

1.1 Thesis Objectives and Methodology

The objective of this thesis was to research, develop, and test the methodology that will form the basis for a novel, general-purpose, distributed feedback (DFB) laser optimization and design tool. A key advantage of this new methodology is its ability to address above-threshold laser design and optimization problems.

It was deemed of interest to build an optimization and design tool with above-threshold modeling and analysis capabilities because of the existence of non-linear laser performance characteristics including gain margin reduction at higher injection currents, wavelength stability with varying injection currents, as well as, considerations that involve maximizing the flatness of light energy along the laser's cavity.

The classical modeling approach is to first design and optimize for a desired performance characteristics at the laser's threshold injection current. This step results in a set of structural parameter values (solution variables) which represents the optimal solution for a given design constraint, such as field flatness at threshold. (Throughout this work, when the term "field" is used, it means "electric field", which is also considered as the "light", or "optical field"). Using these solution parameters, the next step is to test that the desired performance is still maintained in the above-threshold regime or at the target above-threshold injection current [Ghafouri-Shiraz and Lo, 1996], [Yokoyama and Sekino, 1998].

This approach has its advantages in that the threshold computational effort is easily managed, and for certain design considerations, threshold solutions have been adequate. If, for example, one wishes to improve the above-threshold gain margin of a quarter-wave shift (QWS) DFB laser, a threshold optimization (reduction) of the non-uniformity of the laser cavity field has been shown to accomplish this. Based on an understanding of the physical processes involved it is also sometimes possible to make very good

predictions as to the general above-threshold behavior of certain designs developed at threshold; however, it may be difficult to efficiently achieve specific target results in this manner.

In addition to addressing this potential limitation in the current methodology, a new tool with above-threshold optimization capabilities would provide a completely different approach to the problem of laser design, possibly revealing new and useful phenomenon. Any time an existing problem is looked at in a different way, this action typically creates the potential to discover something new.

Thus it was postulated there might be advantages to performing such design optimizations at the particular injection current of interest. However, in order to investigate this possibility a new methodology was needed, one that would be capable of considering multiple non-linear design constraints in the process of obtaining an optimized solution.

The approach used to achieve this objective was to integrate the transfer matrix modeling method with the general-purpose non-linear global optimization solver system, LGO [Pintér, 2000]. This combination provided the basis for a new tool that offers the potential to deal with above-threshold non-linear problems consisting of many degrees of freedom (solution variables) and imposed solution (physical or manufacturability) constraints, and represents a new and original contribution by the author.

The new methodology was tested and validated by a successful application to the difficult problem of optimizing the internal field flatness of a QWS DFB laser operating in its above-threshold regime [Isenor, Pintér, and Cada, 2001a], [Isenor, Pintér, and Cada, 2002c]. Although it was anticipated that field flattening optimizations performed near (at) threshold could not be substantially improved upon in the sense that the fields could not be made substantially flatter by optimizing at the injection current of interest, the real

value of this problem was its ability to provide a reasonable and comparative benchmark test for the new approach.

Optimally flattened field solutions were obtained over the considered range of above-threshold injections currents and found to be comparable to the anticipated results. This successfully verified the effectiveness of the methodology and indicated that other types of above-threshold design optimizations should also be possible.

In the process of obtaining optimally flattened above-threshold field solutions, evidence was found for the existence of multiple near-optimal solutions. This was an unexpected and new finding of potential interest to laser designers and also represents an original contribution by the author.

1.2 Layout and Scope of Thesis

Following this subsection is a brief discussion of the basic theory of laser operation. Also included is an introduction to DFB lasers and consideration of the important issue of longitudinal spatial hole-burning (LSHB) reduction. Beginning with Section 2, the necessary supporting background theory for the new methodology is presented. Field propagation within the laser cavity is described in terms of coupled wave theory, and in Section 3, the transfer matrix method's basic concepts are outlined.

In Section 4 the new methodology is presented and validated by considering in detail the important issue of maximizing the field flatness of a QWS DFB laser operating in a region above its threshold injection current, (thus minimizing the effects of LSHB). The problem was formulated in terms of an objective function that considered both the boundary condition error associated with the laser's internal field solution, and a field "flatness" parameter that corresponded to the non-uniformity of the field. Global optimization strategies were then applied to find a steady state field solution for the DFB laser that minimized the objective function for a given above-threshold injection current,

and in so doing, both an optimal match with the boundary condition and a maximally flat field were obtained within the parameter constraints of the problem.

In order to demonstrate the efficacy of the methodology, various numerical examples were considered. First, the sectional coupling coefficient profile associated with a six (equal-length) section, index-coupled, QWS DFB laser was optimized such that maximized field flatness was obtained for a range of above-threshold injection currents. Following this, phase shifts were introduced between the six laser sections. The effect of optimizing the phase shift profile to obtain maximum field flatness was investigated first independently then in combination with optimization of the sectional coupling coefficient profile. Section 5 continues the analysis, where the behavioral characteristics that resulted from an investigation of (fixed) optimized sectional coupling coefficient and/or inter-sectional phase shift profiles over the full range of injection currents, are presented. Also examined were threshold injection current and single longitudinal mode stability considerations. Finally, discussion and conclusions follow in Section 6.

1.3 Background and Laser Basics

This subsection presents a brief introduction to lasers and their theory of operation. For additional information, the reader may wish to consult the following excellent books: [Agrawal, 1992], [Ghafouri-Shiraz and Lo, 1996], [Green, 1993], [Kawaguchi, 1994], [Keiser, 1993], [Tamir, 1988], [Van Etten and Van der Plaats, 1991], and [Yariv, 1991].

The history of the laser dates back to the 1958 work of Schawlow and Townes, where they proposed a method to synchronize the radiation resulting from a large number of excited atoms by stimulating the exited atoms to emit radiation within a special type of resonant cavity. This was followed in 1960 by the first solid-state ruby laser and helium neon (He-Ne) gas laser. Concurrent research resulted in the 1962 discovery of lasing behavior in semiconductor material and since that time lasers have found increasingly widespread usage. A short and by no means comprehensive list of applications would

include communication systems, laser radars, military weapons guidance systems, range finding, medicine, holography, manufacturing, and home entertainment systems.

The structure and size of a laser varies greatly. Lasers can be as small as the head of a pin to room size, and lasing media can consist of various gases, crystals, liquids, and semiconductor materials. Optical communication systems require a small compact monochromatic (single frequency) laser source, and semiconductor lasers are the choice for this application. However, unless carefully designed, these lasers are not strictly monochromatic. Achievement of an efficient monochromatic source from a semiconductor laser has been an ongoing research goal. Much of the design effort involves numerical modeling of the laser behavior, including the internal field distribution and intensity. A partial list of references would include the work of [Ghafouri-Shiraz and Lo, 1996], [Kogelnik, 1969], [Kogelnik and Shank, 1972], [Makino, 1991], [Makino and Glinski, 1988], [Sargent, Swantner, and Thomas, 1980], [Wang, 1974], and [Yariv, 1973]. Such field solutions must satisfy an increasingly non-linear set of relations as the laser's optical power increases. The solution space in turn is non-linear and multi-extremal. Analysis is extremely complicated and design of optimized laser structures has been a challenging task. In the succeeding sections this challenge will be addressed in a new way, by introducing for the first time a novel and robust numerical method that integrates the transfer matrix method (TMM) and global optimization (GO) strategies. It will be demonstrated that by applying this approach it was possible to both obtain and optimize the DFB laser field solution for maximum flatness over varying levels of optical power (injection current).

All types of lasers operate using the same basic principles, which involve the following three processes: photon absorption, spontaneous emission, and stimulated emission. For illustrative purposes consider a simple two-state system, with energy levels denoted as E_1 and E_2. The lasing medium's electrons will normally exist in their lowest energy or ground energy state, E_1. If an incoming photon has an energy level of $h\nu_{1,2} = E_2 - E_1$, (where h is Planck's constant and ν is frequency), an electron in the ground state can

absorb the photon's energy and be promoted to the excited state, E_2. This is an unstable energy state for the electron and in a short time it will spontaneously return to its ground state, while emitting a photon of energy $hv_{1,2}$. This process occurs at random and does not rely on an external stimulus. Photons produced in this way are not in phase and assume random polarizations and directions within the lasing medium.

Stimulated emission occurs when an electron in the excited state, E_2, is externally induced to make the transition to its ground energy state. This occurs when a photon of energy, $hv_{1,2}$ interacts with the excited electron. The stimulated photon produced when the electron drops to its ground state is also of energy $hv_{1,2}$, but unlike the case of spontaneous emission, this photon is in phase (coherent) with the stimulating photon and has the same polarization.

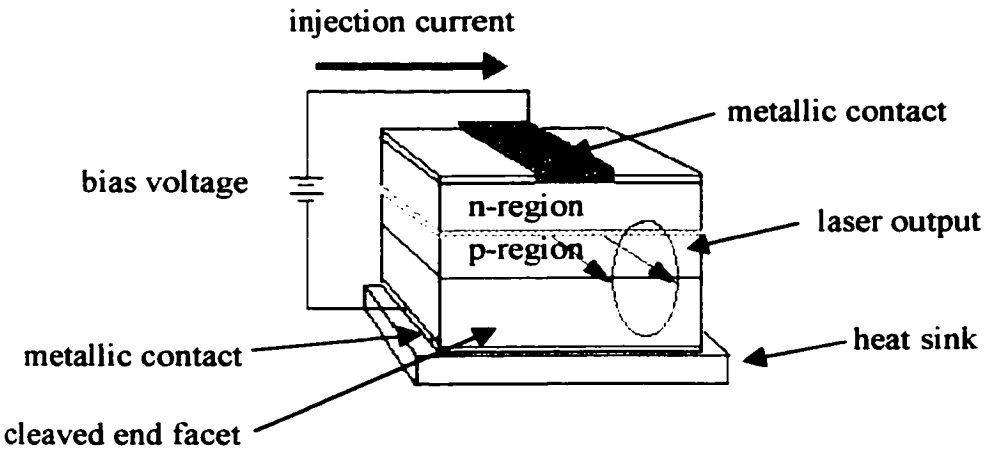

Figure 1.1 Semiconductor Laser Diode

Normally the level of stimulated emission is negligible unless a condition known as population inversion is achieved. This occurs when the number of electrons occupying the excited state is greater than the number of electrons in the ground state. In this situation stimulated emission may dominate over both absorption and spontaneous emission, and a net optical gain will result. In order to achieve this condition the laser

medium is "pumped"; depending on the type of laser this is done either optically (by an external light source), or electrically (by applying a current or voltage to the lasing medium).

Figure 1.1 shows a typical semiconductor laser design. Its approximate dimensions would be in the order of length $\approx 300\ \mu m$, width $\approx 200\ \mu m$, and thickness $\approx 100\ \mu m$. It consists of a higher refractive index active medium sandwiched between heavily p- and n- doped cladding layers with lower refractive indices. Placing the doped semiconductor materials together in the manner depicted in figure 1.1 achieves two important results. Firstly, because of the electrical properties associated with the doping i.e. different band-gap energies, the electron-hole pairs injected from the electrical current source will be confined to the active region only. This means that when recombination takes place the optical gain is also confined to this region. Secondly, the refractive index difference between the layers acts to confine the field transversely and guide it longitudinally. Therefore in the process of the lasing action, the semiconductor laser medium is pumped by application of an injection current at the device's metallic contacts. This process fills the energy states of the conduction and the valence bands associated with the laser's p-n junction. Spontaneous and stimulated emissions involve the transition of electrons from the conduction band to the valance band thus annihilating electron-hole pairs, which is analogous to the E_2 to E_1 energy level transition of the two state system previously introduced. (The reader may wish to consult one of the suggested references for a detailed discussion of these mechanisms.)

Once pumping occurs, all that remains to initiate laser action is to establish a mechanism of optical feedback. In order to set up this situation, the pumped active medium is placed within the confines of an optical resonant cavity. The resonant condition can be achieved in several ways; however, in the case of semiconductor lasers, the earliest methods employed reflective facets at the cavity ends. In very simple terms, as the light bounces back and forth between the reflecting end facets it interacts with the pumped active medium stimulating the emission of photons as the electron-hole pairs recombine. A

longitudinal field builds until internal optical losses are exceeded and the laser begins to exhibit a self–sustained oscillation. This is known as the threshold condition and it is the point that the laser is just "turning on". Less than 100% reflectivity allows a portion of the light to escape through the end facets.

Lasers that employ cavity end reflectivity, whether using reflective facets or external mirrors, are referred to as Fabry–Perot lasers. A semiconductor Fabry-Perot laser has a wide gain spectrum and exhibits multimode longitudinal oscillations. Unlike the simple two-level, single-frequency energy transition model previously discussed, this means that the active medium is capable of emitting radiation across a broad range of frequencies. Because a cavity with facet reflectivity will support oscillations at multiple frequencies, the laser will emit more than one lasing frequency. This makes the Fabry-Perot laser useful, for example, in applications such as a CD player, but undesirable for use in optical communication systems.

A single longitudinal mode oscillation resulting in a monochromatic output can be achieved by changing the nature of the cavity feedback. Removing the mechanism of feedback from the cavity ends and distributing it over the entire length of the cavity in the form of a periodic index variation will accomplish this. A semiconductor laser employing this type of distributed feedback mechanism is known as a distributed feedback (DFB) laser. Refer to figure 1.2 for a simplified schematic of a DFB laser structure.

1.4 DFB Lasers

DFB laser structures are planar and composed of semiconductor materials such as indium gallium arsenide phosphide (InGaAsP) waveguide and active layers as well as n- and p-doped indium phosphide (InP) buffer and substrate layers. Typical dimensions of a DFB laser's active layer are a length of 500 μm, a width of 1.5 μm, and a depth of 0.12 μm. The grating is formed using an etching process. These methods are very precise and

result in an accurate grating depth, pitch, and period, parameters that determine the feedback and operational characteristics of the laser.

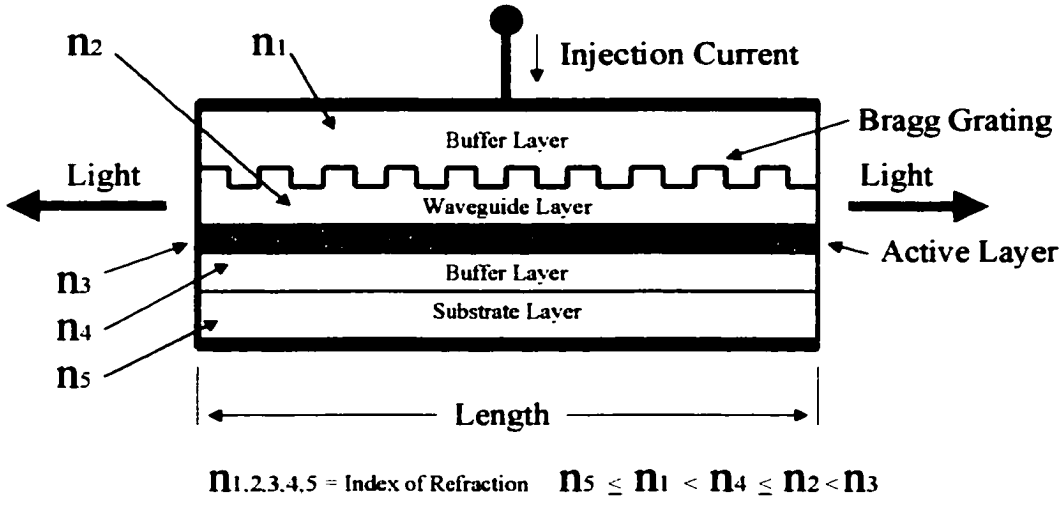

Figure 1.2 Index-Coupled Distributed Feedback Laser

This longitudinal periodic index distribution is known as a Bragg grating and the mechanism of feedback is by Bragg diffraction. A wave that is incident on the Bragg grating will result in reflected wavelets at each grating corrugation. If the phase difference between reflecting wavelets is an integer of 2π, constructive interference will take place. This provides the mechanism for longitudinal mode selectivity. Only the modes with a wavelength, λ_B, which satisfies a condition

$$\Lambda = m(\lambda_B / 2n_e) \qquad [1\text{-}1]$$

where Λ is the grating period, m is a non-zero integer, and n_e is the effective refractive index of the mode, will couple constructively. The examples considered in this work used a first order grating, where $m = 1$. Optical feedback generated in this manner results in two counter-propagating electromagnetic (optical) waves, where the right-traveling wave couples energy into a left-traveling wave, while at the same time the left-traveling

wave couples energy into the right-traveling wave. The strength of this coupling is governed by the coupling coefficient, K, a parameter that is determined by the grating pitch, depth, period, and position relative to the active layer.

When the coupling is restricted to a grating that consists of a periodic index perturbation only, this is referred to as index-coupling. Other classes of coupling include mixed or gain-coupling. The mixed-coupled structure has its corrugation layer fabricated on the upper portion of the active layer. Index-coupling is induced through the periodic variation in the refractive index associated with the corrugation layer; however, the active layer thickness is also modulated by the presence of the corrugation. This in turn results in a longitudinal modulation of the amplitude gain, which induces the gain-coupling effect. Pure gain-coupling is achieved by fabricating a second grating layer on top of the mixed-coupling grating structure. This second grating employs an inverse phase corrugation, which acts to cancel the index-coupling effects of the original grating. These various coupling classes, index, mixed, and gain-coupling, are reflected in K values that are respectively either purely real, complex, or purely imaginary.

Although the forthcoming methods could be applied equally well to the other classes of coupling, the index-coupled DFB laser is extensively used, and for the purpose of this work consideration was restricted to this structure with no obvious loss of generality.

1.5 Longitudinal Spatial Hole-burning

The DFB laser's ability to produce a single longitudinal mode oscillation resulting in a monochromatic output is of fundamental importance in optical communications applications. Much work has gone into the design of such devices in the effort to achieve narrow spectral linewidths, reduced longitudinal spatial hole-burning (LSHB), low threshold (turn-on) current, and efficient power utilization. The introduction of a quarter-wave phase shift at the laser cavity mid-point eliminated a major problem associated with DFB lasers, that of low power mode-degeneracy. This is the appearance of unwanted

side modes at an injection current level that is above, but still close to the threshold injection current. This characteristic is due to insufficient gain margin at the low power level. Unfortunately, addition of the quarter-wave phase shift also resulted in a highly concentrated field at the phase shift plane causing LSHB. At this point the intense field of a QWS DFB structure locally depletes the carrier density, and as the laser power increases, this effect ultimately results in mode-degeneracy now occurring at higher operating powers.

DFB laser design, including the reduction of LSHB, has been the target of intensive research. A partial list of references includes the works of [Fang, Hsu, Chuang, Tanbun-Ek, and Sergent, 1997], [Fessant, 1997], [Morthier and Baets, 1991], [Morthier, David, Vankwikelberge, and Baets, 1990], and [Rabinovitch and Fieldman, 1989]. Recent research by [Wang, Cada, and Makino, 1998], [Wang, Cada, and Sun, 1999], and [Wang and Cada, 2000] has resulted in the development of a novel coupled-power technique, which has also been successfully used to investigate the behavior and the LSHB reduction of a DFB laser.

One method used to reduce LSHB is to introduce a longitudinally distributed coupling coefficient (DCC). The DCC is typically length-normalized and is referred to as the *Kappa-L* product (*KL*). By optimally choosing a *KL* distribution, the field maximum that occurs at the laser cavity midpoint in a QWS structure for a uniform *KL* is reduced, thereby reducing the LSHB effects. The question then is, given a finite number of (fixed) *KL* sections, is it possible to select the *KL* distribution so that the internal field is optimally flattened, or at least approaches a uniform state.

It is also possible to achieve a reduction in the field intensity non-uniformity by moving away from the QWS structure and longitudinally distributing the phase shift (*PS*) profile. This method may be used alone or in combination with a DCC.

Because these approaches have been investigated using designs at threshold power, (see [Ghafouri-Shiraz and Lo, 1996], and [Yokoyama and Sekino, 1998]), this problem provided a useful benchmark to validate the new proposed methodology which conversely entailed designing for maximum field flatness at the threshold current of interest. In other words, for a fixed above-threshold injection current, how does one optimize the *KL* and/or *PS* parameters such that the DFB laser's internal field is optimally flattened?

Based on the known above-threshold performance characteristics of the benchmark threshold designs, a substantial improvement in field flatness was not anticipated by using the new methodology, but the advantage of this expected result was that it provided a required reasonable standard for validation purposes. Therefore, it was considered logical to expect that confirmation of the new methodology's capabilities would depend on achieving field optimization results that were at least comparable to the benchmark results. This established the rationale for using this problem to test and substantiate the performance capabilities of the new methodology. As an additional benefit, there also remained the possibility to gain alternate insights into this problem by approaching it from a new direction.

So to summarize, what has been lacking so far in the literature is a comprehensive optimal design methodology for DFB lasers, particularly when directly tackling non-linear above-threshold considerations such as minimization of LSHB at the specific injection current of interest. This thesis proposes a new methodology that uses global optimization in conjunction with the transfer matrix method above-threshold solution technique as one step towards achieving this objective.

2. COUPLED WAVE THEORY

2.1 The Scalar Wave Equation

The pioneering work of [Kogelnik and Shank, 1972] provided the first theoretical explanation of the operation of a DFB laser structure in terms of the coupled wave theory. Methods based on coupled wave analysis have since been used extensively to model the steady state characteristics of DFB lasers. Coupled wave theory necessarily forms the basis of the TMM as applied to the threshold and above-threshold analysis of DFB lasers and as such will be discussed in this section.

Lateral and transverse field confinement imposed by the structural constraints of the DFB laser necessitates that any longitudinal field solution must satisfy the following one-dimensional time-independent scalar wave equation.

$$\frac{d^2E(z)}{dz^2} + k^2(z)E(z) = 0\,, \qquad [2\text{-}1]$$

where z represents the direction of electric field propagation or longitudinal direction of the laser and $k(z)$ is the wave propagation constant. $E(z)$ is the complex amplitude of a time-harmonic electric field and is considered to be independent of the x (width) and y (thickness or transverse) directions of the laser.

Consider the general case where the Bragg grating consists of both a periodic refractive index and gain variation. Then, using a first order approximation, the index $n(z)$, and gain $\alpha(z)$ profiles are written as

$$n(z) = n + n_1 \cos(2\beta_o z)\,, \qquad [2\text{-}2a]$$

$$\alpha(z) = \alpha + \alpha_1 \cos(2\beta_o z)\,. \qquad [2\text{-}2b]$$

The parameters n and α, are average values while n_1 and α_1 are the maximum amplitudes of the periodic variations in laser medium refractive index and gain, respectively. β_o is

the Bragg propagation constant. The wave propagation constant, k, for a wave propagating in a complex dielectric where the radiation frequency close to the resonance frequency is defined as

$$k^2 = k_o^2 n^2(z)\left(1 + j\frac{2\alpha(z)}{k_o n(z)}\right), \qquad [2\text{-}3]$$

where k_o is the free space propagation constant. Assuming the perturbations in gain and index are much smaller than their average values ($n_1 << n$, $\alpha_1 << \alpha$) and substituting equation [2-2a] and [2-2b] into equation [2-3] result in the following expression for k:

$$k^2 = k_o^2 n^2(z) + j2k_o n(z)\alpha(z) + 4k_o n(z)\left(\frac{\pi n_1}{\lambda} + j\frac{\alpha_1}{2}\right)\cos(2\beta_o z). \qquad [2\text{-}4]$$

Since K is defined as

$$K = \frac{\pi n_1}{\lambda} + j\frac{\alpha_1}{2}, \qquad [2\text{-}5]$$

by replacing $k_o n(z)$ with β, equation [2-5] can be rewritten in the following form

$$k^2 = \beta^2 + j2\beta\alpha(z) + 4\beta K\cos(2\beta_o z). \qquad [2\text{-}6]$$

Substitution of this expression into equation [2-1] yields

$$\frac{d^2E(z)}{dz^2} + [\beta^2 + j2\beta\alpha(z) + 4\beta K\cos(2\beta_o z)]E(z) = 0. \qquad [2\text{-}7]$$

2.2 The Coupled Wave Equations

A necessary condition for coupling and propagation is that the Bragg condition must be nearly satisfied. This means that the actual propagation constant β must be sufficiently close to the Bragg propagation constant β_o such that the absolute difference between them is much less than the Bragg propagation constant or $|\beta-\beta_o| << \beta_o$. With this considered, the solution to equation [2-7] is the total complex electric field amplitude along the grating and results from a linear superposition of two counter-propagating waves (electric fields). The expression is written as

$$E(z) = R(z)e^{-j\beta_o z} + S(z)e^{j\beta_o z}. \qquad [2\text{-}8]$$

Equation [2-8] is the trial solution to the scalar wave equation, and is used to construct a general solution by substitution into equation [2-7]. The electric field solutions vary slowly in amplitude allowing second order derivatives in the complex amplitude terms $R(z)$ and $S(z)$ to be neglected. Similarly because $|\beta-\beta_o| << \beta_o$, rapidly changing phase terms such as $exp(\pm j3\beta_o z)$ can be ignored. It is common practice in the coupled wave theory to neglect the higher order terms because there is no coupling between third order traveling waves.

Finally the following approximation is made

$$\frac{\beta^2 - \beta_o^2}{2\beta_o} \approx \beta - \beta_o = n(\omega - \omega_o)/c = \delta, \qquad [2\text{-}9]$$

where c is the speed of light in vacuum, ω and ω_o are the longitudinal mode and Bragg frequencies, respectively, and the parameter δ is known as the detuning coefficient. It is a measure of the difference between the Bragg propagation constant and the actual propagation constant of the longitudinal mode. When the terms containing similar

exponents are grouped together, the general solution, which consists of the following pair of coupled wave equations, is obtained

$$-\frac{dR(z)}{dz} + (\alpha_o - j\delta)R(z) = jKS(z) \qquad [2\text{-}10a]$$

$$\frac{dS(z)}{dz} + (\alpha_o - j\delta)S(z) = jKR(z). \qquad [2\text{-}10b]$$

Expressing the trial solution to the coupled wave equations in terms of the complex propagation constant, γ, the following relations are obtained

$$R(z) = R_1 e^{\gamma z} + R_2 e^{-\gamma z} \qquad [2\text{-}11a]$$

$$S(z) = S_1 e^{\gamma z} + S_2 e^{-\gamma z}, \qquad [2\text{-}11b]$$

where R_1, R_2, S_1, and S_2, are complex coefficients that depend on the boundary conditions that the field encounters at the left-and right-hand facets. These boundary conditions in turn depend on facet reflectivities, which are understood to be zero as a simplifying but in no way limiting assumption for the purpose of this analysis. The dispersion relation determines the complex propagation constant, γ, with

$$\gamma^2 = K^2 + (\alpha - j\delta)^2. \qquad [2\text{-}12]$$

In the case of zero facet reflectivity, the exact solutions to the coupled wave equations are written as

$$R(z) = \sinh \gamma(z + \frac{1}{2}L), \qquad [2\text{-}13a]$$

$$S(z) = \sinh \gamma(z - \frac{1}{2}L). \qquad [2\text{-}13b]$$

where L is the longitudinal dimension (length) of the DFB laser. Equation [2-1], the scalar wave equation, is classified as a two-point linear homogeneous boundary problem. The non-trivial solutions to equation [2-1] are expressed in terms of eigenvalues and corresponding eigenfunctions. In this case, equations [2-13a], and [2-13b] form a set of eigenfunctions with corresponding eigenvalues γ, which determine the oscillation modes of the laser as a function of L and K.

2.3 Threshold Oscillation Condition

The threshold equation for zero facet reflectivities is written as [Ghafouri-Shiraz and Lo, (1996)]

$$j\gamma L = \pm KL \sinh(\gamma L). \qquad [2\text{-}14]$$

For a fixed value of the length-normalized coupling coefficient, KL, it is possible to solve equation [2-14] for the various oscillation modes of the DFB laser. These modes are expressed in terms of the detuning parameter, δ, and the threshold gain, α. Typically these parameters are also normalized relative to the length of the DFB laser and are written as δL and αL.

Equation [1-1] and equations [2-1] to [2-14] form the basis on which to describe the oscillating mode characteristics and resultant field profiles of a DFB laser at threshold, i.e. the point where the laser is just turning on. At threshold the number of stimulated photons are considered negligible. As the injection current increases, so does the dynamic range of the laser's longitudinal carrier density and the stimulated photon density profiles. This interrelationship is also reflected by an increase in the dynamic range of the laser's internal electric field intensity profile. The non-linear interactions between these profiles must now be considered because of their effects on the laser's oscillating mode characteristics. The next section will illustrate how the transfer matrix method is used to address the above-threshold problem.

3. TRANSFER MATRIX METHOD

3.1 Transfer Matrix Method and Global Optimization

The concept presented in this section uses as its starting point the above-threshold transfer matrix methodology originally proposed by [Ghafouri-Shiraz and Lo, 1996]. Starting at the left-hand facet, and using sectional transfer matrices, the DFB laser's internal electric field is longitudinally propagated through the structure until the right-hand facet is reached. Using their approach, the oscillation mode characteristics of the laser, for an above-threshold injection current, are obtained by matching the internal field's right-hand boundary condition (RBC). This is done iteratively where, based on the RBC error in the previous iteration, new potential solution values are selected and evaluated by re-propagating the electric field. Their heuristic strategy utilizes an adaptable numerical grid over the solution space to select each new set of potential solution values. This method, which is dependent on the result of the previous iteration, "walks around" the solution space until the RBC error is minimized. Because of the multi-extremal nature of the error function, one has to carefully select a starting point when solving the problem at a given injection current. Solutions are obtained for increasing injection current by using a previous lower injection current result as a starting point. These increases must be sufficiently small to avoid ending up in a local minimum of the error function, which would represent a non-physical field solution.

By integrating this above-threshold transfer matrix method with the robust global optimization strategies as implemented by the LGO software [Pintér, 2000], to globally search the entire solution space and select the solution that minimizes the RBC error, it was possible to directly and rapidly solve for injection currents that varied from 1.1 to 5 times the threshold injection current. [Ghafouri-Shiraz and Lo, 1996] selected this range of injection currents to explore the behavior of a bulk semiconductor lasing around 1550 *nm*. This range was chosen primarily because it covered a sufficient span to permit the material saturation effects to fully mature. In order to obtain a valid comparison with the new methodology, identical laser structural and material parameters, as well as the same injection current range, were used in this work.

Using the new methodology, the simplest possible case was first considered [Isenor, Pintér, and Cada, 2001b]. This consisted of finding the valid internal field solutions for the QWS DFB laser in terms of the optimal values of the lasing wavelength, λ, and the dimensionless coefficient, C_o, a parameter which relates the normalized electric field to the actual total electric field. The solutions were obtained over a range of selected injection currents, initially without the requirement to optimize the flatness of the laser's internal field. Encouragingly, these results compared very favorably to the referenced results achieved by Ghafouri-Shiraz and Lo.

This represented an initial success; however, the most important realization was that no inherent limit existed on the number of solution variables this process was theoretically capable of dealing with, although practical limits based on the computational load obviously existed. By defining the error function (objective function) to include a field flatness parameter and by expanding the solution space to include the structural parameters that affect field flatness, it became possible to simultaneously obtain an optimally flattened field while achieving the boundary match condition required for a valid field solution.

3.2 Transfer Matrix Method Theory

The TMM approach requires dividing the DFB laser into a large number of equal-length sections while within each section all physical parameters are considered constant.

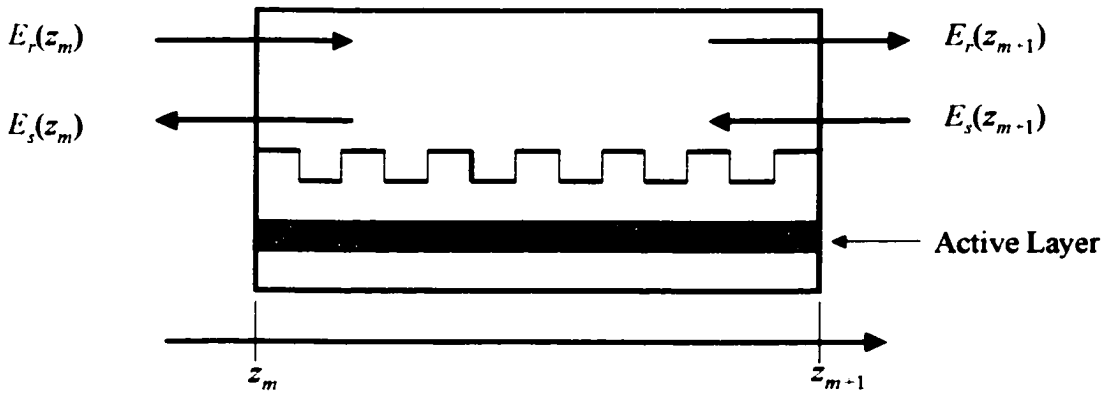

Figure 3.1 DFB Section of a Semiconductor Laser Diode

This is the key to the method. In the case of the DFB laser's electric field distribution, it allows a simple 2x2 matrix relationship to be developed between the input and the output electric fields for any section. Refer to figure 3.1 for a schematic of an arbitrary (m^{th}) section of a DFB semiconductor laser diode.

For any laser section of the type described, it is possible to rewrite the trial solutions, equations [2-11a] and [2-11b], in such a fashion that the input and the output electric fields are related by a matrix equation of the form

$$\begin{bmatrix} E_r(z_{m+1}) \\ E_s(z_{m+1}) \end{bmatrix} = \begin{bmatrix} t_{11} & t_{12} \\ t_{21} & t_{22} \end{bmatrix} \cdot \begin{bmatrix} E_r(z_m) \\ E_s(z_m) \end{bmatrix} \qquad [3\text{-}1]$$

where the matrix elements, t_{ij}, are written as

$$t_{11} = \left(E - \rho^2 E^{-1}\right) \cdot e^{-j\beta_o(z_{m+1}-z_m)} / \left(1-\rho^2\right) \qquad [3\text{-}2a]$$

$$t_{12} = -\rho\left(E - E^{-1}\right) \cdot e^{-j\beta_o(z_{m+1}-z_m)} / \left(1-\rho^2\right) \qquad [3\text{-}2b]$$

$$t_{21} = \rho\left(E - E^{-1}\right) \cdot e^{j\beta_o(z_{m+1}-z_m)} / \left(1-\rho^2\right) \qquad [3\text{-}2c]$$

$$t_{22} = -\left(\rho^2 E - E^{-1}\right) \cdot e^{j\beta_o(z_{m+1}-z_m)} / \left(1-\rho^2\right), \qquad [3\text{-}2d]$$

with

$$\rho = \frac{jK}{(\alpha - j\delta + \gamma)}, \qquad [3\text{-}3]$$

and

$$E = e^{\gamma(z_{m+1}-z_m)}, \qquad E^{-1} = e^{-\gamma(z_{m+1}-z_m)}. \qquad [3\text{-}4]$$

The matrix product of the individual section transfer matrices, written in the following manner

$$\mathrm{Y}\left(z_{M-1}|z_1\right)=\mathrm{T}^{M}\cdot\mathrm{T}^{M-1}\cdots\mathrm{T}^{2}\cdot\mathrm{T}^{1}, \qquad [3\text{-}5]$$

forms the complete transfer matrix, Y, for a DFB laser of M sections.

This overall matrix fully describes the propagation characteristics of the right-and left-traveling waves for the entire DFB laser. The initial numerical example considered in the next section used a quarter-wave phase shift (QWS) section positioned at the midpoint of the laser to ensure single longitudinal mode stability. In a QWS structure, input and output electric fields are considered continuous, encountering only a shift in phase as they travel through this section.

The quarter-wave phase shift section can be described by a matrix

$$P=\begin{bmatrix} e^{j\frac{\pi}{2}} & 0 \\ 0 & e^{-j\frac{\pi}{2}} \end{bmatrix}. \qquad [3\text{-}6]$$

Any (mid-point) phase shift section is easily incorporated into equation [3-5] in the following manner

$$\mathrm{Y}\left(z_{M-1}|z_1\right)=\mathrm{T}^{M}\cdot\mathrm{T}^{M-1}\cdots\mathrm{T}^{\frac{M}{2}+1}\cdot P\cdot\mathrm{T}^{\frac{M}{2}}\cdots\mathrm{T}^{2}\cdot\mathrm{T}^{1}. \qquad [3\text{-}7]$$

This expression gives the complete transfer matrix representation of a QWS DFB laser. In order to ensure symmetry, an even number of equal-length sections is chosen, allowing the phase shift section to be placed at exactly the midpoint of the DFB laser. This consideration is reflected in equation [3-7]. In the forthcoming numerical examples, M

was chosen to be 5000, and the phase shift section was placed after the section 2500. The midpoint QWS section is a plane of quarter-wave phase transition for the longitudinal electric fields. Because this transition takes place over one corrugation period, which is three orders of magnitude less than the length of the laser, the actual physical length of the transition can reasonably be neglected. Using equation [3-7], it is now possible to relate the electric fields that appear at the right-hand facet of a QWS DFB to the electric fields at the left-hand facet by the following matrix equation

$$\begin{bmatrix} E_r(z_{M+1}) \\ E_s(z_{M+1}) \end{bmatrix} = \mathrm{Y}\left(z_{M+1} | z_1\right) \cdot \begin{bmatrix} E_r(z_1) \\ E_s(z_1) \end{bmatrix}. \qquad [3\text{-}8]$$

It should be noted that equation [3-7] reflects an ideal QWS DFB laser structure with zero facet reflectivities at both facets as well as no residual grating phase at either facet. Non-zero residual grating phases at the facets as well as facet reflectivities would necessarily be accounted for in the transfer matrix formulations and could easily be incorporated into equation [3-7] and equation [3-8] if needed. However, for the purpose of this work these considerations are an unnecessary complexity.

3.3 Laser Threshold Condition Using the TMM

A laser at threshold is an optical oscillator. Applying coupled wave theory means that at threshold the right-traveling electric field with a value of zero at the left-hand facet would grow in intensity as it travels to the right through the laser until it reaches the right-hand facet. The same consideration would, of course, equally apply to the left-traveling electric field. In order for this to occur, the transmission gain of both the left-and right-traveling fields must be theoretically infinite.

Using equation [3-8] the following relationship is obtained for the transmission gain, A_t, of the left-traveling field

$$A_t = \frac{E_s(z_1^-)}{E_s(z_{M-1}^-)} = \frac{1}{y_{22}(z_{M-1}|z_1)}, \qquad [3\text{-}9]$$

where

$$y_{22}(z_{M-1}|z_1) = 0. \qquad [3\text{-}10]$$

When equation [3-9] approaches zero, the transmission gain for the left traveling-field approaches infinity and the cavity becomes resonant. Solving equation [3-9] is analogous to solving equation [2-14], and results in the oscillation mode parameters of the laser at threshold, again expressed in terms of the detuning parameter, δ, and the threshold gain, α.

4. ABOVE-THRESHOLD OPTIMIZATION

4.1 Theory and Methodology

Any study of the above-threshold behavior of a DFB laser must incorporate the non-linear interactions between the longitudinally varying parameters of electric field intensity distribution, carrier density, photon density, and refractive index for a given injection current. Because the physical parameters in any given laser section are assumed to be homogeneous, it is possible to obtain the electric field intensity, carrier density, photon density, and refractive index for that section, and by using a large enough number of transfer matrix sections, it is also possible to numerically extend the localized results to a continuous distribution.

This investigation considered the field flatness optimization of a QWS DFB laser consisting of six equal length sections symmetrically arranged about the laser's midpoint. A schematic of this structure is presented in figure 4.1. Associated with each section were length-normalized coupling coefficients, *KL1* to *KL6*, while phase shift planes, *PS1* to *PS5*, separated each section. Given the problem symmetry, the following simplifications were possible: *KL1* equals *KL6*, *KL2* equals *KL5*, *KL3* equals *KL4*, *PS1* equals *PS5*, and *PS2* equals *PS4*. The plane of symmetry was *PS3*, the laser's midpoint. This arrangement reduced the numerical complexity by three variables with coupling coefficient only optimization, and by five variables when both phase and coupling coefficient optimization were considered simultaneously.

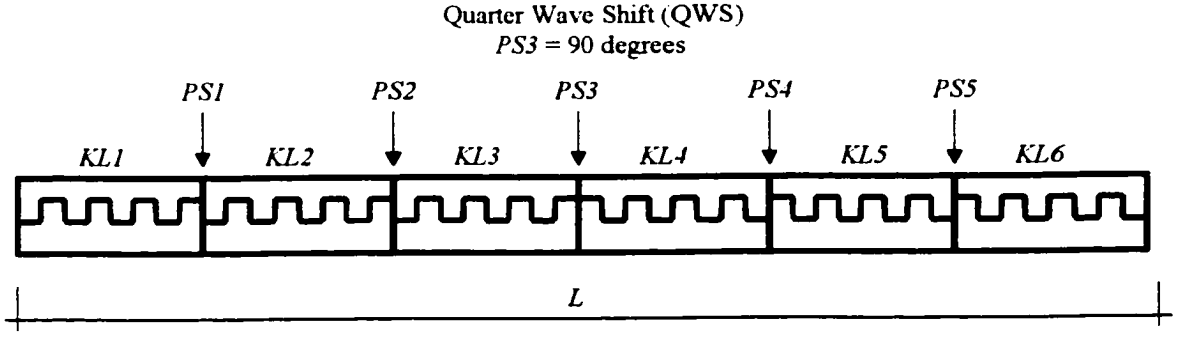

Figure 4.1 Schematic of DFB Laser Structure

As a matter of clarification the following convention with respect to sectional coupling coefficient and phase shift sections was adopted. The parameter *KL* refers to the overall sectional coupling coefficient profile, *KL1* to *KL6*, and similarly the phase shift profile parameter, *PS*, refers to the collection of phase shifts, *PS1* to *PS5*, which separate the various coupling coefficient sections. This is also illustrated in figure 4.1.

The primary objective was to apply global optimization methodology to minimize the objective function derived from the above-threshold TMM, and in so doing, to select the *KL* and *PS* design parameters as well as the lasing wavelength, λ, and the dimensionless coefficient, C_o, such that the field flatness was maximized. C_o, relates the actual total electric field, $\bar{E}$, to the normalized total electric field, E, in the following manner

$$\bar{E}(z) = C_o E(z) = C_o\left[E_r(z) + E_s(z)\right]. \qquad [4\text{-}1]$$

There are fundamentally two conditions that must be simultaneously considered when solving the above problem. The first condition is the requirement that the field solution must match the right-hand facet boundary condition. TMM field propagation is chosen to start from the left-hand facet and moves through the laser structure section by section until the right-hand facet is reached. Providing the laser structure is symmetric, and the facets are anti-reflective, at this point the normalized left-traveling field intensity should be zero and the normalized right-traveling field intensity should be one. Under these considerations the right-hand boundary condition is met if equation [3-10] is satisfied, [Ghafouri-Shiraz and Lo, 1996]. One may use this fact directly in the iterative process to find the best solution or opt to consider the actual left-traveling field intensity's requirement to be zero at the right-hand facet. The latter approach was considered in this investigation. It should be noted that with either approach equation [3-10] is still directly or indirectly minimized.

Finding the above-threshold field solution for fixed *KL* and *PS* profiles involves the iterative selection of the λ and C_o that results in the best field boundary condition match

at the right-hand facet. This in itself is an optimization problem where the objective or merit function to be minimized is the boundary condition error.

The second condition is maximizing the actual field flatness. *KL* and *PS* values have to be optimized such that the field is maximally flattened while at the same time the boundary condition constraint must be met. Utilizing the problem definition capabilities of the LGO software and constructing an objective function that incorporates both requirements simultaneously accomplish this. To the best of the author's knowledge this approach has not been used before and as such represents an original contribution.

The field flatness function F is defined as

$$F = \frac{1}{L}\int_{z_1}^{z_{M-1}} \left(I(z) - I_{avg}\right)^2 dz\,, \qquad [4\text{-}2]$$

and the objective function becomes

$$Objf = F + scal \times RBC\,error\,, \qquad [4\text{-}3]$$

where *I(z)* is the sectional field intensity, I_{avg} is the average field intensity over the laser length, *RBCerror* is the right-hand boundary condition error, and *scal* is a suitable scaling (penalty) parameter. This represents (one of) the simplest possible objective functions for this problem. The design of the objective function depends on the problem complexity and the relationships between the solution parameters. If additional considerations are required such as inclusion of a residual phase corrugation and non-zero end facet reflectivities, it may become necessary to redesign the objective function to better reflect the ensuing solution parameter dependencies. However, for the purposes of this work, equation [4-3] provided a reasonable starting point and yielded acceptable results. Based on the outcome of several trial runs using a selection of scaling parameters, a value of *scal* = 1000 was selected and used in the evaluation of the succeeding numerical examples.

Observe that it is necessary to constrain the solution such that minimization of *RBCerror* takes precedence over maximizing the field flatness. This is accomplished by also specifying *RBCerror* as an explicit independent constraint, which ensures that the boundary condition criterion at the right-hand facet is met and the field solution, however optimally flattened, is a valid solution (reference Appendix E, page 109). LGO uses its combination of global and local search strategies on the defined parameter space to seek a minimized objective function. With LGO's selection of each new set of *KL* and *PS* values, as well as λ and C_o, the internal parameters of each transfer matrix section are subsequently modified.

The carrier rate equation must be included to consider the relationship between the injection current, i, the carrier density, N, the stimulated photon density, S, and the net (material) gain, g, in each laser section and is expressed as

$$\frac{i}{qV} = \frac{N}{\tau} + BN^2 + CN^3 + \frac{v_g g S}{1+\sigma S}. \qquad [4\text{-}4]$$

The volume, V, is determined from the geometry of the active region. The parameter σ accounts for saturation effects at high photon densities. The remaining equation parameters consist of the bimolecular recombination coefficient, B, the Auger recombination coefficient, C, the linear recombination lifetime, τ, and the group velocity at the Bragg wavelength, v_g.

The amplitude gain and detuning in each matrix section depend on the carrier density and are written as

$$\alpha = (\Gamma g - \alpha_{loss})/2, \qquad [4\text{-}5]$$

$$\delta = \frac{2\pi}{\lambda} n - \frac{2\pi n_g}{\lambda \lambda_B}(\lambda - \lambda_B) - \frac{\pi}{\Lambda}, \qquad [4\text{-}6]$$

where Γ is the optical confinement coefficient, α_{loss} is the internal cavity loss, n is the effective index, n_g is the group refractive index, λ_B is the Bragg wavelength, and λ is the lasing wavelength. The effective index dependence on the carrier density is defined as

$$n = n_e + \Gamma \frac{\partial n}{\partial N} N, \qquad [4\text{-}7]$$

where n_e is the effective refractive index at zero injection current, and the term $\partial n / \partial N$ is the differential index.

The stimulated photon density in each laser section, S_z, is given by the following expression

$$S_z \approx \frac{2\varepsilon_o n(z) n_g \lambda}{hc} \cdot C_o^2 \left[|E_r(z)|^2 + |E_s(z)|^2 \right], \qquad [4\text{-}8]$$

where ε_o is the permittivity of free space, h is Planck's constant, and c is the speed of light in vacuum. C_o is the dimensionless normalization coefficient. Both λ and C_o need to be determined in the calculation such that the corresponding field profile matches the boundary conditions at the laser facets. Finally, the following parabolic gain model is used to characterize the active medium's gain

$$g = A_0 (N - N_o) - A_1 \left[\lambda - \left(\lambda_o - A_2 (N - N_o) \right) \right]^2. \qquad [4\text{-}9]$$

At the transparency carrier density, N_o, this expression reduces to

$$\lambda_o = \lambda_{th} + A_2 (N_{th} - N_o). \qquad [4\text{-}10]$$

The wavelength λ_o is the wavelength at which the material gain is zero, at the transparency carrier density, and is defined as the peak gain wavelength at zero gain transparency. In the above expression, A_0 is the differential gain, and the parameters A_1

and A_2 are associated with the width of the gain spectrum and changes in gain, respectively, that result from shifts in the peak wavelength.

The flow chart depicted in figure 4.2 illustrates the use of the LGO global optimization software in the solution methodology for obtaining a DFB laser's above-threshold optimized field solution. Consult [Pintér, 2000] for a complete description of the LGO software system, and [Pintér, 1996] discusses the theory behind LGO. Note that LGO can be used in both global and local search modes and that both were applied in this study.

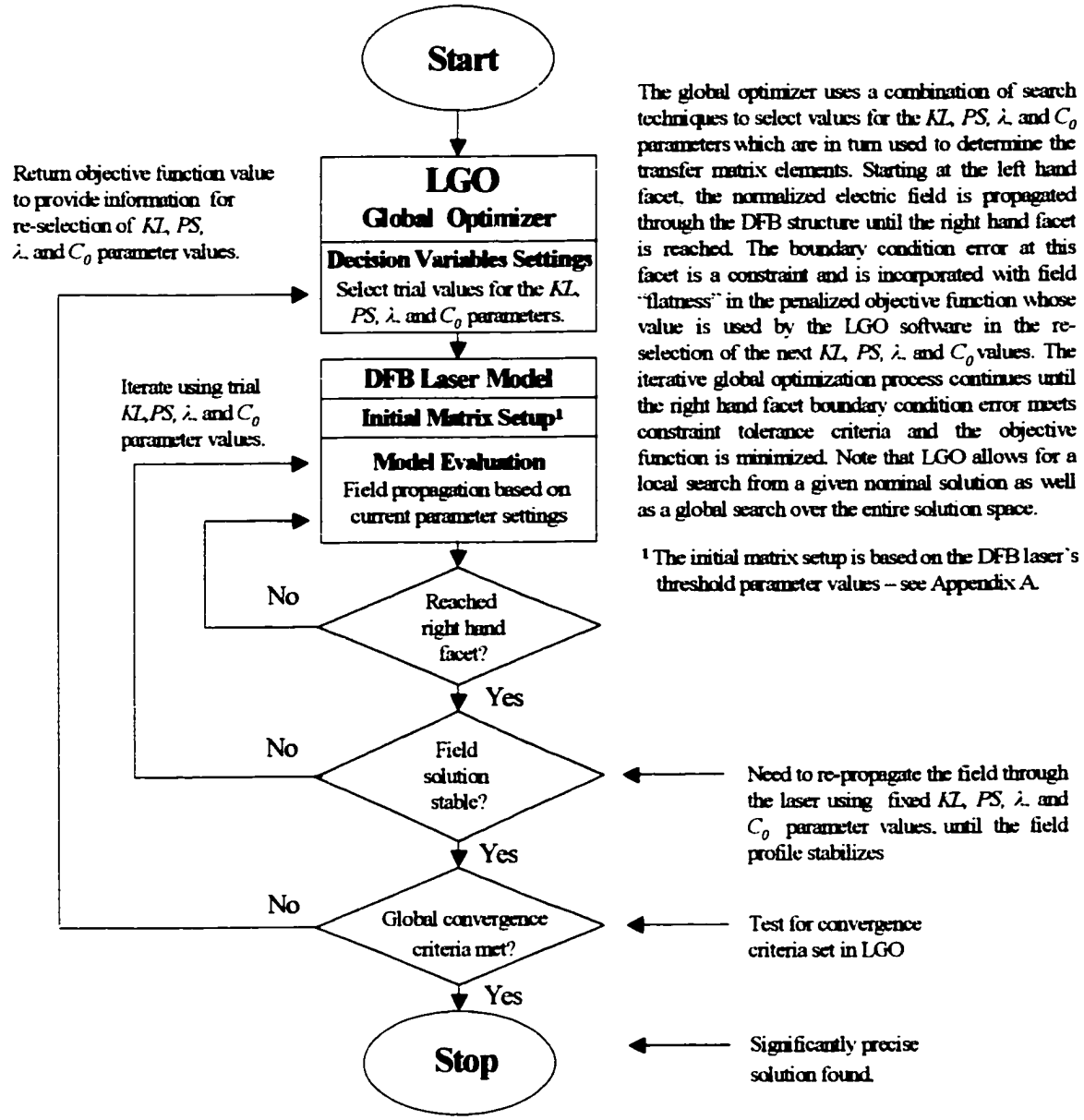

Figure 4.2 Flow Chart of Numerical Procedure

From the preceding description it is clear that the problem solution entails optimization of the behavior of a highly non-linear "black box" (complicated) system. In such cases, there is no guarantee of convexity in the model structure, therefore the "traditional" repertoire of (convex non-linear) optimization is insufficient per se, and a genuine global scope optimization methodology is required to solve the optimal laser design problem discussed.

The calculation proceeds by first obtaining the laser's threshold condition, α_{th} and δ_{th}, from equation [3-10]. Following this, equation [4-1] and equations [4-4] to [4-10] determine all other threshold parameters, N_{th}, n_{th}, λ_o, λ_{th}, and i_{th} , which are used to initialize each sectional transfer matrix. The normalized field is propagated through each laser section, starting at the left-hand facet, until the right-hand facet is reached. The final self-consistent field solution is obtained iteratively such that with each left-to-right pass through a laser section its effective index is updated to reflect the revised sectional carrier density. Because of the complex non-linear interrelationship between the longitudinal field, the longitudinal carrier density, the refractive index, and the photon density profiles, structural iterations must continue until there are no changes in the profiles with each subsequent pass. In so doing, the field solution quickly stabilizes for a given set of *KL*, *PS*, λ, and C_o values. Once the profiles have stabilized, the model function values are evaluated by LGO and based on the search technique employed, LGO selects new *KL*, *PS*, λ, and C_o values.

Using the objective function equation [4-3], and the boundary match constraint, $RBCerror = 0$, the global optimization method, as implemented by the LGO software, searches the entire solution space and selects the solution that minimizes the objective function for a given injection current. This process continues until either the iteration limit set by the user has been exceeded or the numerical optimization criteria have been met. Once this occurs, the *KL1*, *KL2*, *KL3*, *PS1*, *PS2*, *PS3*, λ, and C_o, values as well as the associated longitudinal profiles that correspond to the smallest objective function value are accepted as the solution. The reader may wish to refer to Appendix A for a detailed step-by-step description of the complete calculation process.

4.2 Numerical Examples

In order to evaluate and validate the effectiveness of the new methodology, as well as investigate the characteristics of performing above-threshold field flatness optimizations, three cases were separately considered and compared. Field optimizations were performed using first variations in the coupling coefficient only, then in the phase only, and finally in the coupling coefficient and in the phase. The optimized laser's relative characteristics for the three cases were then compared to each other and to the characteristics of an un-optimized QWS structure with an overall normalized coupling coefficient value of two. All results presented were based on a 500-μm long DFB laser with its model parameters listed in table 4.1. The injection current was normalized relative to the threshold current, i_{th}, and values ranging from 1.1 times i_{th} to 5 times i_{th} were considered.

Therefore, in order to meaningfully compare the new methodology's optimization results to the reference structure's field characteristics, as a starting point for the optimization process, all six equal-length *KL* sections *KL1* to *KL6*, as illustrated in figure 4.1, were also initialized to the value of two. This meant the overall normalized coupling coefficient for the entire structure to be optimized by the new methodology initially matched that of the reference.

The first requirement in the optimization process is to determine the structure's threshold lasing parameters. These values are required to initialize the structural transfer matrices prior to starting the field propagation iterations. In the case of the coupling coefficient only optimization threshold conditions were determined from the indicated QWS structure (with *PS3* = 90 degrees). All the remaining phase shifts were considered zero. In effect the laser remained a QWS structure throughout the entire optimization process. In the other two cases evaluated, the five phase shift planes, *PS1* to *PS5*, were assumed to each have an initial value of 36 degrees each while each of the six *KL* sections were initialized to the normalized (sectional) coupling coefficient value of two, once again matching the reference.

Because of the symmetry conditions previously discussed, (Section 4.1), the first and the second cases resulted in a problem with five degrees of freedom (optimization parameters) whereas the third case, with the combination of both the phase shift and the coupling coefficient optimization parameters, had eight degrees of freedom.

Feasible solutions with objective function minimizations on the order of 10^{-6} were obtained for the various injection currents using a global search termination criterion parameter of 10,000 and 20,000 iterations or model function evaluations. The relatively long runtimes of five to ten hours dictated the restriction of function evaluations to $O(10^4)$ for the purposes of this work; however, satisfactory solution accuracy was still reliably achieved while keeping within this range.

The model was coded using Lahey Fortran LF95, from Lahey Computer Systems Inc. [2000], and implemented together with LGO on an 800 MHz personal computer. Examples of the problem Fortran code are presented in Appendix E. Numerical solutions were obtained in under five hours with a 10,000 iteration run. According to the extensive numerical experience gained with LGO, the use of 10,000 (20,000) function evaluations in the global scope search (before switching over to standard search techniques) was sufficient for the five to eight variable global optimizations performed in this work.

Table 4.1 Model Parameters

Parameter	Symbol	Value	Unit
Material Parameters			
Spontaneous emission rate	τ^{-1}	2.5×10^{8}	s^{-1}
Bimolecular recombination coefficient	B	1×10^{-16}	m^3/s
Auger recombination coefficient	C	3×10^{-41}	m^6/s
Differential gain	A_0	2.7×10^{-20}	m^2
Gain curvature	A_1	0.15×10^{20}	m^{-3}
Differential peak wavelength	A_2	2.7×10^{-32}	m^3
Internal cavity loss	α_{loss}	4×10^{3}	m^{-1}
Refractive index at zero injection	n_c	3.41351524	
Carrier concentration at transparency	N_o	1.5×10^{24}	m^{-3}
Carrier concentration at threshold	N_{th}		m^{-3}
Differential index	$\partial n / \partial N$	-1.8×10^{-26}	m^3
Group velocity at Bragg wavelength	v_g	$3 \times 10^{8}/3.7$	m/s
Nonlinear gain coefficient	σ	1.5×10^{-23}	m^3
Peak gain wavelength at transparency	λ_o	1.63×10^{-6}	m
Lasing wavelength	λ		m
Lasing wavelength at threshold	λ_{th}		m
Structural Parameters			
Active layer width	d	1.2×10^{-7}	m
Active layer thickness	w	1.5×10^{-6}	m
Coupling coefficient	K	4×10^{3}	m^{-1}
Laser cavity length	L	500×10^{-6}	m
Optical confinement factor	Γ	0.35	
Grating period	Λ	2.27039×10^{-7}	m
Bragg wavelength	$\lambda_B = 2\Lambda n_o$	1.55×10^{-6}	m
Threshold current	i_{th}		A
Injection current	i		A

The parameters listed in table 4.1 have been used extensively [Ghafouri-Shiraz and Lo, 1996] in the threshold and the above-threshold analysis of a bulk semiconductor DFB laser, and are considered to be valid for such a device lasing around 1550 *nm*.

4.2.1 Coupling Coefficient Optimization

Results of the coupling coefficient only optimization are presented in this subsection. Starting with a QWS structure based on the parameters defined in table 4.1, field intensity profile optimizations were carried out for injection current values ranging from 1.1 to 5 times the threshold current. In this case the threshold injection current was determined to be 19.82 mA. Figure 4.3 graphically illustrates the results achieved at the various normalized injection currents relative to un-optimized QWS profiles for 10,000 iteration runs. (Similar results were produced with 20,000 iteration runs.) For clarity only the QWS profiles at the injection current extremes are presented in the graph. (The remaining QWS profiles would populate the space between these two extremes.)

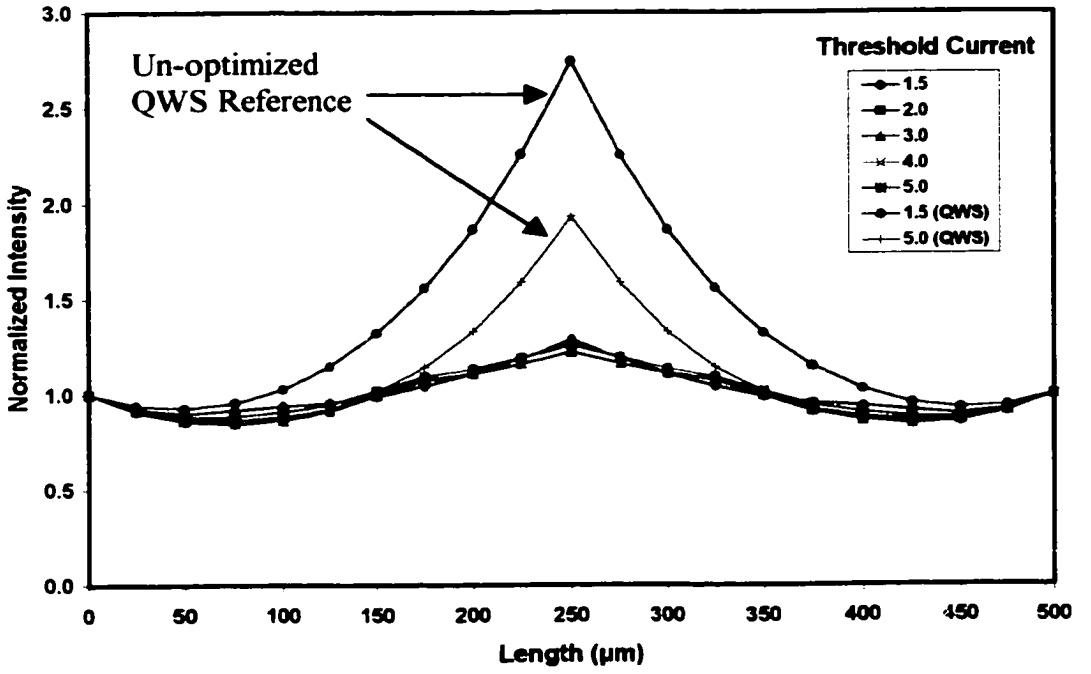

Figure 4.3 Coupling Coefficient Optimization versus Un-optimized QWS Structure: Normalized Longitudinal Field Intensities (10,000 Iterations)

The first fact that is immediately obvious from figure 4.3 is that the longitudinal field intensity profiles were drastically reduced from those of the un-optimized QWS structure for the complete range of injection currents evaluated. This is extremely significant as it clearly indicates that the optimization process worked successfully in the above-threshold region of the laser operation, and resulted in significantly flattened profiles. It is also of importance to note that only minor differences existed between the optimized profiles regardless of the value of the injection current at which the optimization was carried out. In other words, the optimized normalized field intensity profile of the laser operating at 1.1 times the threshold current denoted by 1.1 x i_{th} was virtually identical to the normalized field intensity profile of the laser operating at any other injection current up to and including 5 x i_{th}.

Normalized intensity, carrier density, refractive index, and photon density profiles are presented in figures 4.4 to 4.7 for an injection current value of 3 x i_{th}. Similar characteristics were observed for all the remaining injection currents evaluated.

These results, obtained from 10,000 and 20,000 iteration runs respectively, were compared against the un-optimized QWS DFB laser with a fixed KL of two. Most significantly, there was a marked reduction in the peak field intensity at the midpoint of the laser, which was slightly improved from 10,000 to 20,000 iterations. This reduction was reflected in a corresponding decrease in the depletion of carriers at the laser midpoint. LSHB was thus reduced significantly compared to the un-optimized structure. A decrease in the photon density at the midpoint followed from the decrease in the field intensity, and the refractive index also decreased as a result of the increase in the carrier density.

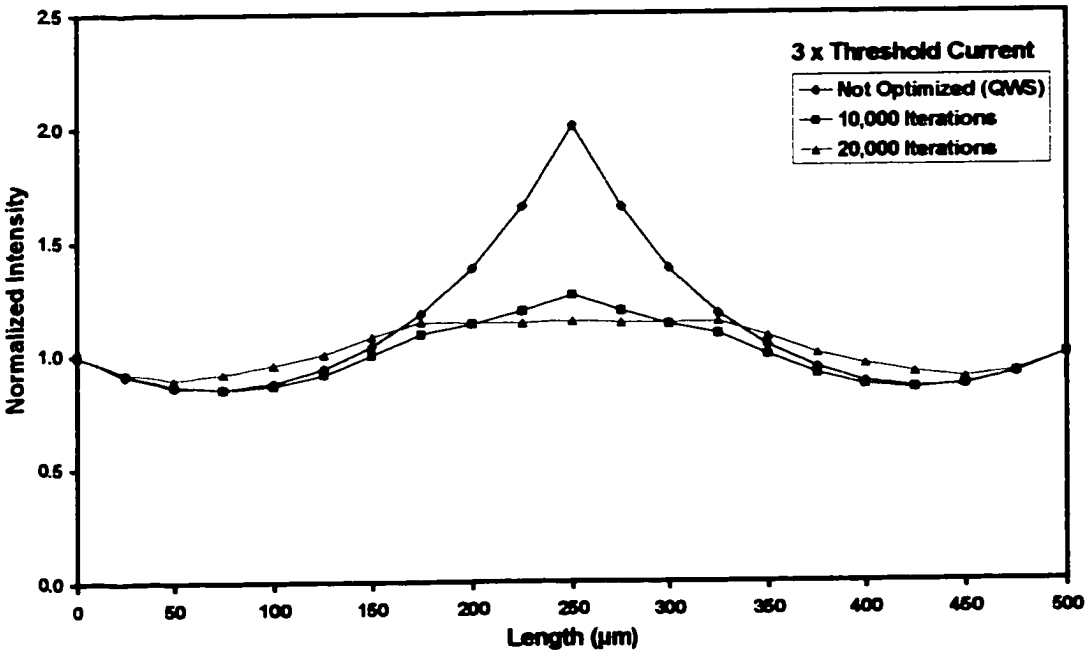

Figure 4.4 Field Intensity (*KL* Optimization at 3 x i_{th})

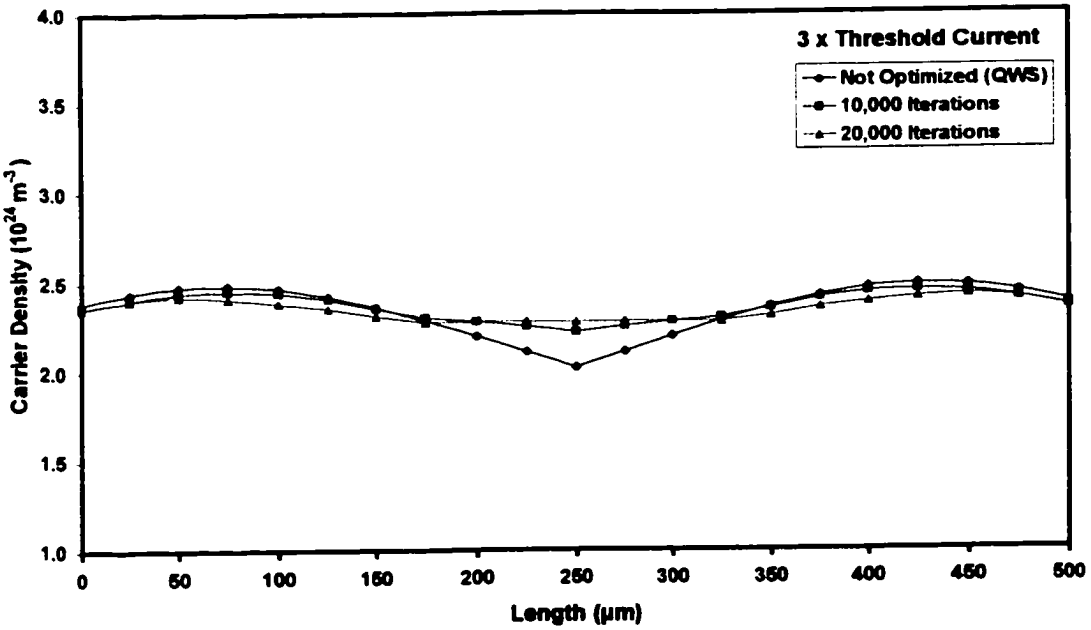

Figure 4.5 Carrier Density (*KL* Optimization at 3 x i_{th})

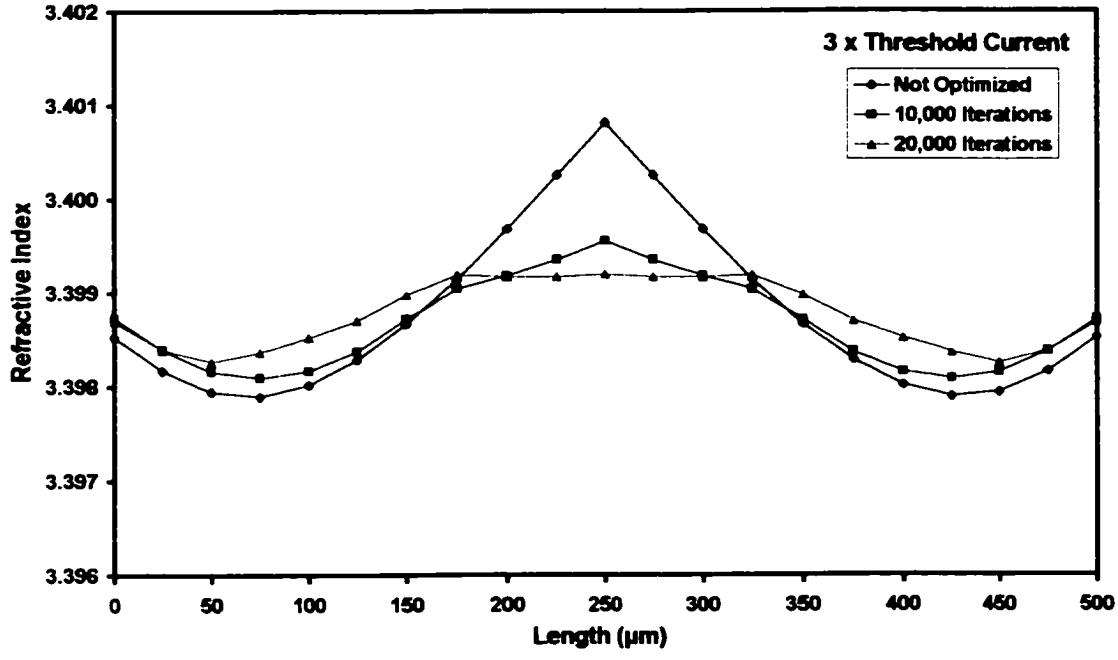

Figure 4.6 Refractive Index (*KL* Optimization at 3 x i_{th})

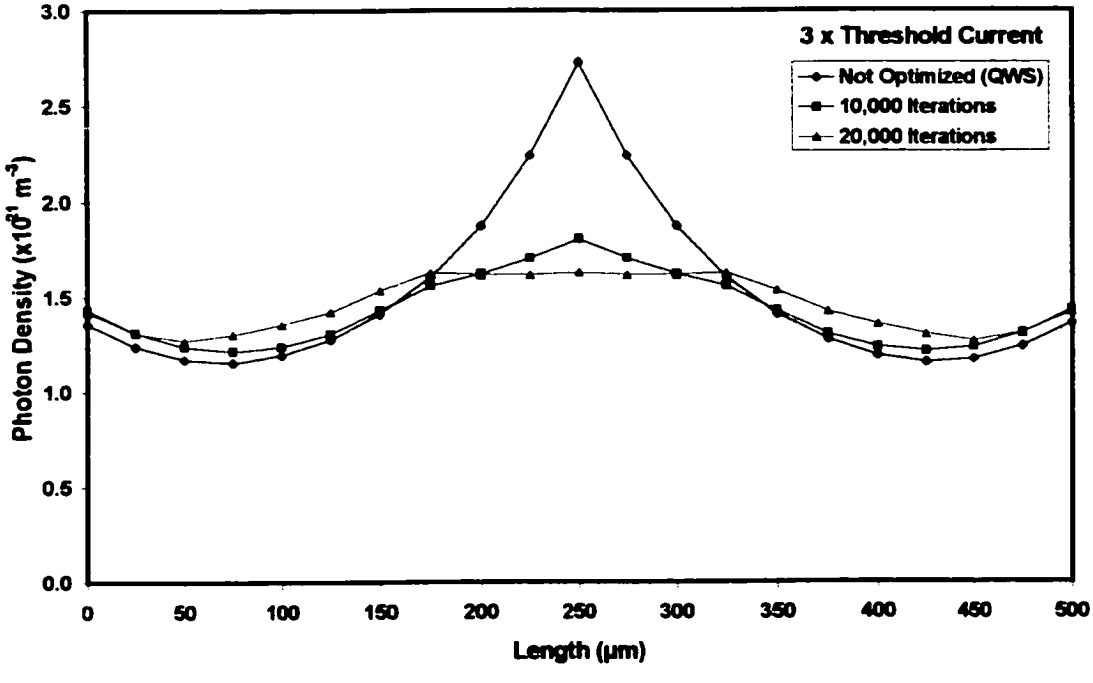

Figure 4.7 Photon Density (*KL* Optimization at 3 x i_{th})

The next set of figures summarizes the operational characteristics for various normalized (i/i_{th}) injection levels above-threshold. Field flatness is compared in figure 4.8.

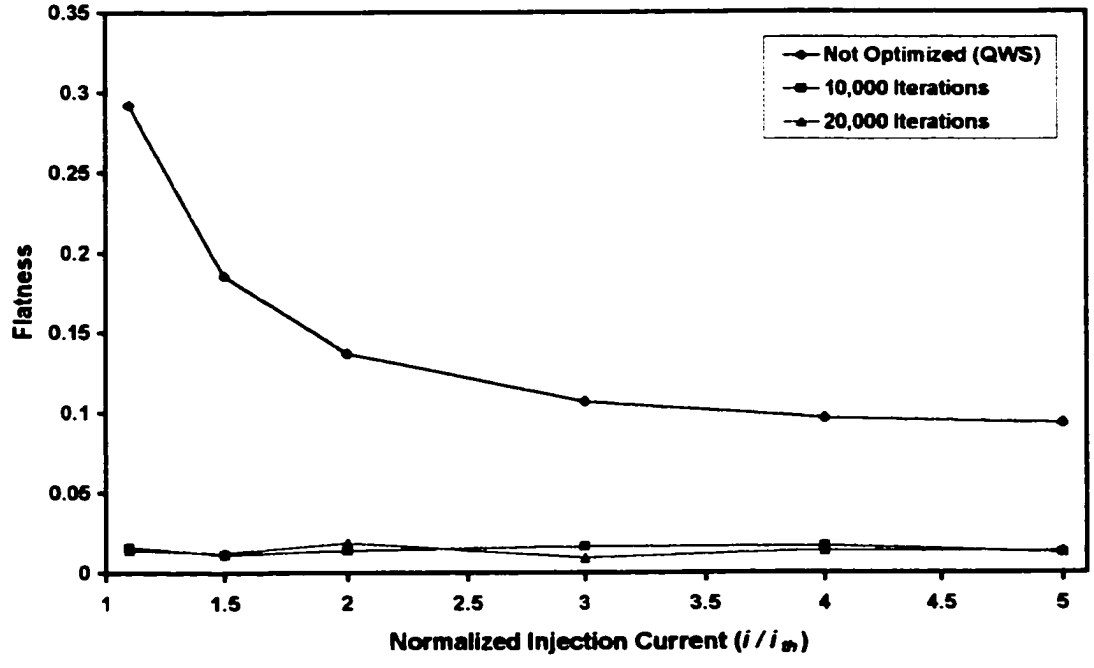

Figure 4.8 Field Intensity Flatness (*KL* Optimization)

Both the 10,000 and 20,000 iteration runs indicated a significant reduction in field flatness over the un-optimized structure, with the greatest improvement at the lower injection currents. This was expected as the relative normalized field intensity profile of a QWS structure with a constant *KL* tends to flatten at higher injection currents. There was an average of a 90% improvement in flatness across the range of injection currents evaluated. Little difference was seen between the 10,000 and 20,000 iteration flatness results indicating a near optimum solution.

The coupling coefficient optimized solution values obtained are presented in table 4.2a and table 4.2b. Examination of these results revealed interesting differences between the corresponding 10,000 and 20,000 iteration *KL* values. In some cases there were significant differences yet the intensity profile solutions as well as the corresponding field intensity flatness showed only minor variations. This behavior is thought to be reflective

of more than one "almost optimal" solution. This fact may prove very useful to a designer faced with constraints imposed by a fabrication process.

Table 4.2a Optimized *KL* Parameters (10,000 iterations)

Injection Current	*KL1*	*KL2*	*KL3*	Average *KL*
1.1 x i_{th}	2.22	0.75	1.18	1.38
1.5 x i_{th}	2.12	1.00	0.84	1.32
2 x i_{th}	2.00	1.36	0.61	1.32
3 x i_{th}	1.85	1.65	0.60	1.37
4 x i_{th}	1.89	1.62	0.64	1.38
5 x i_{th}	1.96	1.47	0.55	1.33
		Overall	Average =	1.35

Table 4.2b Optimized *KL* Parameters (20,000 iterations)

Injection Current	*KL1*	*KL2*	*KL3*	Average *KL*
1.1 x i_{th}	2.11	1.12	0.74	1.32
1.5 x i_{th}	2.21	0.91	0.88	1.33
2 x i_{th}	1.97	1.37	0.85	1.40
3 x i_{th}	2.21	1.30	0.11	1.21
4 x i_{th}	1.93	1.56	0.56	1.35
5 x i_{th}	2.01	1.27	0.85	1.38
		Overall	Average =	1.33

Figure 4.9 shows that the for both iteration counts, the average *KL* over the range of injection currents for the optimized structure remained constant at approximately KL_{avg} = 1.34, which is reduced from *KL* = 2 corresponding to the un-optimized structure. There is little change (0.02) in the average *KL* between both iteration counts, which is interesting in light of the results presented in tables 4.2a and 4.2b. Again this behavior is thought to be representative of more than one near-optimal solution and may also be indicative of an underlying (unknown) relationship between sectional coupling coefficient values and an optimal solution.

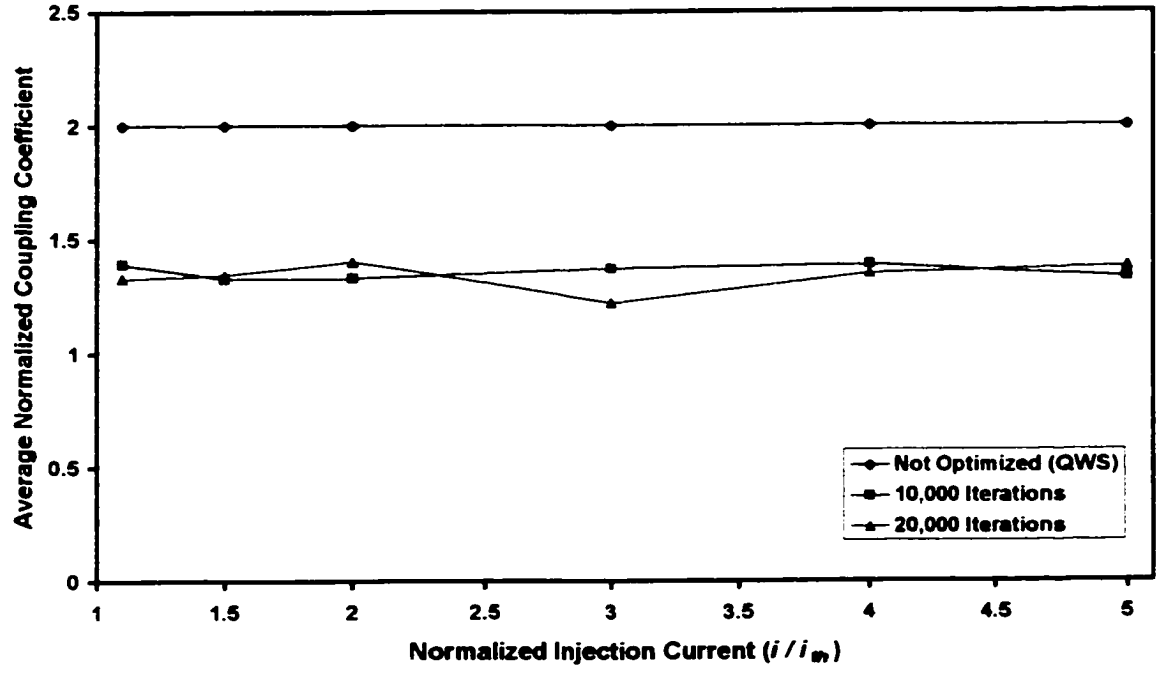

Figure 4.9 Average *KL* (*KL* Optimization)

It should be noted that KL_{avg} slightly exceeded 4/3, which is considered as a practical upper limit for overall average coupling; however, at no time did a sectional *KL* value exceed the considered practical limit of 2.5, [Yokoyama, Sekino, 1998]. Using the new methodology, which incorporates LGO, it would be a simple matter to constrain KL_{avg} to remain below 4/3.

The lasing wavelength of the optimized structure was observed to blue-shift by approximately 0.1 *nm* from the un-optimized structure's wavelength, (see figure 4.10). Again, no significant change was apparent between the 10,000 and 20,000 iteration optimization runs with the optimized structure's wavelength remaining constant over the full range of injection currents.

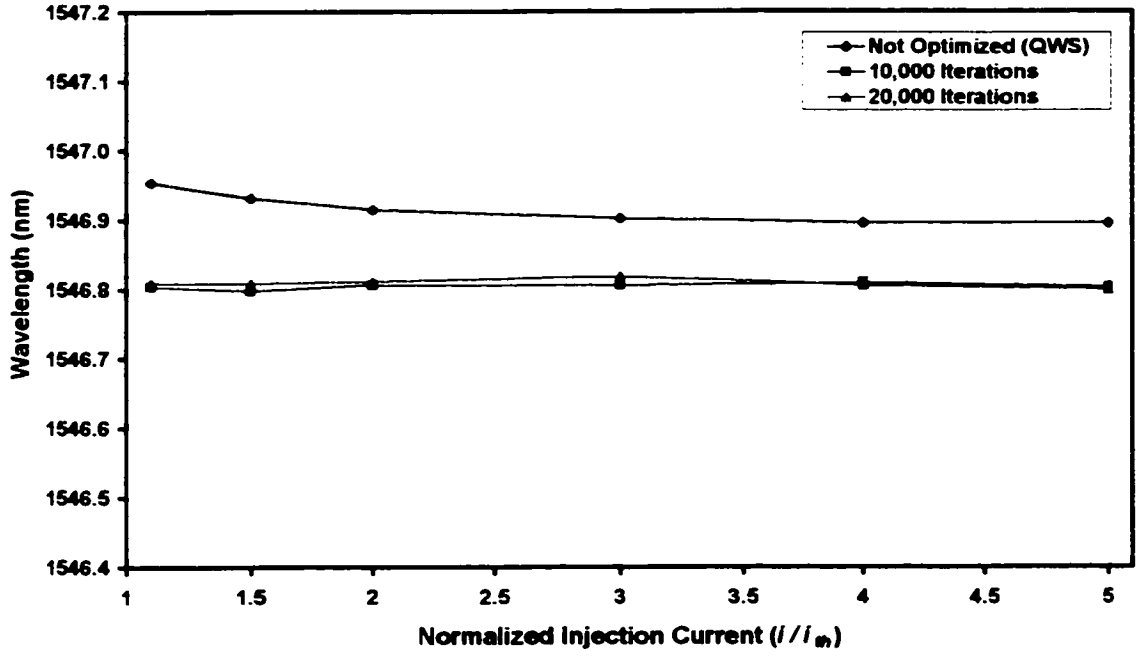

Figure 4.10 Wavelength (*KL* Optimization)

Typically, similar DCC QWS DFB laser structures with fixed coupling coefficient parameters exhibit a blue-shift in the order of 0.05 to 0.1 *nm* over the range of injection currents studied, with the greatest change being at the lower injection currents. Other than the initial wavelength blue-shift from the average wavelength of the un-optimized structure, there was no observable change with increasing injection current. One possible explanation for this behavior is that with optimization, a more uniform field flatness is obtained over the range of injection currents. The optimally flattened field has an associated optimally flattened carrier density distribution. This characteristic, through the relationship established by equation [4-7], leads to an average refractive index value that shows less of an overall change with injection current than observed for the un-optimized QWS structure. The uniformity is present even though there is an observed minor variation between both optimization runs (see figure 4.11). This in turn results in uniform wavelength versus injection current behavior. It is worthwhile noting that this behavior is in marked contrast with the average refractive index of the un-optimized structure, which exhibits a rapid decrease with increasing injection current and has the

largest change at the lower current values. Because the variation in the average refractive index with the injection current was minimal, it followed that the change in the lasing wavelength was also minimal. This behavior may prove beneficial in the reduction of the so-called chirping effect, i.e. a wavelength variation with the injection current; this is also a system limitation in high-speed optical communications networks.

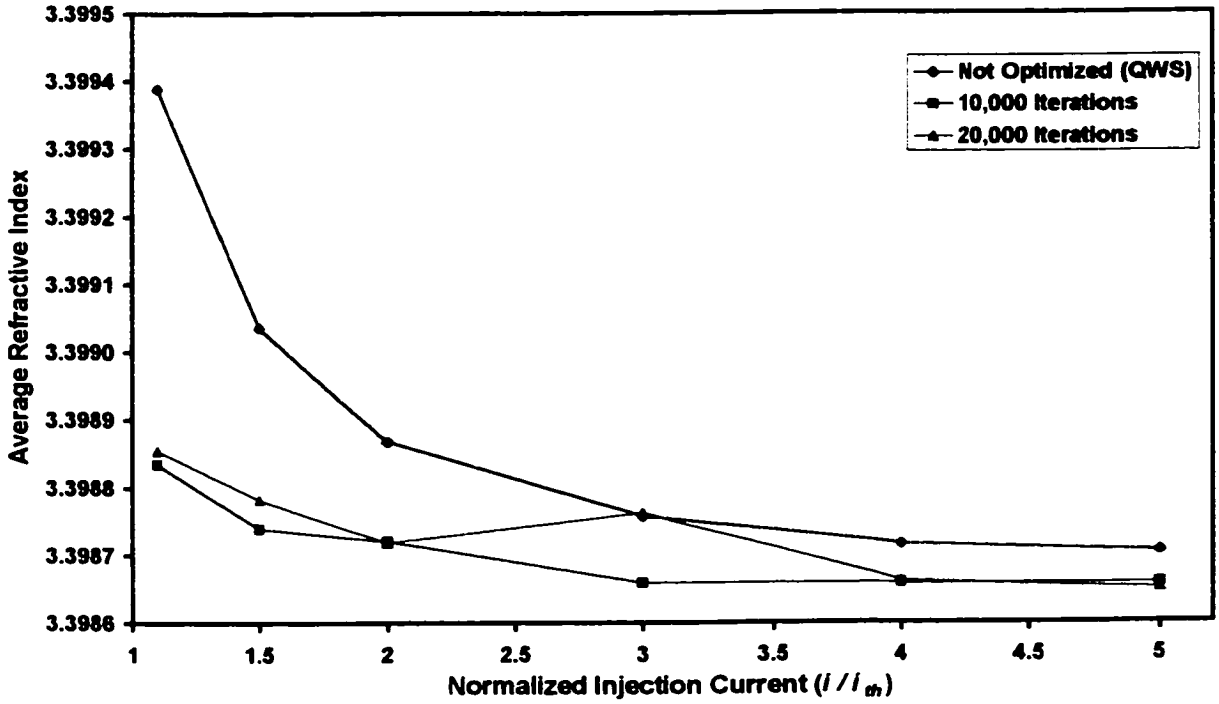

Figure 4.11 Average Refractive Index (*KL* Optimization)

The average normalized (Bragg) detuning coefficient and average normalized amplitude gain results are presented in figure 4.12 and figure 4.13. With optimization, both the detuning and the amplitude gain resulted in slightly less variation with increasing injection current over the un-optimized structure. Because the wavelength did not change appreciably with the increasing injection current, changes in detuning were also minimal over the range of injection currents.

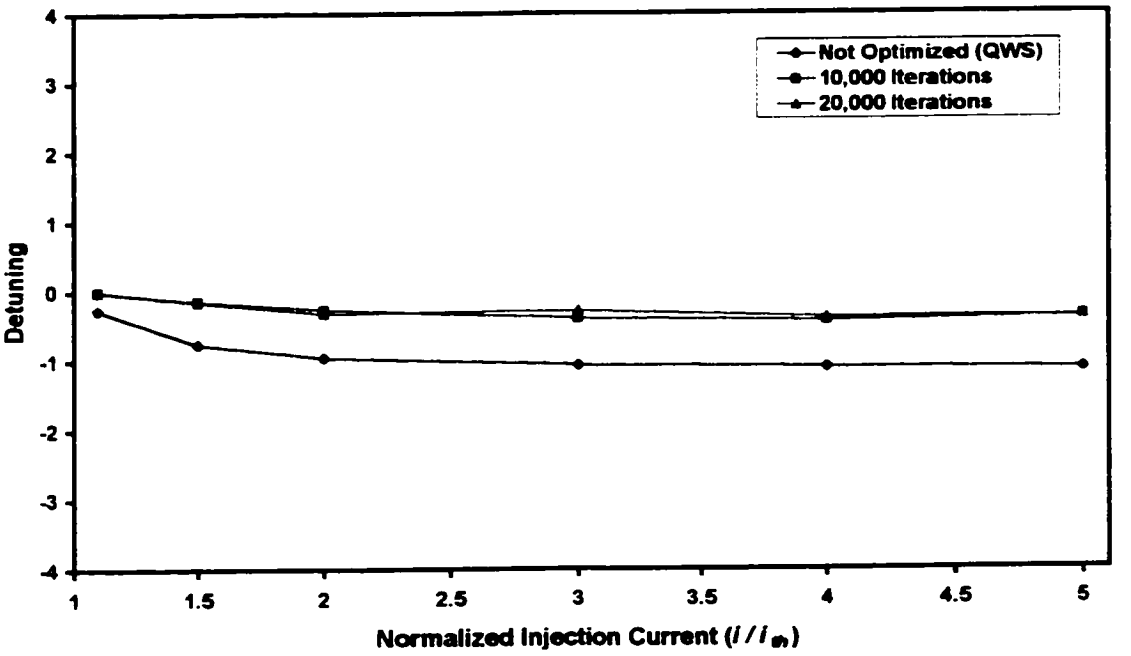

Figure 4.12 Average Normalized Detuning (*KL* Optimization)

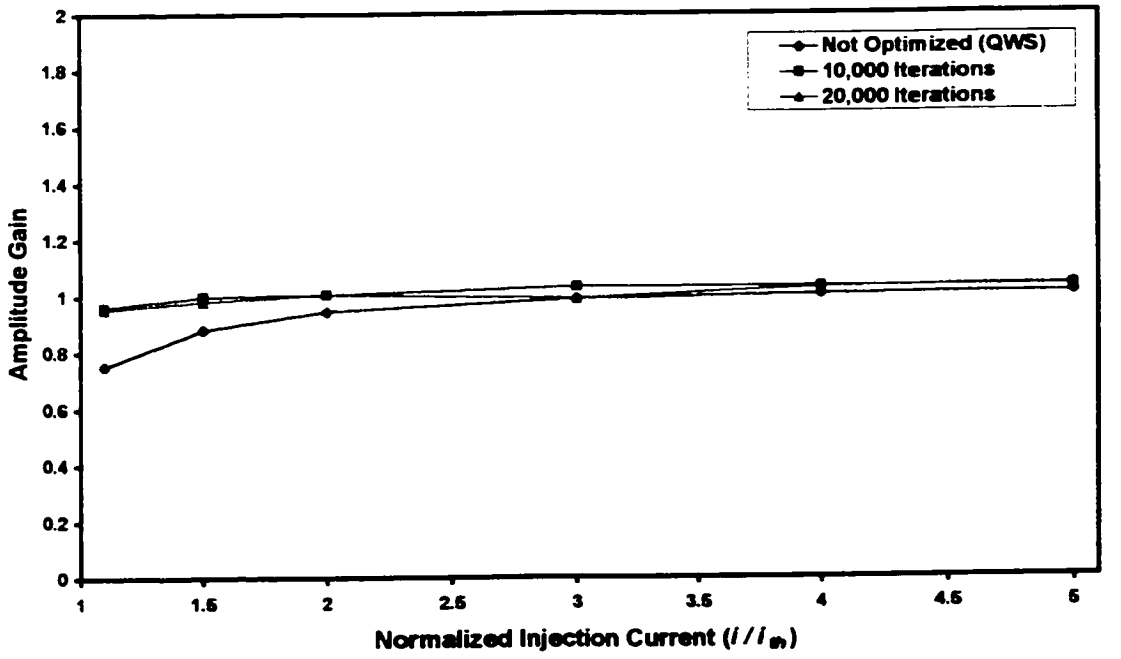

Figure 4.13 Average Normalized Amplitude Gain (*KL* Optimization)

The highly non-linear nature of the objective function associated with the DCC QWS DFB laser is clearly revealed for the first time by figure 4.14 (Appendix B figure B1).

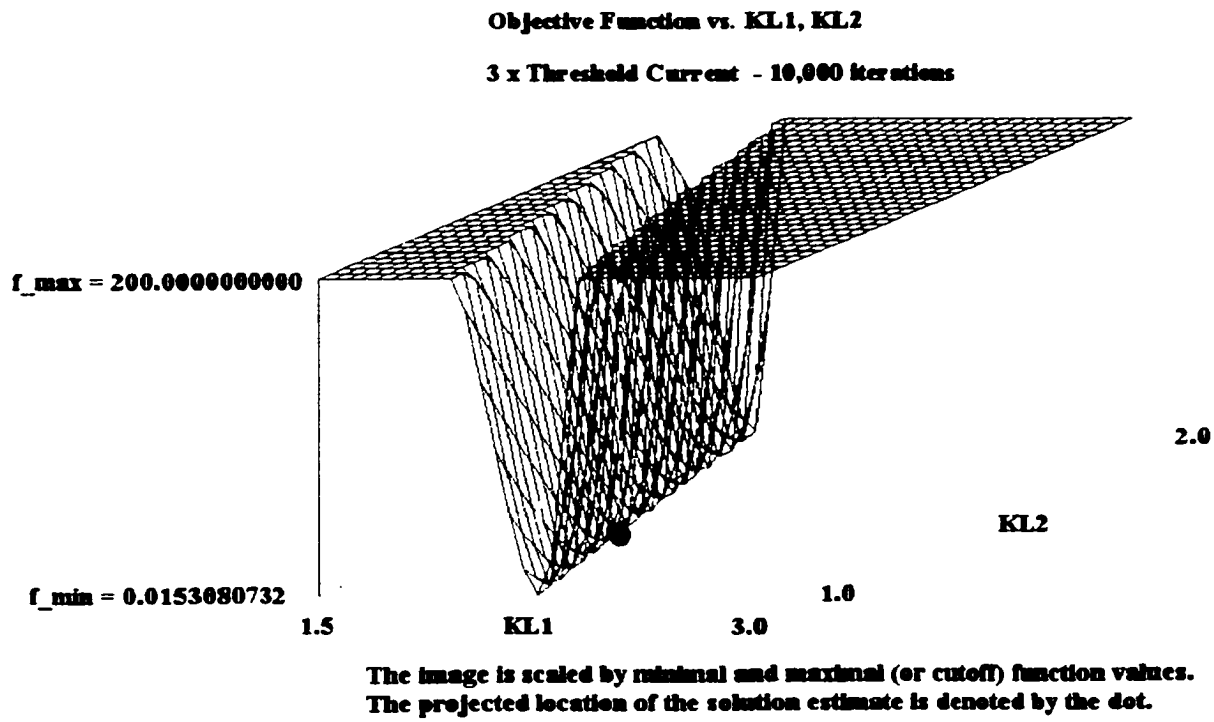

Figure 4.14 Objective Function versus *KL1*, *KL2* (*KL* Optimization at 3 x i_{th})

Please refer to Appendix B, figures B1 to B8 for the complete set of objective function visualizations. These figures are optimal solution sub-space projections for several of the laser's independent solution parameters. In figure B7 and figure B8 the objective function cut-off value was reduced from 200 to 20, thus revealing some of the non-linearities' finer details. The "blue dot" indicates the position of the optimal solution estimate.

It appears from figure B1, (figure 4.14), and figure B2 that the objective function was highly sensitive to the behavior of *KL1*, and less influenced by *KL2* and *KL3*. Note that the *KL1* (and *KL6*) sections were at the extreme ends of the laser, and included the end facet boundaries. Although the exact mechanism is unclear, one possible explanation for the sensitivity may be related to the fact that the field profiles must accurately satisfy the facet boundary conditions associated with these sections. This behavior was also

observed in figure B4 to figure B6 and indicated the same objective function sensitivities when coupling coefficients and the lasing wavelength were considered. Figures B1 to B8 (generated interactively by LGO) visually demonstrated the numerical difficulty of the laser model parameterization issue explored in this work.

4.2.2 Phase Optimization

Using a fixed *KL* profile of two for all coupling coefficient sectional values, phase shift planes with initial nominal values of 36 degrees were introduced between the six coupling coefficient sections resulting in a total starting phase shift of 180 degrees. Although in this study no attempt was made to design for single longitudinal mode (SLM) operation by maximizing the threshold gain difference, threshold studies performed by [Ghafouri-Shiraz and Lo, 1996] indicated that a total phase shift of 180 degrees over three phase shift sections (60 degrees per phase shift) appeared to offer the largest threshold gain difference relative to other values of total phase shift. Based on this fact it was reasoned that the total phase shift of 180 degrees over five sections (36 degrees per phase shift) might also result in an adequate threshold gain difference, and as such provide reasonable nominal values for the optimization process. In reality this assumption turned out not to be valid (section 4.3); however, by using the new methodology, drastic field flatness optimizations were still achieved from this initial nominal phase shift profile.

Figure 4.15 reveals the same general field flatness optimization behavior as observed in the case of coupling coefficient only optimization. (Again, similar results were produced with the 20,000 iteration runs.) Careful examination of the obtained profiles indicated slightly more variability in the profile shape with the various levels of the injection current evaluated.

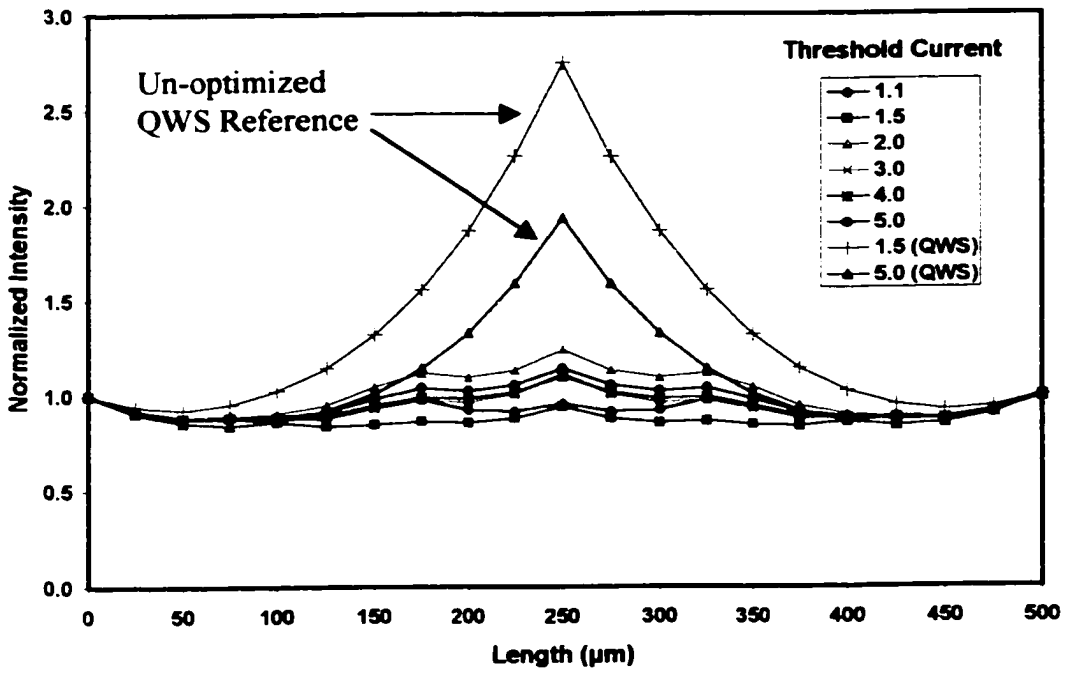

Figure 4.15 Phase Optimization versus Un-optimized QWS Structure: Normalized Longitudinal Field Intensities (10,000 Iterations)

The normalized intensity, the carrier density, the refractive index, and photon density profiles for phase optimization are presented in Appendices C1 to C4 for an injection current value of 3 x i_{th}. As with the case of coupling coefficient optimization only, similar characteristics were observed for all the remaining injection currents evaluated.

A marked reduction in the peak field intensity at the midpoint of the laser was again observed, as well as a slight improvement from 10,000 to 20,000 iterations. In a similar fashion as the coupling coefficient optimization, this reduction was reflected in a corresponding decrease in the depletion of carriers at the laser midpoint; LSHB was thus reduced significantly from the un-optimized structure. A decrease in the photon density at the midpoint followed from the decrease in the field intensity, and the refractive index also decreased as a result of the increase in the carrier density.

Figure C5 indicates that the reductions in field flatness achieved with phase only optimization were equivalent to the coupling coefficient results of the previous section, with little variation again seen between the 10,000 and 20,000 iteration runs.

Significant differences in corresponding phase shift values *PS1*, *PS2*, and *PS3* were observed between the 10,000 and 20,000 iteration runs (table 4.3a, and 4.3b), yet the overall average optimized phase shift showed little change (< 3 %). The previous results revealed that the overall average optimized coupling coefficient exhibited an analogous behavior.

Table 4.3a Optimized *PS* Parameters (10,000 iterations)

Injection Current	*PS1* (deg.)	*PS2* (deg.)	*PS3* (deg.)	Average *PS* (deg.)
1.1 x i_{th}	37.61	34.93	19.12	32.84
1.5 x i_{th}	39.36	16.57	25.33	27.44
2 x i_{th}	22.26	37.64	36.36	31.23
3 x i_{th}	35.05	28.83	39.62	33.48
4 x i_{th}	26.67	24.19	30.80	26.50
5 x i_{th}	21.37	29.19	31.05	26.43
		Overall	Average =	29.65

Table 4.3b Optimized *PS* Parameters (20,000 iterations)

Injection Current	*PS1* (deg.)	*PS2* (deg.)	*PS3* (deg.)	Average *PS* (deg.)
1.1 x i_{th}	41.68	44.18	33.12	40.97
1.5 x i_{th}	19.37	29.17	36.44	26.70
2 x i_{th}	35.66	25.96	17.91	28.23
3 x i_{th}	19.65	31.95	27.72	26.18
4 x i_{th}	17.66	40.55	22.43	27.77
5 x i_{th}	20.22	29.12	30.13	25.76
		Overall	Average =	29.27

This is interesting in light of the fact that the average phase shift values versus the injection current (table 4.3a and 4.3b) in some cases showed ten times the percentage variability between the 10,000 and the 20,000 iteration runs than did the reasonably constant, average *KL* percentage variability between the 10,000 and the 20,000 iteration

runs of the previous case, indicated in table 4.2 and figure 4.9. These results coupled with the negligible difference in field flatness observed in figure C5 are thought to lend further strength to the argument for the existence of multiple near-optimal solutions.

Phase shift only optimization produced an initial approximate 0.2 *nm* blue-shift in the lasing wavelength relative to the lasing wavelength of the un-optimized QWS DFB structure, in comparison to the 0.1 *nm* shift observed with coupling coefficient optimization. This behavior is illustrated in figure C6. The observed wavelength shift occurred at the lowest value of the injection current evaluated, 1.1 x i_{th}, but as the current increased, the lasing wavelength tended on average to gradually red-shift such that by 5 x i_{th}, the difference between the un-optimized QWS DFB's lasing wavelength and the lasing wavelength of the phase-shift optimized DFB was on the order of 0.05 *nm*. This trend plus the noticeable wavelength variability were thought to be related to a stronger manifestation of multiple near-optimal solution effects, first observed in the case of *KL* only optimization.

This increased wavelength variability, as expected, was reflected in the average refractive index, the average detuning, and the average amplitude gain behaviors of the optimized laser, and may be observed in the figures C7, C8, and C9, respectively.

4.2.3 Combined Coupling Coefficient and Phase Optimization

The results obtained from the combined coupling coefficient and phase optimization are presented in this section. Starting with the nominal initial values for the sectional coupling coefficient and the phase used in the previous two sections, 10,000 and 20,000 iteration numerical studies were performed. Both previous optimizations considered a problem with five degrees of freedom (optimization variables); however, with the combination of the coupling coefficient and the phase, the problem expanded to eight degrees of freedom.

The normalized intensity profiles for the various injection currents studied are presented in figure 4.16. The complete set of longitudinal profiles obtained for the 3 x i_{th} injection current level are presented in Appendix D, figures D1 to D4.

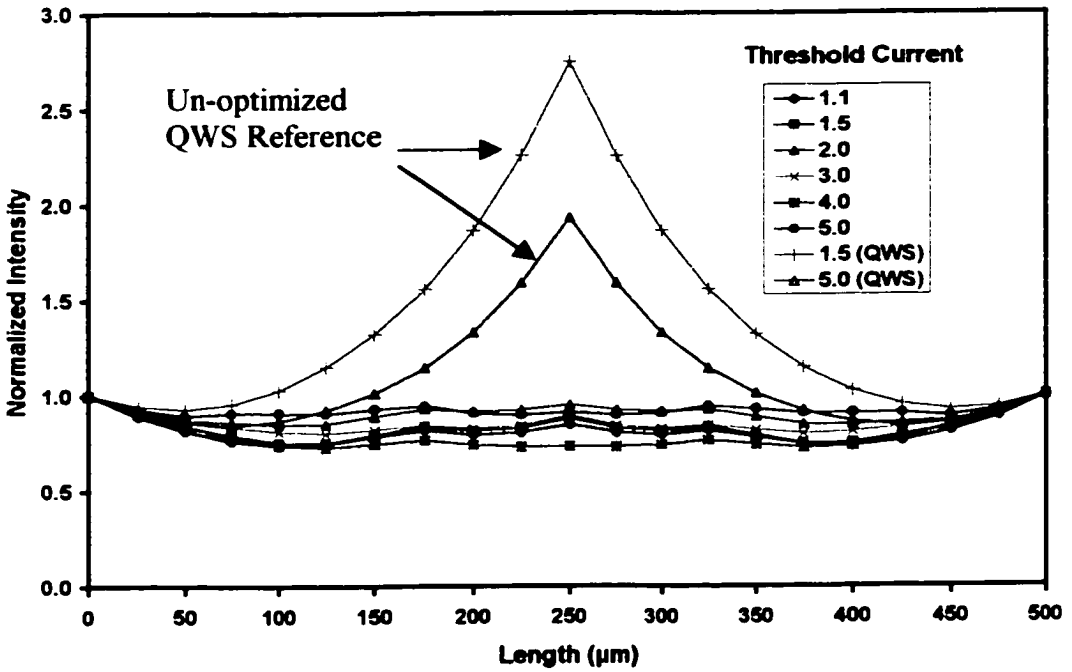

Figure 4.16 Coupling Coefficient Plus Phase Optimization versus Un-optimized QWS Structure: Normalized Longitudinal Field Intensities (10,000 Iterations)

These intensity profile results are comparable to the results obtained for both previous cases. Figure D5 indicated that the reductions in the field non-uniformity were of a similar magnitude across the spectrum of injection currents evaluated. The representative 3 x i_{th} longitudinal profiles also showed little deviation from the previous results, other than that slightly smaller solution variability was observed between the 10,000 and 20,000 iteration runs when compared to the variability observed for the case of the phase optimization only.

Optimized sectional coupling coefficient and phase solution values are presented in table 4.4a and 4.4b. Again, a significant variability between the 10,000 and 20,000 iteration results was evident for both individual and average *KL* and *PS* values for given injection

currents, yet as with the previous two cases, the overall average values of *KL* and *PS* differed by less than 3%.

Table 4.4a Optimized Combined *KL* and *PS* Parameters (10,000 iterations)

Injection Current	*KL1*	*KL2*	*KL3*	Average *KL*
1.1 x i_{th}	1.34	1.79	1.70	1.61
1.5 x i_{th}	1.44	2.31	1.81	1.86
2 x i_{th}	1.84	1.56	0.75	1.38
3 x i_{th}	1.67	1.59	1.54	1.60
4 x i_{th}	1.18	1.56	0.38	1.04
5 x i_{th}	2.10	1.08	0.87	1.35
		Overall	Average =	1.47

Injection Current	*PS1* (deg.)	*PS2* (deg.)	*PS3* (deg.)	Average *PS* (deg.)
1.1 x i_{th}	21.49	34.95	24.26	27.42
1.5 x i_{th}	36.92	29.63	27.27	32.07
2 x i_{th}	31.13	27.51	32.10	29.88
3 x i_{th}	32.12	27.65	29.79	29.87
4 x i_{th}	13.26	19.48	18.45	16.79
5 x i_{th}	29.71	39.44	17.16	31.09
		Overall	Average =	27.85

Table 4.4b Optimized Combined *KL* and *PS* Parameters (20,000 iterations)

Injection Current	*KL1*	*KL2*	*KL3*	Average *KL*
1.1 x i_{th}	1.18	1.81	1.10	1.36
1.5 x i_{th}	1.62	0.97	1.52	1.37
2 x i_{th}	2.05	1.26	2.06	1.79
3 x i_{th}	1.50	2.01	1.14	1.55
4 x i_{th}	1.06	2.21	1.28	1.52
5 x i_{th}	1.83	1.06	1.12	1.34
		Overall	Average =	1.49

Table 4.4b (continued)

Injection Current	*PS1* (deg.)	*PS2* (deg.)	*PS3* (deg.)	Average *PS* (deg.)
1.1 x i_{th}	14.52	28.14	33.81	23.83
1.5 x i_{th}	14.03	30.37	23.62	22.49
2 x i_{th}	33.33	35.84	35.84	34.54
3 x i_{th}	31.44	31.44	30.40	28.52
4 x i_{th}	20.94	29.21	32.89	26.64
5 x i_{th}	27.90	19.86	39.43	26.99
		Overall	Average =	27.17

Following an initial blue-shift of approximately 0.25 *nm* from the 1.1 x i_{th} injection current un-optimized QWS DFB results, combined coupling coefficient and phase optimization produced a flat wavelength response with an increasing injection current. A negligible variability was also observed between the 10,000 and 20,000 iteration runs. This behavior is presented in figure D6.

Interestingly enough, the average refractive index, the average detuning, and the average amplitude gain behaviors of the combined coupling coefficient and phase optimized laser, showed a significant variability over the full spectrum of the injection current studied, with little difference indicated between the 10,000 and 20,000 iteration runs. These results are illustrated in figures D7, D8, and D9 respectively; however, in contrast to the previous case of phase only optimization, this variability was not reflected in the wavelength behavior. Typically the suppression of spatial hole-burning by field intensity optimization is anticipated to produce a refractive index that does not change significantly over the considered range of injection currents. This in turn should result in an almost constant wavelength over the same range of injection currents. If one assumes the opposite must also be true, it is surprising in this case that the wavelength apparently did not reflect the observed refractive index variability suggesting some other unknown relationship was at work influencing the wavelength behavior.

4.3 Summary of Optimization Effects

Utilizing the previously described above-threshold TMM and global optimization methodologies, maximally flattened above-threshold field intensity profiles were obtained with sectional coupling coefficient and/or phase shift optimization for normalized injection currents that ranged from 1.1 x i_{th} to 5 x i_{th}. In the case of coupling coefficient only optimization, a $\pi/2$ phase shift was maintained at the laser's midpoint ensuring that the fully optimized laser still remained a QWS structure. In the case of phase or combined coupling coefficient and phase optimization, a phase shift of $\pi/5$ between each coupling coefficient section was employed as the initial distribution. In all cases, a normalized sectional coupling coefficient value of two was used for each laser section as the starting coupling coefficient profile distribution (*KL1*, *KL2*, and *KL3* = 2).

At the lowest injection current evaluated, 1.1 x i_{th}, the lasing frequency in all three cases considered exhibited an initial blue-shift from the lasing frequency of the reference QWS DFB laser. The coupling coefficient only optimization produced a lasing wavelength blue-shift of ~ 0.1 *nm* and the coupling coefficient plus phase shift optimization resulted in an initial blue-shift of ~ 0.2 *nm* when compared with the reference QWS DFB laser's wavelength. In both cases the shifted wavelength remained (basically) unchanged over the full range of injection currents. The phase shift only optimization also produced an initial blue-shift of ~ 0.2 *nm*, but in this case an average gradual red-shift of ~ 0.1 *nm* back towards the QWS DFB laser's wavelength was seen over the range of injection currents. In addition to this the phase shift only optimization produced a higher degree of variability in the blue-shifted wavelength over the range of injection currents than did either the coupling coefficient only or the coupling coefficient plus phase optimizations. The reason for these differences is presently unknown.

A negligible variation in field flatness was observed across the range of injection currents as well as combinations of coupling coefficient and phase shift parameters employed indicating no practical restrictions over the range studied. In all cases it was possible to obtain a maximally flattened field.

Results from optimizations carried out using the coupling coefficient and/or phase shift variables show strong evidence for the existence of multiple near-optimal solutions. This is reflected in the differences in specific and average optimization parameter (*KL* and *PS*) values between the 10,000 and 20,000 iteration runs for any given injection current. More importantly, the average of these (average) values over the range of injection currents, i.e. the overall average, shows almost no variation between the two iteration runs. This is suggestive of the anticipated result: that the value of the injection current makes very little difference in the outcome of the optimization process. In other words if the laser is optimized for an injection current of 1.1 x i_{th} such that a maximally flattened field profile is obtained, then holding the resulting *KL* and/or *PS* parameters fixed, it should be possible to find an equivalent optimally flattened field intensity solution at all other injection current values over the range studied. This assertion is further explored in section 5.1, along with the threshold injection current and the single mode stability behavior as a function of the optimization process.

5. FURTHER ANALYSIS OF OPTIMIZED PROFILES

5.3 Optimized Profile Flatness Behavior

In the preceding section, the effectiveness of using the transfer matrix method combined with global optimization in reducing a DFB laser's internal field non-uniformity was clearly demonstrated. Maximally flattened field profiles were obtained for all values of injection currents investigated, using variable coupling coefficient and/or phase shift parameters. The results indicated that it was possible to optimize a DFB laser at any of the given above-threshold injection currents. The optimization process would in turn produce a set of KL and PS values that corresponded to a near-optimally flattened field. Marked variability of the solution parameters between the 10,000 and 20,000 iteration runs over the range of injection currents contrasted sharply with an equally marked insensitivity in the behavior of the optimized value of field flatness. This behavior was thought to be indicative of the presence of multiple near-optimal solutions across the spectrum of the injection currents evaluated, and also raised the question as to whether or not there actually was a particular advantage to optimize the laser's KL and/or PS parameters for each specific injection current. In other words, if one seeks to operate a laser at 3 x i_{th} with a maximally flattened field profile, is it necessary to perform the optimization at 3 x i_{th} or, as anticipated, would a near-threshold optimization suffice? Stated another way, would an optimization performed at a given injection current still result in optimally flattened fields if the same KL and PS solution parameters were now used in obtaining the laser's field solutions at all the other given injection currents. (In the second case, only the λ and C_o parameters would be permitted to vary in order to obtain the necessary boundary condition match at the right-hand facet.). With the results of the previous section this question could now be explored in more detail.

In order to further investigate these issues, an additional series of numerical studies were performed where field solutions at all the given threshold currents were obtained using (fixed) optimized solution parameters resulting from optimizations performed at 1.1 x i_{th} and 3 x i_{th}. In this study both coupling coefficient and phase shift optimizations were investigated. (Based on the results obtained it was reasonable to assume that the

combined coupling coefficient and phase shift optimization solution parameters would have produced similar behavior; therefore, to avoid redundancy, this combination was not included.)

Using data from 10,000 iteration runs, the normalized field flatness versus injection current results are presented in figure 5.1, where field flatness behaviors resulting from the fixed solution parameters obtained through optimizations performed at 1.1 x i_{th} and 3 x i_{th} were compared to the field flatness results from coupling coefficient and phase optimizations performed at each of the given threshold currents.

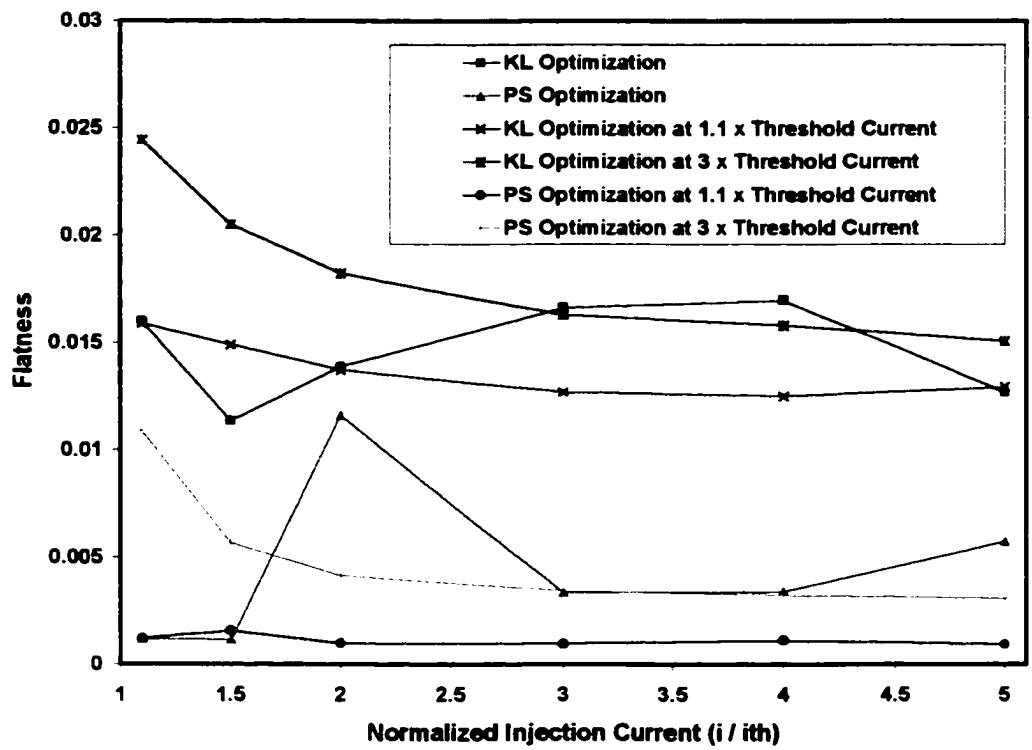

Figure 5.1 Field Flatness – Fixed Solution Profiles (1.1 x i_{th} and 3 x i_{th})

In the legend of figure 5.1, the terms "KL Optimization" and "PS Optimization" refer to coupling coefficient (*KL*) optimizations or phase shift (*PS*) optimizations, respectively, that were performed at each value of the injection current resulting in different sets of *KL* and *PS* solution parameters, which of course are the Section 4.2.1 and 4.2.2 results. (Also

see figures 4.8 and C5.) The next term in the legend, "KL Optimization at 1.1 x Threshold Current", corresponds to the case where the structural coupling coefficient profile was obtained through an optimization carried out at 1.1 x i_{th}. This profile was held fixed, and above-threshold field solutions were obtained for all the other values of injection currents. The field flatness parameters corresponding to these field solutions are presented in the figure. The remaining three terms in the legend are to be similarly interpreted.

As a matter of observation, intersections between the fully-optimized QWS DFB laser flatness results and the corresponding fixed (optimized at 1.1 x i_{th} and 3 x i_{th}) *KL* and *PS* parameter results were seen to occur at 1.1 x i_{th} and 3 x i_{th}. This was anticipated and it confirmed that the solution procedure was consistent. The most significant result revealed in figure 5.1 is that all flatness values across the range of injection currents are of the same magnitude, remaining better than 90% reduced relative to the flatness behavior of the un-optimized QWS DFB laser. (In order to maintain a reasonable scale, the un-optimized QWS DFB laser's flatness results were omitted from figure 5.1).

These results provide reasonable evidence that an optimization carried out at or near-threshold, or for that matter at any other fixed injection current in the given range, is sufficient and will produce a (near) optimally flattened field intensity over the full range of injection currents. In light of this fact there appears to be no particular advantage to performing multiple above-threshold optimizations if achieving a maximally flattened field is the sole aim. Again, this was an anticipated result that both confirmed both the validity and consistency of the new methodology, and of performing the (computationally simpler) threshold optimizations.

It is also interesting to note that the field flatness values resulting from optimizations conducted using the fixed *KL* and *PS* structural parameters, showed less variability over the range of injection currents than the field flatness values obtained by optimizing at each injection current. This was attributed to the fact that the numerical process now

consisted of only two degrees of freedom, λ and C_o, whose values were iteratively determined such that the right-hand facet field boundary condition was optimally matched. One possible explanation for this behavior is that by reducing the number of degrees of freedom to just two, the hypothesized multiple near-optimal solution effect was also reduced (or eliminated).

In addition to the reduction in variability it was also observed that the field flatness behavior resulting from the fixed *KL* or *PS* field solutions showed in general a decrease in flatness value over the range of injection currents, with the greatest decrease at the low injection current. This is easily explained by the fact that the resulting field profiles are only optimally flattened at the injection current for which the original optimization was carried out. At any other value the field is slightly non-optimally flattened and will exhibit the same type of flatness versus injection current behavior as a non-optimized QWS DFB laser except to a much lesser extent.

Finally, the field flatness values over the range of injection currents evaluated, were observed to be smaller if the 1.1 x i_{th} optimized values for *KL* or *PS* were used to produce the field solutions across this range, instead of the 3 x i_{th} optimized values for *KL* or *PS*. This suggests that there may actually be a slight overall advantage to performing the field flattening optimization at or near the threshold injection current.

Other than the primary result, which indicates that optimization at any injection current will produce a near-optimally flattened field at all other injection currents, the remainder of the above results produced effects that are thought to be too small to be of much immediate practical significance. However, the effects were consistent with expected behavior and as such they further support the validity and consistency of the optimization methodology used.

5.2 Optimized Profile Wavelength Behavior

Using data from 10,000 iteration runs, the lasing wavelength versus injection current results are presented in figure 5.2, where wavelength behaviors resulting from the fixed solution (*KL* or *PS*) parameters obtained through optimizations performed at 1.1 x i_{th} and 3 x i_{th} are compared to the wavelength results from coupling coefficient (*KL*) and phase (*PS*) optimizations performed at each given injection current.

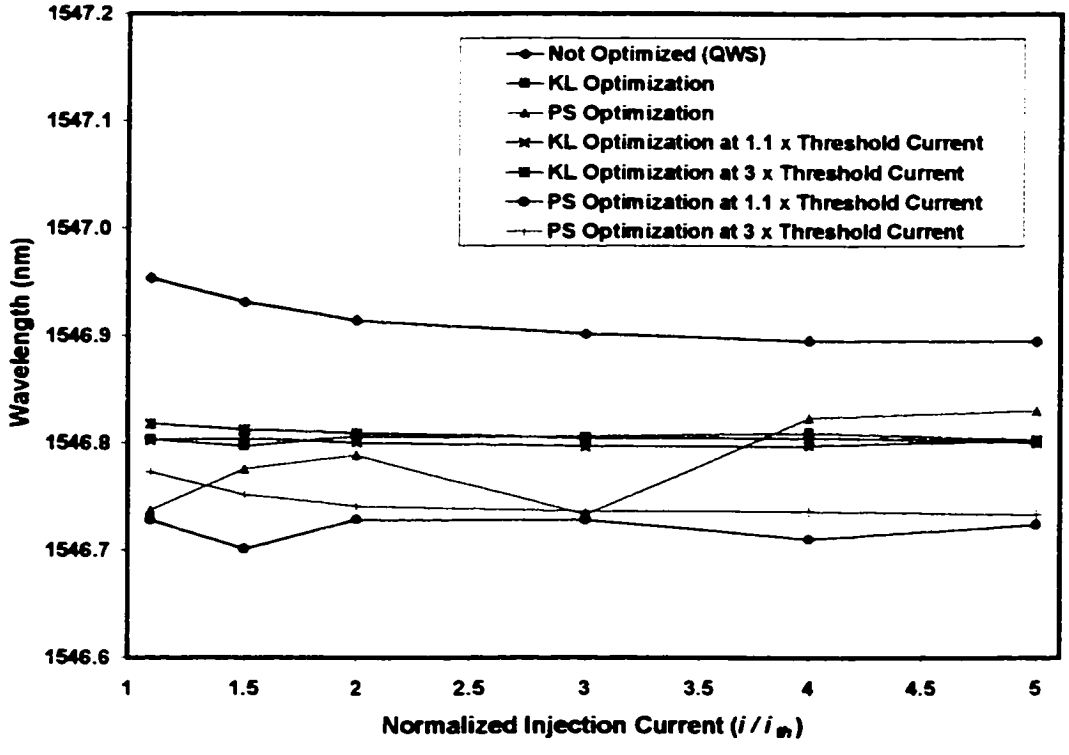

Figure 5.2 Lasing Wavelength – Fixed Solution Profiles (1.1 x i_{th} and 3 x i_{th})

Consistent with the results presented in figure 5.1, and as expected, intersections between the fully optimized QWS DFB laser wavelength results and the corresponding fixed (optimized at 1.1 x i_{th} and 3 x i_{th}) *KL* and *PS* parameter results were again seen to occur at 1.1 x i_{th} and 3 x i_{th}. It was also observed that wavelength values resulting from the field solutions derived from the fixed (optimized) *KL* and *PS* structural parameters showed less variability over the range of injection currents evaluated than the cases of *KL* or *PS* optimizations performed at every injection current. As with the previous section the

reason for this was attributed to the reduction in the number of degrees of freedom and consequently the reduction of the effects from the hypothetical multiple near-optimal solutions.

Two interesting observations resulted from the data presented in figure 5.2. The first significant behavior was that by using the 1.1 x i_{th} or 3 x i_{th} optimized *KL* structural parameters, a noticeable improvement in the overall wavelength change with injection current (wavelength chirp) was achieved relative to the wavelength chirp of the reference un-optimized QWS DFB laser. Although there was evidence of improvement in the wavelength chirp when using the 1.1 x i_{th} optimized *PS* structural parameters, some wavelength variability was seen over the range of injection currents used. The reason for this variability is not known. Wavelength chirp improvement also occurred at the injection current of 3 x i_{th} for the optimized *PS* structural parameters, but to a much smaller extent. Therefore, in all cases, using either the *KL* or the *PS* structural parameters associated with the field flattening optimizations carried out at 1.1 or 3 x i_{th}, some improvement in wavelength chirp was realized. This behavior's apparent (unknown) relationship to field flatness and the structural parameters used in the field flattening optimizations, may potentially lead to a method to control and minimize the wavelength chirp in a DFB laser.

The second interesting observation made from the data presented in figure 5.2 was the presence of the overall wavelength blue-shifts of approximately 0.15 to 0.2 *nm* relative to the wavelength of the reference un-optimized QWS DFB laser. These blue-shifts occurred to varying degrees with either the *KL* or the *PS* field flattening optimizations. In all the cases except one, the shifted wavelength remained relatively constant over the full range of injection currents evaluated. The exception was the case where a *PS* optimization was carried out at each of the considered injection currents. This behavior was first observed and discussed in Section 4.2.2. Displaying this wavelength data in figure 5.2 illustrates its enhanced variability over the full range of injection currents as compared to the relatively trivial to non-existent wavelength variability associated with

the remaining optimization results. With *PS* only field flattening optimizations conducted at each threshold current, a wavelength variability of approximately 0.1 *nm* occurred over the full range of injection currents. This variability, as discussed in Section 4.2.2, was attributed to a stronger manifestation of the effects from multiple near-optimal solutions.

Although the mechanism remains unclear, the important point here is that in all cases the amount of blue-shift observed was apparently related in some unknown and complicated way to the process of field flattening optimization as well as to the appearance of multiple near-optimal solutions. This behavior may offer the potential to tune a DFB laser over a range of at least 0.2 *nm* by using an appropriately constrained optimization process, one where an optimally flattened field would not necessarily be the target objective.

5.3 Threshold Current

Figure 5.3 details the behavior of the threshold current with the various combinations of optimization parameters evaluated. It is apparent from the data that the un-optimized QWS DFB laser had the lowest overall threshold injection current, which increased depending on the type of optimization used. This was an expected result and is related to the increase in the associated number of the coupling coefficient and/or the phase shift discontinuities with the various optimizations performed. As more coupling coefficient and/or phase shift discontinuities were introduced into the structure, the threshold injection current increased. The largest overall values were associated with the combined *KL* plus *PS* optimization, where a total of ten overall transitions in the coupling coefficient and the phase were present in the optimized structure. This compared to five transitions in either the *KL* or *PS* optimized structure, or one in the case of the QWS un-optimized structure. Any discontinuity, whether associated with a change in the sectional coupling coefficient or the phase, increases spontaneous emission. This results in the

need for a larger injection current; clearly there is a tradeoff if one wishes to optimize a DFB structure.

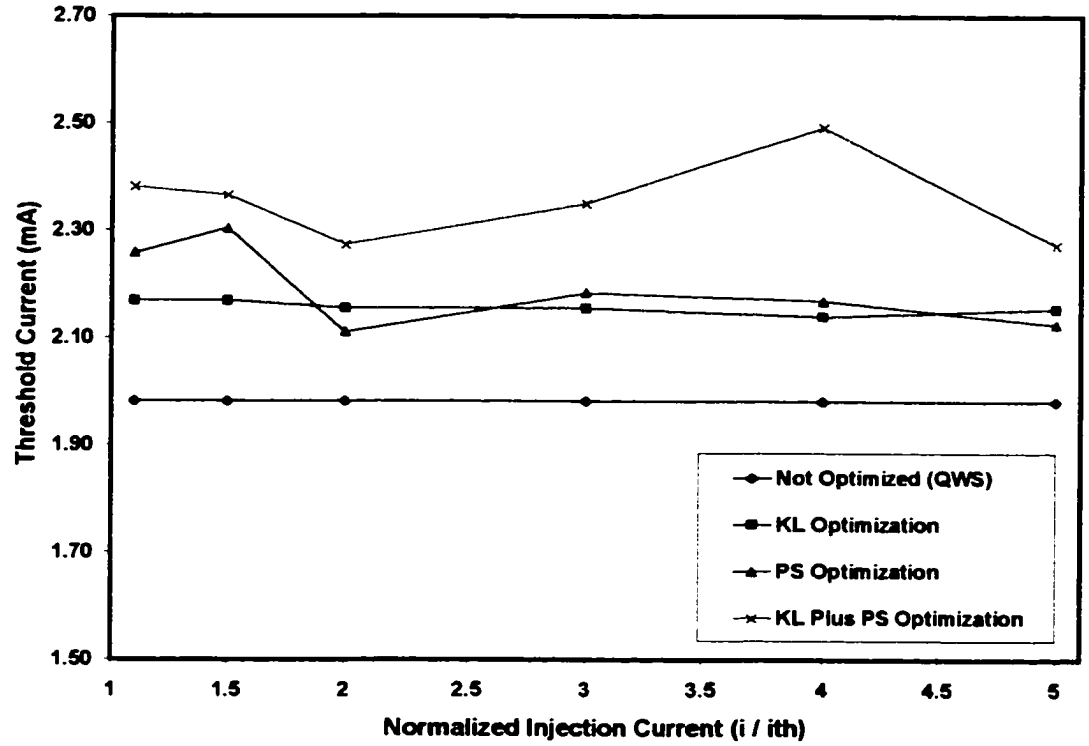

Figure 5.3 Threshold Current – Optimized Solutions

The variability observed in the threshold injection current, especially for *PS*, and *KL* plus *PS* optimization, is fully congruent with the earlier hypothesis that multiple near-optimal solutions exist.

5.4 Single Longitudinal Mode Stability

Up to this point the effect of optimization on side modes has been largely ignored. In order for a DFB laser to maintain a single longitudinal mode, i.e., a single wavelength output, it is necessary that the side modes remain non-lasing. Typically, the normalized gain margin between the lasing and the most probable non-lasing side modes should be at least 0.25 in order to guarantee single longitudinal mode (SLM) oscillation. The most

probable side modes are usually closest (but not always) to the lasing mode. As the injection current increases, the amplitude gain of the lasing mode moves from its threshold gain value, relative to the amplitude gains of the side modes, which also move accordingly. Thus, the normalized gain margins change in a complicated way with increasing injection current. If at some injection current the normalized gain margin between a side mode and the lasing mode drops below 0.25, mode competition can occur resulting in multi-modal oscillation.

[Ghafouri-Shiraz and Lo, 1996] proposed a method of evaluating the normalized gain margin by using a transfer matrix approach that introduced a complex wavelength to mathematically suppress the dominant lasing mode. The real part of the imaginary wavelength was interpreted to be the actual side mode wavelength and the imaginary part provided the additional (mathematical) gain the side mode would need to reach its threshold value. In this way the side mode's amplitude gain as well as the dominant lasing mode's amplitude gain, and hence normalized gain margins, could be found for any injection current. Although mathematically this approach provides answers, the physical interpretation of what is actually taking place is not obvious. Rather than rigorously applying this type of analysis to the resulting optimized profiles, the simplifying assumption was made that if a sufficient gain margin existed at threshold (0.25 plus 20%) then it was reasonable to assume that as the injection current increased, any reduction in gain margin would still be insufficient to initiate a multi-mode oscillation. At the very least it was assumed that the onset of multi-modal oscillation should be delayed until the higher injection currents were reached. If however, there were not sufficient gain margin at threshold, then there would be little chance of maintaining SLM oscillation as the injection current was increased.

With this in mind, the lasing and the $\pm$ 1 mode amplitude threshold gain values were determined by a threshold evaluation of equation [3-10], the results of which are presented in tables 5.1a, 5.1b, and 5.1c. Also refer to Appendix F for a listing of the Lahey Fortran 95 code used in the threshold mode calculations.

Table 5.1a Normalized Gain Margin at Threshold – *KL* Optimized Profiles

KL Optimization	Injection Current	+1 Mode Gain Margin	-1 Mode Gain Margin
	1.1	0.38	0.38
	1.5	0.38	0.38
	2	0.40	0.40
	3	0.46	0.46
	4	0.46	0.46
	5	0.42	0.42

Table 5.1b Normalized Gain Margin at Threshold – *PS* Optimized Profiles

PS Optimization	Injection Current	+1 Mode Gain Margin	-1 Mode Gain Margin
	1.1	-0.06	0.64
	1.5	-0.16	0.76
	2	0.34	0.60
	3	0.12	0.72
	4	0.12	0.72
	5	0.24	0.66

Table 5.1c Normalized Gain Margin at Threshold – *KL* plus *PS* Optimized Profiles

KL Plus *PS* Optimization	Injection Current	+1 Mode Gain Margin	-1 Mode Gain Margin
	1.1	0.22	0.74
	1.5	-0.04	1.02
	2	0.10	0.58
	3	0.06	0.68
	4	0.14	0.76
	5	0.08	0.34

It is evident from the results presented in table 5.1a that *KL* optimization alone provided the best chance of maintaining SLM oscillation in the numerical examples studied. Evaluation of the amplitude gains from the *KL* profiles resulting from optimizations carried out over the full range of injection currents resulted in normalized gain margins at least 20% greater than the required 0.25. As expected the upper and lower mode gain margin values were equivalent. This is characteristic of the behavior both at threshold and above-threshold for a QWS structure. Although optimized for the given injection currents, with *KL* optimization alone, the $\pi/2$ phase shift was still held fixed at the laser's midpoint, hence throughout the optimization process the DFB laser remained a QWS structure. It was evident that the SLM characteristics inherent to a QWS structure were apparently maintained when the structure was optimized to achieve maximum field flatness.

The converse was seen to be true for *PS*, and *KL* plus *PS* optimizations. Results presented in tables 5.1b and 5.1c showed normalized gain margin values below the 0.25 minimum threshold value for the upper modes, and indicated a high probability of multi-mode oscillation between the lasing mode and the +1 mode with the increasing injection current for all cases except with the *PS* optimization carried out at 2 x i_{th}. In this particular instance, there appeared to be a sufficient gain margin to support SLM oscillation. The reason for this behavior was not obvious. This appears to be an anomaly and may warrant future investigation.

In the cases where the sign of the gain margin was observed to be negative, the +1 mode would have been already oscillating. In these instances, the optimized structure profile resulted in the gain margin asymmetry between upper and lower modes to such a degree that the +1 mode had the lowest threshold amplitude gain value.

From these results it appeared that the advantages derived from the introduction of a quarter-wave shift at the DFB laser's midpoint were not lost under the optimization process. Although the preceding analysis was limited to a specific DFB laser, it is

reasonable to assume that if both an optimally flattened field and SLM oscillation are design requirements, then an optimization process that preserves the QWS structure would offer a reasonable chance of success.

6. DISCUSSION AND CONCLUSIONS

6.1 Results Summary

The primary objective of this work was to research and develop the underlying principles for a novel laser modeling and design methodology with optimization capabilities and the potential to address above-threshold, non-linear laser design problems. As a requirement the new methodology had to be capable of dealing with multiple degrees of freedom (model parameters) and imposed solution (physical or manufacturability) constraints. This was successfully achieved through the integration of the above-threshold transfer matrix method with LGO implemented global optimization strategies and represents a new advancement in the approach to laser modeling.

The new methodology's principles were validated by its application to the problem of reducing the longitudinal field non-uniformity of a QWS DFB laser over a given range of above-threshold injection currents. Results obtained from performing the field flattening optimizations at the various target injection currents compared favorably to the reference optimally flattened field profile results, which were derived from extrapolating near-threshold optimizations over the full range of the injection currents studied.

Relative to the field flatness of the un-optimized reference QWS DFB laser, more than 90% reduced field flatness values were consistently achieved by carrying out optimizations using various combinations of sectional coupling coefficients and/or phase shifts for normalized injection currents that ranged from 1.1 x i_{th} to 5 x i_{th}. Within the given constraints, in all cases it was possible to obtain, with only minor differences, near maximally flattened fields.

Analysis of the optimized *KL* and/or *PS* solution parameters revealed significant variations with the different values of injection currents evaluated, and between 10,000 and 20,000 iteration runs, yet the changes in field flatness were minimal. This result was not anticipated and strongly supported the possibility of the existence of multiple near-optimal solutions.

Investigating this further, selected above-threshold optimized solutions with their corresponding optimized *KL* or *PS* profiles were evaluated across the full range of injection currents. In these cases the optimized (solution) *KL* or *PS* profiles were held fixed and field solutions, now only in terms of λ and C_o, were sought at each injection current. Note that further field flattening optimizations were not being carried out at this stage. Field solutions were obtained by iteratively selecting λ and C_o such that the field boundary conditions were matched at the laser's facets. In all cases, except for minor differences, the field profiles obtained remained near-optimally flattened.

Ill-conditioning of the problem may provide some insight into this behavior. Ill-conditioning points out where one must be very precise, and also where there may be some flexibility in the selection of solution (design) parameters. Changes in the "insensitive" solution parameters have a minimal effect on the objective function and hence the field flatness value and associated field profile solution. Examination of the objective function visualization presented in figure 4.14 reveals some of the complexity of the various sensitivities. It can be seen that along a particular "direction" in the *KL1* – *KL2* "solution space", the objective function was relatively insensitive to the values of the solution parameters, while highly sensitive in other directions. Further evidence of this behavior is also seen in the remainder of the objective function visualizations presented in Appendix A. Although additional study is needed, these results further support the argument for the existence of multiple near-optimal solutions.

By using the *KL* and/or *PS* parameters obtained from optimizations performed near-threshold (1.1 x i_{th}), or above-threshold (3 x i_{th}), it was possible to produce equivalently flattened field profiles across the full range of injection currents. This was an anticipated result based on the original work of [Ghafouri-Shiraz, and Lo, (1996)]. This behavior also validated the principles of the new methodology and confirmed that a DFB laser optimized for maximum field flatness at or just above-threshold will also produce a similarly flattened field as the injection current increases and saturation affects become dominant. This is both a consequence of ill-conditioning and important from a

computational point of view in so far as it is much easier to solve the boundary value/optimization problem if the non-linear effects resulting from the carrier rate equation are minimal and can be ignored. At the threshold condition the problem is considered linear because there are essentially no stimulated photons. This allows the longitudinal refractive index to be considered as constant, i.e. not appreciably modified by the weak optical field. The requirement for multiple iterations is therefore eliminated allowing a quick and straight-forward solution of the internal optical field.

In all cases the optimization produced an initial blue-shift from the lasing wavelength of the reference un-optimized QWS DFB structure, which varied from 0.1 to 0.2 nm depending on the parameters being considered in the optimization process. Once shifted, the wavelength, again depending on the optimization parameters used, displayed differing degrees of variability over the range of injection currents evaluated. This behavior was in part attributed to the existence of multiple near-optimal solutions. These results may offer a method to precisely tune the laser's wavelength while still optimizing its physical parameters to obtain maximum field flatness under this constraint. If multiple solutions exist, as the evidence seemed to indicate, then in theory by absolutely constraining the wavelength to a specific value, it may be possible to optimize the DFB laser structure to achieve a significantly flattened field profile while at the same time solve for a specific target operating wavelength. Exploring the potential of this approach is considered a topic for possible future study.

The threshold current value, as anticipated, was found to relate to the number of degrees of freedom, i.e. to the number of model parameters used in the optimization process. The more transitions resulting from discontinuities between the sections of differing coupling coefficient values, as well as inter-sectional phase shifts, the higher the threshold current. Clearly a tradeoff was seen to exist, but an excellent degree of field flattening was produced by applying the optimization method to a DFB laser with a conservative number of sectional coupling coefficient and/or phase transitions, which varied from six to ten depending on the optimization parameters used. Based on this, by

keeping the number of sectional transitions at a minimum, it should be possible to obtain excellent field flatness design results while still maintaining the threshold current at an acceptable level.

The following statements thus summarize the main results achieved in this work. Firstly, the primary objective has been completed, i.e. a new above-threshold modeling and optimization methodology for the DFB laser has been developed and its principal functionality has been validated. Secondly, by using the new methodology to re-examine the problem of minimizing the internal field non-uniformity of a QWS DFB laser, evidence was observed indicating the possibility of the existence of multiple near-optimal field flatness solutions. The discovery of these new results, which only became evident by performing the field flattening optimizations in the above-threshold region, served to highlight one facet of the new methodology's potential.

6.2 Sensitivity Considerations

The introduction of any modeling and design methodology would not be complete without recognizing and addressing solution sensitivity concerns in at least a cursory manner. The question of how a given solution behaves within the constraints of the laser device's parameter manufacturability tolerances needs to be understood. It is not a simple matter to determine how the "optimal" solution (vector) varies relative to changes in the model parameter values. Two possible approaches follow.

The first approach, a direct sensitivity analysis, entails obtaining the optimal solution vector based on "nominal" or "average" model parameter values. Following this, the parameter value to be studied is selected and varied as per its defined probability distribution function. The optimization process is repeated while holding the remaining parameters at their original values, and a new solution vector is obtained. In this way it is possible to establish the solution vector's sensitivity to variations in any given model parameter value, in the form of an empirically derived probability distribution function

for each of the vector elements (solution variables). It is also possible to extend this approach to combinations of model parameter values.

The second approach, an indirect sensitivity analysis, involves establishing the model parameters directly from their defined probability distribution functions, i.e. a "joint instance". Multiple optimization runs based on model parameters determined in this way result in an empirically derived probability distribution function for each of the solution vector's variables that collectively are based on the model parameters' probability distribution functions.

It is possible to investigate the problem of determining real life tolerances in this manner; however, these or similar approaches are computationally intensive and need detailed study, which includes development of the appropriate probability distribution function models.

6.3 Non-linear Considerations

Any solution of a non-linear differential equation, whether obtained through analytical or numerical means, requires close scrutiny. The differential equation numerically solved in this work is considered non-linear because its solution, which consists of a pair of counter-directional, coupled, traveling waves, act by their presence, to modify in a complicated, non-linear fashion, the propagation characteristics of the medium in which they exist. Unlike a linear differential equation, even if a solution to a non-linear differential equation is achieved, it is usually very difficult, if not practically impossible, to say with certainty that it is unique. Because there is no way, in general, to obtain the exact analytic solutions of non-linear differential equations, iterative numerical methods become very important; however, solutions that are obtained in this manner may still be unstable or non-physical in nature. Therefore, it is necessary to examine any solution relative to the physical constraints of the non-linear problem and to ask the question: does the solution represent physical reality?

The above-threshold, optimally flattened field solutions obtained during this work exhibited clear physical relationships to corresponding optimally flattened field solutions similarly obtained near-threshold, where the non-linear effects were minimal. In addition to this, the above-threshold, optimally flattened field solutions displayed a gradual and predictable evolution with the increasing injection current relative to the near-threshold solutions, with no evidence of solution instability. Therefore, based on the stated observations, it was reasoned that these solutions could be considered as physically real.

6.4 Suggestions for Future Research

The optimization analysis in this work focused on an index-coupled DBF laser with bulk device characteristics. One possible direction of future research would be to extend the new methodology to multiple quantum well (MQW) devices. If the bulk model equations that deal with parameters such as the material gain and the optical confinement factor are replaced with those appropriate to an MQW structure, it should be possible to define and solve for an objective function that similarly minimizes the facet boundary condition error while incorporating a term that maximizes the field flatness. Other than these changes, the remainder of the solution methodology should remain the same.

It should also be a straightforward process to extend the new methodology to gain-coupled and partly gain-coupled devices. Gain-coupling is known to enhance the gain margin and promote single longitudinal mode (SLM) oscillation. It is possible to incorporate gain-coupling into the TMM portion of the optimization model by introducing an imaginary term to the coupling coefficient. Construction of the objective function and application of the global optimization methodology would remain exactly the same.

Up to this point the physical parameters have been allowed to vary within set limits with no thought as to the manufacturability of the optimized devices. Optimized KL and PS

parameters producing near maximally flattened fields were obtained within a set of "box" constraints. Based on the potential limitations in the ability to fabricate structures that completely reflect the (theoretical) optimized parameters, additional manufacturability constraints may have to be imposed on the optimization process. This should not pose a problem, as the LGO implemented optimization component of the new methodology is theoretically capable of handling multiple constraints that restrict the solution space to such particular criteria.

6.5 Concluding Comments

The original contribution of this work consists of the successful integration of the above-threshold transfer matrix method with LGO implemented global optimization strategies resulting in a new methodology for DFB laser modeling and design. As a first validation of its novel optimization capabilities, it provided a robust and efficient technique to address the difficult numerical challenges associated with finding optimally flattened internal field solutions for a QWS DFB laser operating in the above-threshold regime.

It should be noted that the success achieved with the new methodology was in part dependent on the capabilities of a sophisticated global optimizer, in this case LGO. With a less sophisticated optimization or solution methodology that involves the use of some form of fixed or adaptable numerical grid to select the solution values, unless the initial guess is very close to the actual globally best solution, the probability of ending up in a local minimum exists. This problem becomes even more significant with higher injection currents necessitating first obtaining a near-threshold solution and then incrementally increasing the injection current to gradually step up to the higher optical power solutions. The iterative process uses the previous solution parameters as the starting point for the next injection current increment. This process must be continued until the desired injection current is finally reached. In practice these increments are quite small, typically around 0.2 times i_{th}.

In addition, the techniques that use numerical grids to determine the globally best solution would become quickly impractical beyond a few degrees of freedom (solution variables). This results from the fact that the dimensionality of the numerical (solution) grid has to expand to match the dimensionality of the solution space. Assuming that a 5x5 numerical grid is utilized in the case of a problem with two-degrees of freedom (two-solution variables), then for n-degrees of freedom, 5^n evaluations would be necessary to determine the next location for the grid in the process of "walking" the grid around the solution space, searching for the globally best solution. Clearly a more sophisticated approach is called for.

With the integration of a genuine global optimization approach, these considerations were largely unnecessary. A proper global solver will eventually find the globally approximate correct solution. The presented solutions were obtained directly, by immediately solving the optimization problem at the desired injection current, eliminating the need for incremental solutions with gradually increasing injection current. Robust global optimization strategies as implemented by the LGO software, were used to globally search the entire solution space, and select the solution that was constrained to minimize the RBC error, and at the same time achieved maximum field flatness. This approach did not need a starting point, making it possible to directly and rapidly solve for injection currents that varied from 1.1 to 5 times the threshold injection current. LGO directly interfaced to the associated model code and rapidly converged to a global minimum. In the numerical examples presented, optimum KL, PS, λ, and C_o values were obtained for the given range of injection currents that in all cases resulted in a significant reduction in the longitudinal field non-uniformity and associated LSHB effects.

In conclusion, the presented work has revealed the general need for using a methodology that incorporates a true global optimization approach, and its potential for solving many of the highly non-linear problems associated with above-threshold laser modeling and design. The fundamental result of this work and original contribution by the author is a novel above-threshold modeling and optimization methodology that includes these

characteristics, is easily adapted and is one step towards developing a practical tool for the above-threshold design and analysis of DFB lasers. Evidence observed for the possible existence of multiple near-optimal solutions when optimizing the internal field flatness of QWS DFB lasers is the second major result of this work and also considered an original contribution by the author, revealing what is thought to be hitherto unknown behavior. Finally, based on the validation results and using LGO's ability to constrain the solution space to physically realizable parameters, it should be possible to extend the new methodology's principles and techniques beyond the optimization examples presented in this work, to address difficult issues such as designing for maximum above-threshold gain-margin, and to include advanced multiple quantum-well (MQW) and gain-coupled devices.

BIBLIOGRAPHY

Agrawal G., (1992) *Fiber-Optic Communication Systems*, John Wiley & Sons Inc., New York / Chichester / Brisbane / Toronto / Singapore.

Fang W., A. Hsu, S.L. Chuang, T. Tanbun-Ek, and A.M. Sergent, (1997) Measurement and Modeling of Distributed-Feedback Lasers with Spatial Hole Burning, IEEE Journal of Selected Topics In Quantum Electronics, Vol. 3, No. 2, pp.547-554.

Fessant T., (1997) Threshold and above-threshold analysis of corrugation-pitch-modulated DFB lasers with inhomogeneous coupling coefficient, IEE Proceedings on Optoelectronics, Vol. 144, No. 6.

Ghafouri-Shiraz H., and B. Lo, (1996) *Distributed Feedback Laser Diodes*, John Wiley & Sons Inc., Chichester / New York / Brisbane / Toronto / Singapore.

Green Jr. P., (1993) *Fiber Optic Networks*, Prentice-Hall Inc., New Jersey.

Isenor G., J.D. Pintér, M. Cada, (2001a) Design of Distributed Feedback Lasers with Drastically Reduced Intensity Profile Non-uniformity Using the Global Optimization Method, CLEO/Europe-EQEC proceedings, Munich, pp. 80.

Isenor G., J.D. Pintér, M. Cada, (2001b) *Determination of a Distributed Feedback Laser's Field Solution Using Global Optimization*, Global Optimization-Selected Case Studies, Kluwer Academic Publishers, Dordrecht / Boston / London (To Appear).

Isenor G., J.D. Pintér, M. Cada, (2001c) Globally Optimized Steady State Characteristics of a Distributed Feedback Laser: The Reduction of Non-uniformity of the Intensity Profile, Optimization and Engineering, Kluwer Academic Publishers, Dordrecht / Boston / London (To Appear).

Kawaguchi H., (1994) *Bistabilities and Nonlinearities in Laser Diodes*, Artech House, Boston / London.

Keiser G., (1993) *Optical Fiber Communications*, (2nd Edn.) McGraw-Hill, Inc., New York.

Kogelnik H., (1969) Coupled Wave Theory for Thick Hologram Gratings, The Bell System Technical Journal, Vol.48, No.9, pp. 2902-2947.

Kogelnik H., C.V. Shank, (1972) Coupled-Wave Theory of Distributed Feedback Lasers, Journal of Applied Physics, Vol. 43, No. 5, pp. 2327-2335.

Lahey Computer Systems, (2000), LF\95 *User's Guide*, Incline Village NV.

Makino T., (1991) Transfer-Matrix Formulation of Spontaneous Emission Noise of DFB Semiconductor Lasers, Journal of Lightwave Technology, Vol. 9, No. 1, pp. 84-91.

Makino T., and J. Glinski, (1988) Transfer Matrix Analysis of the Amplified Spontaneous Emission of DFB Semiconductor Laser Amplifiers, IEEE Journal of Quantum Electronics, Vol. 24, No. 8, pp. 1507-1518.

Morthier G., and R Baets, (1991) Design of Index-Coupled DFB Lasers with Reduced Longitudinal Spatial Hole Burning, Journal Of Lightwave Technology, Vol. 9, No. 10, pp. 1305-1313.

Morthier G., K. David, P. Vankwikelberge, and R. Baets, (1990) A New DFB-Laser Diode with Reduced Spatial Hole Burning, IEEE Photonics Technology Letters, Vol. 2, No. 6, pp 388-390.

Pintér J.D., (1996) *Global Optimization in Action*, Kluwer Academic Publishers, Dordrecht / Boston / London.

Pintér J.D., (2000) *Model Development, Solution, and Analysis in Global Optimization. In: Global Optimization — Selected Case Studies*, Kluwer Academic Publishers, Dordrecht / Boston / London.

Rabinovich W.S., and B.J. Feldman, (1989) Spatial Hole Burning Effects in Distributed Feedback Lasers, IEEE Journal Of Quantum Electronics, Vol. 25, No. 1, pp. 20-30.

Sargent III M., W. H. Swantner, and J. D. Thomas, (1980) Theory of a Distributed Feedback Laser, IEEE Journal of Quantum Electronics, Vol. QE-16, No. 4, pp. 465-472.

Tamir T., (1988) *Guided-Wave Optoelectronics*, Springer-Verlag, Berlin / Heidelberg.

Van Ettenon W., and J. Van der Plaats, (1991) *Fundamentals of Optical Fiber Communications*, Prentice Hall, New York / London / Toronto / Sydney / Tokyo / Singapore.

Wang J.-Y., M. Cada, and J. Sun, (1998) Theory for Optimal Design and Analysis of Distributed-Feedback Lasers, IEEE Photonics Technology Letters, Vol. 11, No. 1, pp.24-26.

Wang J.-Y., and M. Cada, (2000) Analysis and Optimum Design of Distributed Feedback Laser Using Couple-Power Theory, IEEE Journal Of Quantum Electronics, Vol. 36, No. 1, pp. 52-58.

Wang J.-Y., M Cada, and T. Makino, (1998) Coupled-Power Theory of Nonlinear Distributed –Feedback Lasers, Yielding Reduced Longitudinal Spatial Hole Burning, Applied Physics Letters, Vol. 72, No. 25, pp. 3255-3257.

Wang S., (1974) Principles of Distributed Feedback and distributed Bragg-Reflector Lasers, IEEE Journal of Quantum Electronics, Vol. QE-10, No. 4, pp. 413-427.

Yariv A., (1991) *Optical Electronics (4th Edn.)*, Saunders College Publishing, Philadelphia/ Chicago/ Fort Worth/ San Francisco/ Montreal/ Toronto/ London/ Sydney/ Tokyo.

Yariv A., (1973) Coupled-Mode Theory for Guided-Wave Optics, IEEE Journal of Quantum Electronics, Vol. QE-9, No. 9, pp. 919-933.

Yokoyama K., and N. Sekino, (1998) Numerical Optimization of DFB LD Grating Structure for Uniform Longitudinal Intensity Distribution, Computational Electronics, IWCE-6 Extended Abstracts of 1998 Sixth International Workshop, pp. 116-119.

APPENDIX A

SOLUTION METHODOLOGY

APPENDIX A

SOLUTION METHODOLOGY

The following is a step-by-step description of the integrated transfer matrix, global optimization numerical procedure used to optimize the example DFB laser's above-threshold field solution profiles for maximum field flatness.

Step 1. Solving the optimization problem at a given above-threshold injection current involves first determining the threshold conditions of the DFB laser. Using equation [3-10], threshold values for α_{th} and δ_{th} are determined. Solution of equation [3-10] gives the various oscillation modes of the laser and the mode corresponding to the smallest α will be the first to oscillate at threshold. This value is chosen as α_{th} along with its corresponding δ_{th}.

Step 2. The Bragg wavelength is next evaluated as

$$\lambda_B = 2\Lambda n_e, \qquad \text{[A1]}$$

where equation [A1] is simply equation [1-1] for the first order Bragg grating, and the parameter n_e is the mode's effective refractive index with zero injection current.

Step 3. Using α_{th} arrived at in Step 1, the threshold carrier density, N_{th}, can be found as

$$N_{th} = N_o + (\alpha_{loss} + 2\alpha_{th})/\Gamma A_o. \qquad \text{[A2]}$$

Step 4. Having obtained N_{th}, the threshold index, n_{th}, is found using the following expression

$$n_{th} = n_e + \Gamma \frac{\partial n}{\partial N} N_{th}, \qquad \text{[A3]}$$

which defines how the effective refractive index of the laser depends on the carrier density. The term, $\partial n/\partial N$, is the differential index and Γ is the optical confinement factor (refer to table 4.1).

Step 5. The detuning coefficient for the first order Bragg grating is determined as

$$\delta = \frac{2\pi}{\lambda} n - \frac{2\pi n_g}{\lambda \lambda_B}(\lambda - \lambda_B) - \frac{\pi}{\Lambda}, \qquad [A4]$$

where n is the effective refractive index for the corresponding wavelength λ. Substitution of δ_{th} and n_{th}, obtained in Steps 1 and 4, into equation [A4] results in the following expression for λ_{th}, the threshold wavelength or the longitudinal mode oscillation wavelength of the DFB laser when it is just turning on:

$$\lambda_{th} = \frac{2\pi\lambda_B(n_{th} + n_g)}{\delta_{th}\lambda_B + 2\pi n_g + \lambda_B \pi / \Lambda}. \qquad [A5]$$

The parameter n_g is the group refractive index, which is defined for a given mode propagating in a medium of refractive index n, as the velocity of light in vacuum divided by the group velocity of the mode.

Step 6. Starting with the parabolic gain model used to characterize the active medium gain

$$g = A_0(N - N_o) - A_1[\lambda - (\lambda_o - A_2(N - N_o))]^2, \qquad [A6]$$

the peak gain wavelength at zero gain transparency, λ_o, is obtained by setting the gain, g, equal to zero and N to N_{th}. The material gain of a bulk medium is dependent on both the carrier density and the wavelength. When this gain is zero, the medium is considered transparent. The wavelength λ_o at which the

material gain is zero, at the transparency carrier density, N_o, is defined as the peak gain wavelength at zero gain transparency. In the above expression, A_0 is the differential gain, and the parameters A_1 and A_2 are associated with the width of the gain spectrum and changes in gain that result from shifts in the peak wavelength. With these substitutions, equation [A6] reduces to the expression for the zero gain transparency wavelength given as

$$\lambda_o = \lambda_{th} + A_2(N_{th} - N_o). \qquad \text{[A7]}$$

Step 7. Finally, the threshold injection current, i_{th}, is determined from the steady state carrier rate equation

$$\frac{i}{qV} = R + R_{st}, \qquad \text{[A8-a]}$$

where

$$R = \frac{N}{\tau} + BN^2 + CN^3 \qquad \text{[A8-b]}$$

and

$$R_{st} = \frac{v_g g S}{1 + \sigma S}. \qquad \text{[A8-c]}$$

This equation relates the injection current, i, the carrier density, N, and the stimulated photon density, S. Equation [A8-a] equates the injected charge density to the sum of R_{st}, the stimulated emission rate per unit volume (equation [A8-c]), and R, the rate of other non-coherent charge recombination per unit volume (equation [A8-b]). The volume V is determined from the geometry of the active region, and q is the electronic charge. The other parameters used are defined in table 4.1. The parameter σ accounts for saturation effects at high photon densities. At threshold, the numbers of coherent photons are minimal; hence the photon density, S, is considered as zero. Setting the carrier density $N = N_{th}$, it is then a straightforward process to obtain i_{th}.

Step 8. At this point the search domain is specified for LGO, the global optimizer. The maximum, the minimum, as well as nominal values are chosen for *KL*, and/or *PS*, λ, and C_o parameters. Typically these values are selected somewhere close to the midpoint of the search domain. Now the laser is divided into a sufficiently large number of matrix sections such that the concatenation of all the sections will accurately approximate a smooth longitudinal variation of the laser parameters. For this example 5000 transfer matrix sections were found to yield acceptable results.

Step 9. Field propagation is initiated by first determining the photon density, *S*, at the inside surface of the left facet. Initially, the refractive index at this point is unknown so the threshold refractive index, n_{th}, is used as a starting approximation. This approximation is subsequently applied to all 5000 of the laser sections.

Starting with the normalized electric field intensity at the left-hand facet, the photon density at this point is evaluated for the first TMM section from

$$S_z \approx \frac{2\varepsilon_o n(z) n_g \lambda}{hc} \cdot C_o^2 \left[|E_r(z)|^2 + |E_s(z)|^2 \right], \qquad \text{[A9]}$$

where ε_o is the permittivity of free space. The values of λ and C_o used in this calculation are the first values provided by LGO following initialization. Once the photon density has been determined, the carrier density, *N*, is determined by solving equation [A8], the carrier rate equation. Using the following relationship, the amplitude gain coefficient, α, is expressed as

$$\alpha = (\Gamma g - \alpha_{loss})/2, \qquad \text{[A10]}$$

and the detuning coefficient, δ, is determined from equation [A4]. It is now possible, using equations [A17], [A18], and [A19], to determine all of the parameters for the first transfer matrix section. In addition to this, the section refractive index, n, is revised using equation [A3], where the threshold carrier density, N_{th}, is replaced with the newly determined carrier density. This value is stored for the next iterative pass through the section.

Step 10. Once this is accomplished using equation [A22], the field is propagated towards the right-hand facet of the first transfer matrix section and becomes the input field to the second transfer matrix section. The parameters α and δ are again determined along with the second section's transfer matrix values, and the fields are propagated to the right-hand facet of the third transfer matrix section. The process outlined in Step 9 and this step is continued until the right-hand facet of the entire structure is reached.

Step 11. At this point the entire longitudinal refractive index profile has been redefined by the stored values in Step 9. Using the same values of KL, PS, λ and C_o, it is necessary to repeat Steps 9 and 10 until the refractive index profile no longer changes significantly with each pass down the laser.

Step 12. Once the refractive index profile stabilizes, the field profile will also stabilize. Now the right-hand boundary error is determined. Minimization of this error is both an imposed explicit constraint, and coupled with the field flatness parameter comprises the objective function, which itself is also minimized (equations [4-2] and [4-3]). LGO stores the objective function value and proceeds to select new KL, PS, λ and C_o parameters for the next iterative cycle.

Step 13. Using these new values, Steps 9 through 12 are again repeated with the process continuing until the objective function (and the right-hand boundary condition error) has been minimized to the desired tolerance set in LGO. Now the final

solutions of the field intensity, carrier density, refractive index, and photon density profiles for the laser are obtained.

Step 14. With a final pass through the structure, the average amplitude gain coefficient and the average detuning coefficient are determined from the following expressions

$$\overline{\alpha_L} = \sum_{m=1}^{M} \alpha_m / M \qquad \text{[A11]}$$

$$\overline{\delta_L} = \sum_{m=1}^{M} \delta_m / M \,, \qquad \text{[A12]}$$

where M is the total number of transfer matrix sections.

APPENDIX B

OBJECTIVE FUNCTION VISUALIZATIONS

APPENDIX B

OBJECTIVE FUNCTION VISUALIZATIONS

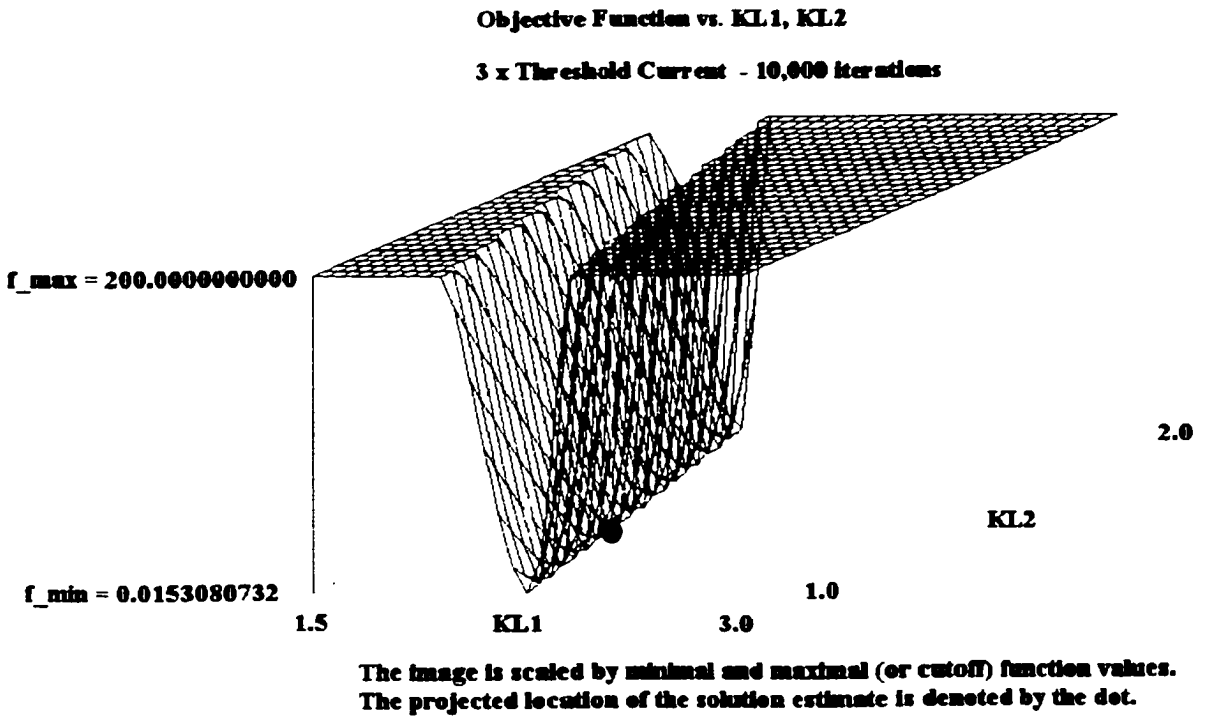

Figure B1 Objective Function versus *KL1, KL2* (*KL* Optimization at 3 x i_{th})

APPENDIX B (Continued)

OBJECTIVE FUNCTION VISUALIZATIONS

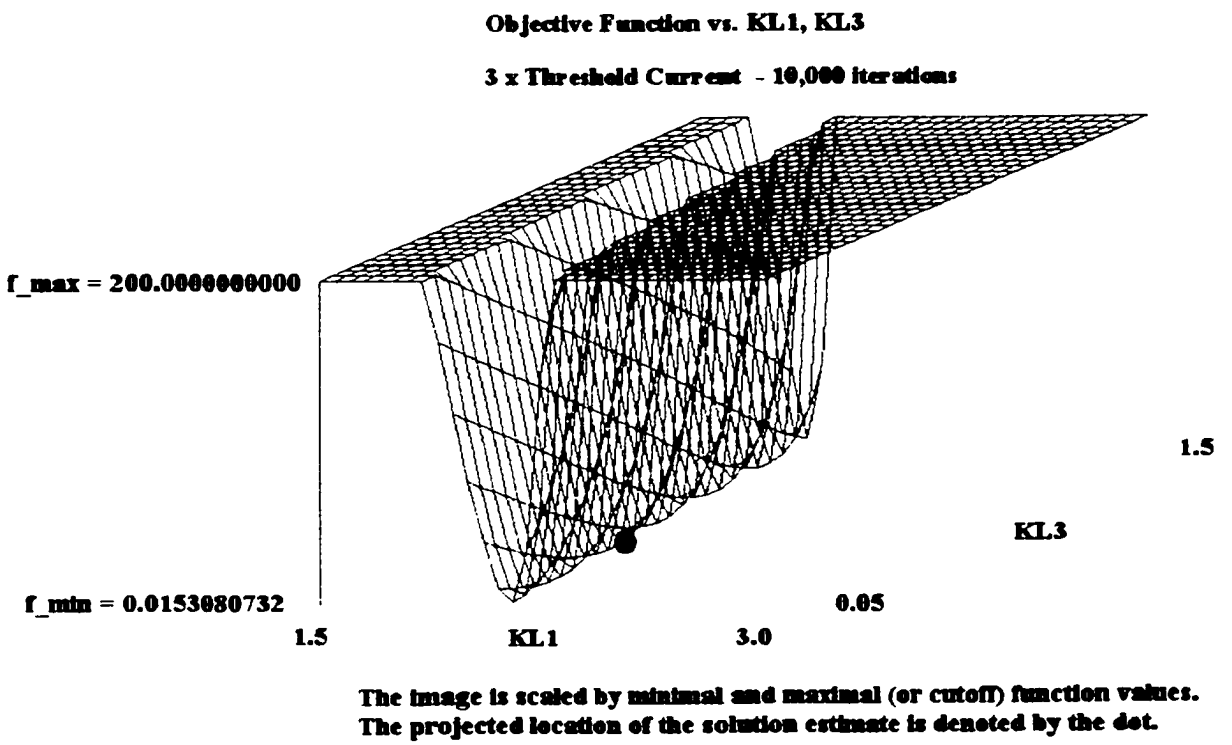

Figure B2 Objective Function versus *KL1, KL3* (*KL* Optimization at 3 x i_{th})

APPENDIX B (Continued)

OBJECTIVE FUNCTION VISUALIZATIONS

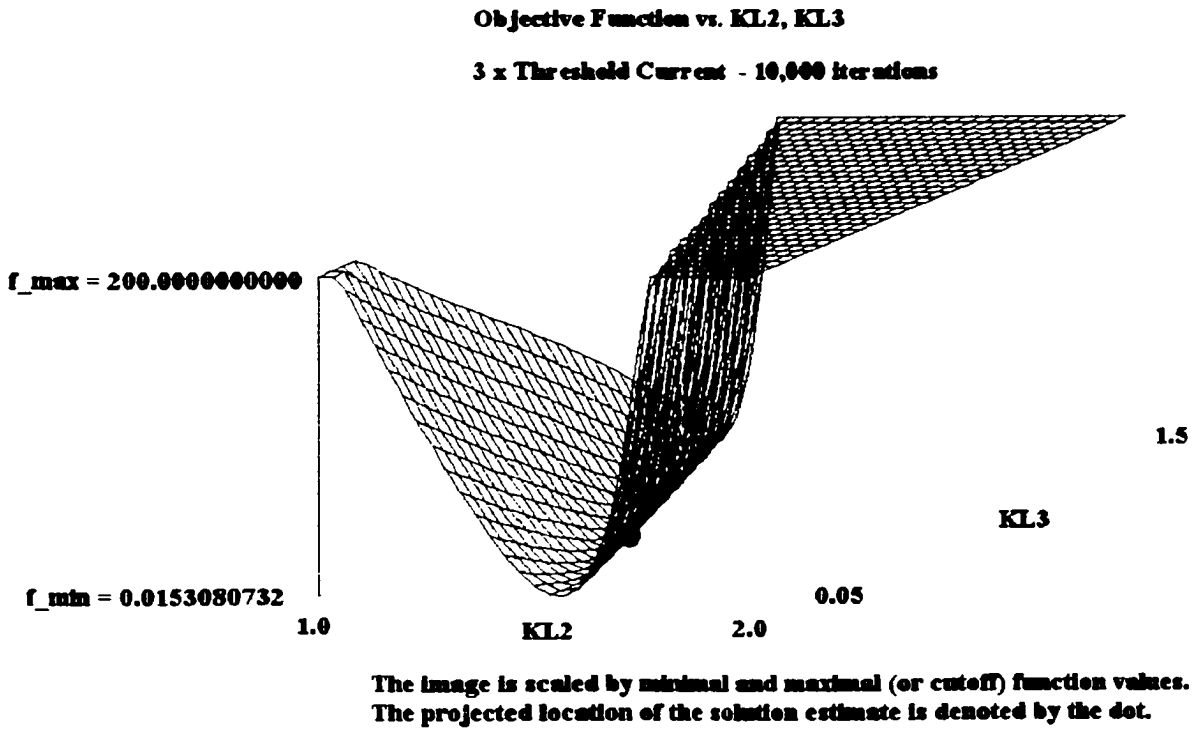

Figure B3 Objective Function versus *KL2, KL3* (*KL* Optimization at 3 x i_{th})

APPENDIX B (Continued)

OBJECTIVE FUNCTION VISUALIZATIONS

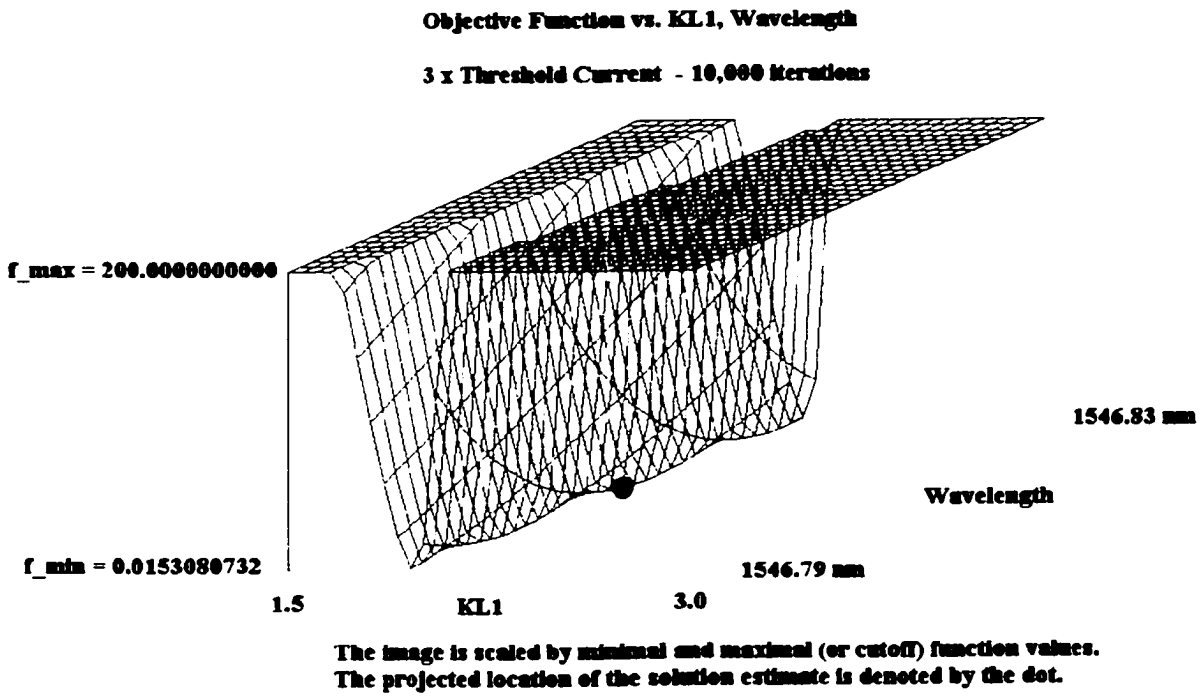

Figure B4 Objective Function versus *KL1*, Wavelength (*KL* Optimization at 3 x i_{th})

APPENDIX B (Continued)

OBJECTIVE FUNCTION VISUALIZATIONS

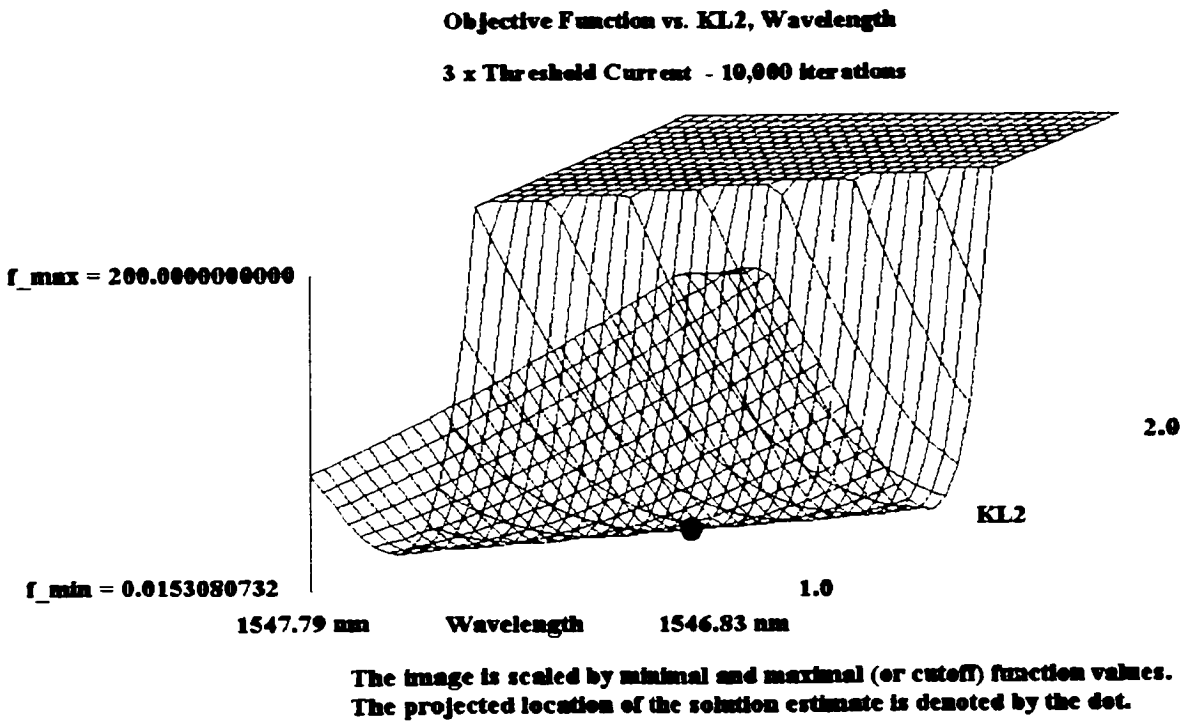

Figure B5 Objective Function versus *KL2*, Wavelength (*KL* Optimization at 3 x i_{th})

APPENDIX B (Continued)

OBJECTIVE FUNCTION VISUALIZATIONS

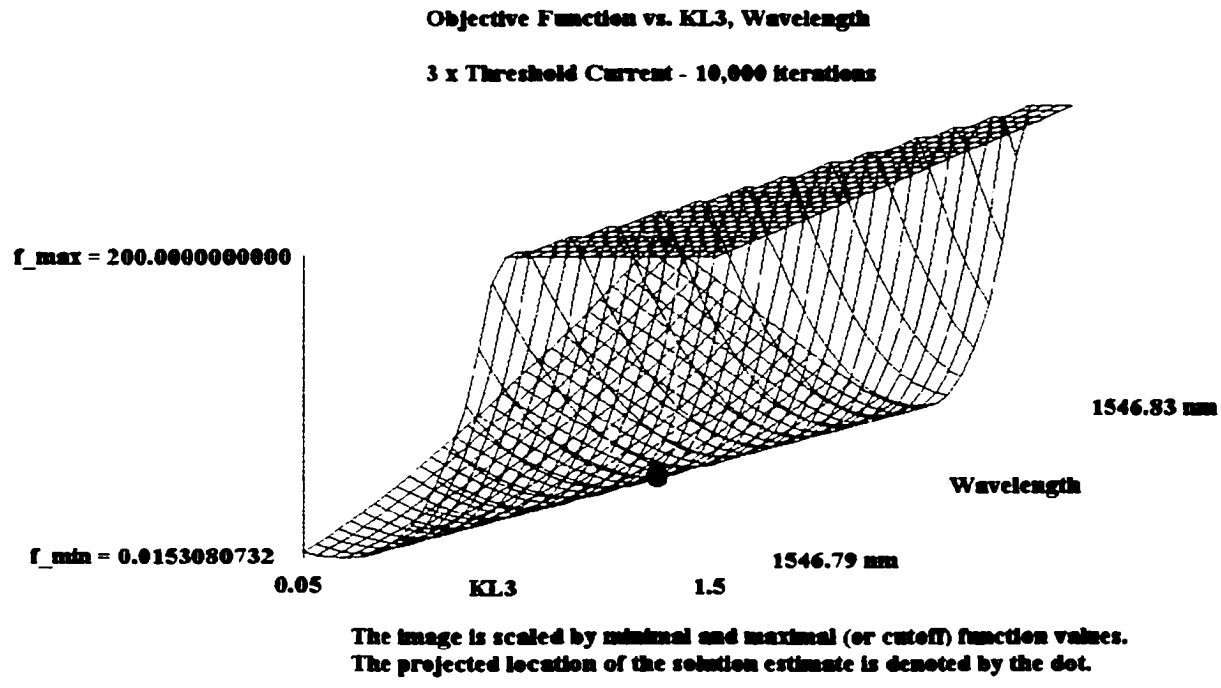

Figure B6 Objective Function versus *KL3*, Wavelength (*KL* Optimization at 3 x i_{th})

APPENDIX B (Continued)

OBJECTIVE FUNCTION VISUALIZATIONS

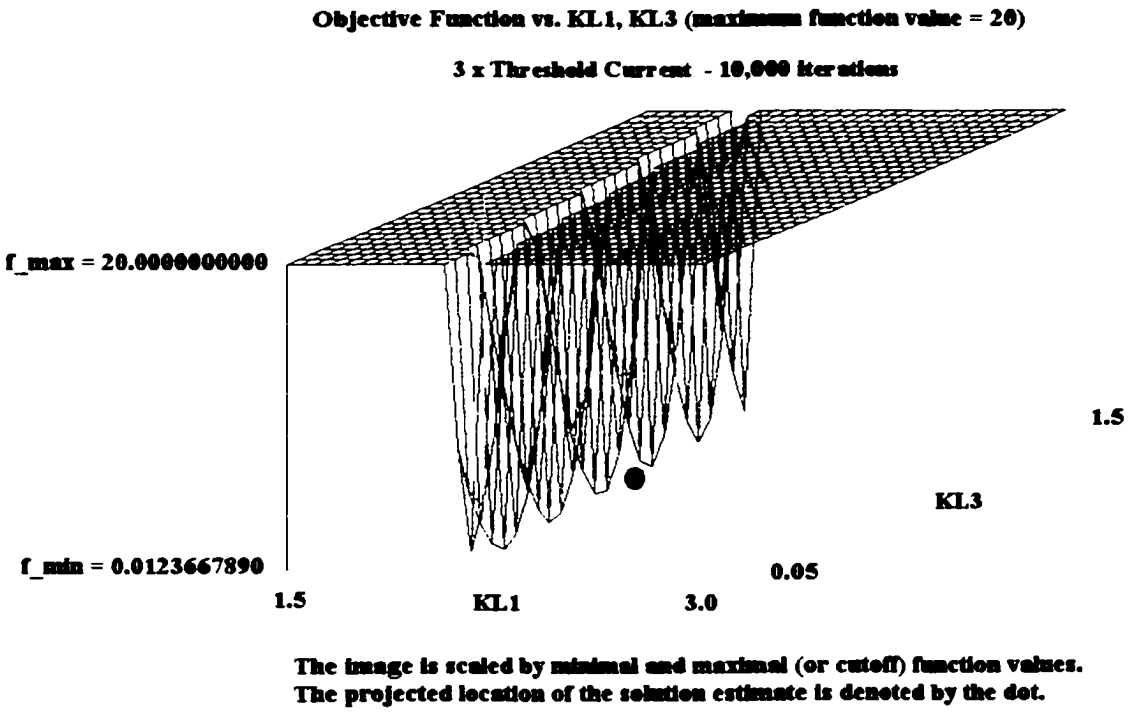

Figure B7 Objective Function versus *KL1, KL3* with maximum function value = 20 (*KL* Optimization at 3 x i_{th})

APPENDIX B (Continued)

OBJECTIVE FUNCTION VISUALIZATIONS

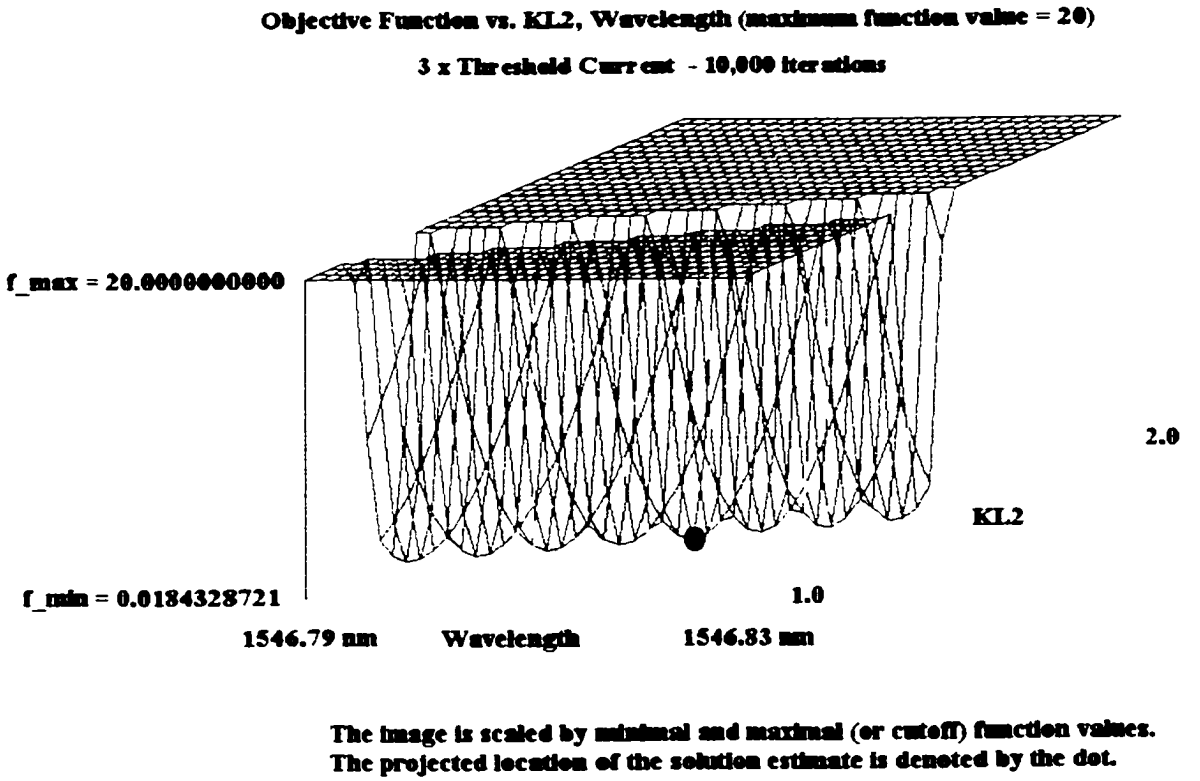

Figure B8 Objective Function versus *KL2*, Wavelength with maximum function value = 20 (*KL* Optimization at 3 x i_{th})

APPENDIX C

PHASE OPTIMIZATION GRAPHS

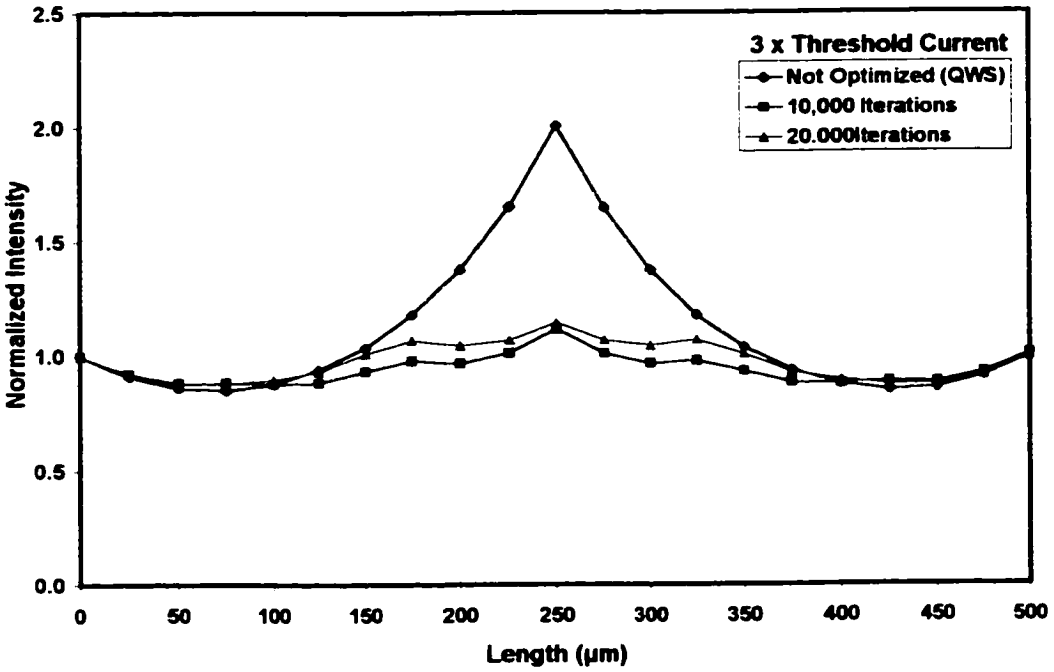

Figure C1 Field Intensity (*PS* Optimization at 3 x i_{th})

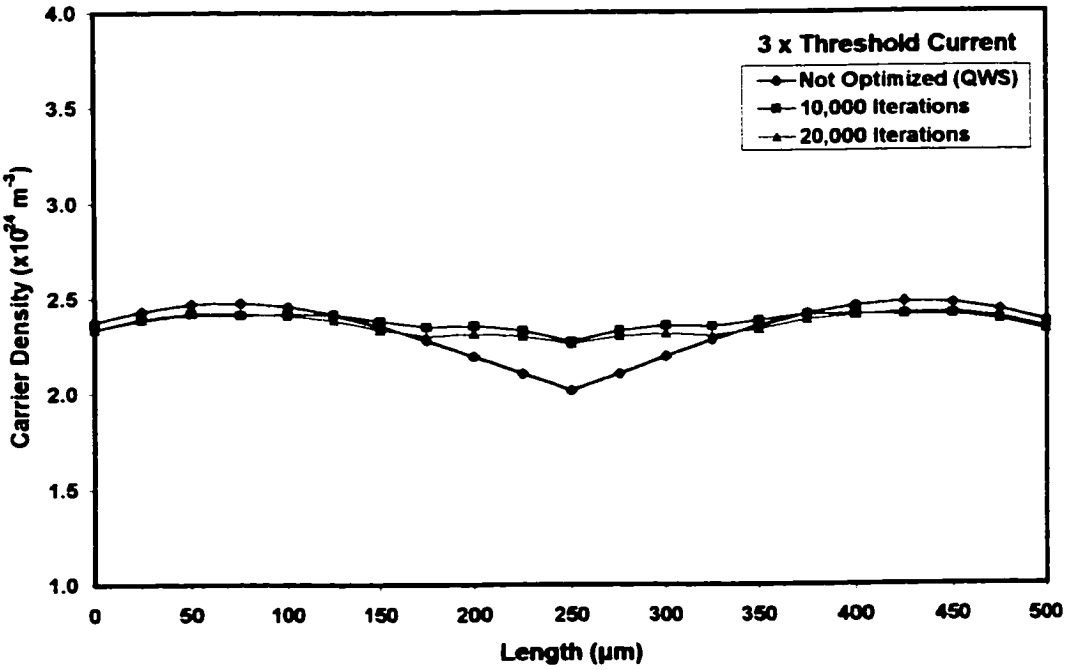

Figure C2 Carrier Density (*PS* Optimization at 3 x i_{th})

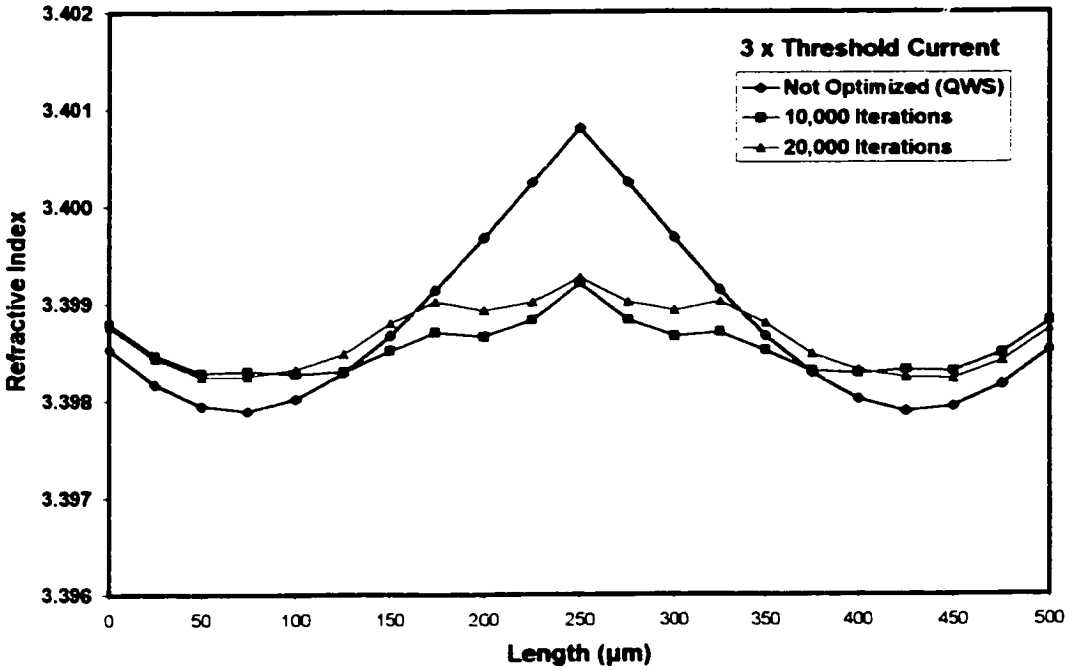

Figure C3 Refractive Index (*PS* Optimization at 3 x i_{th})

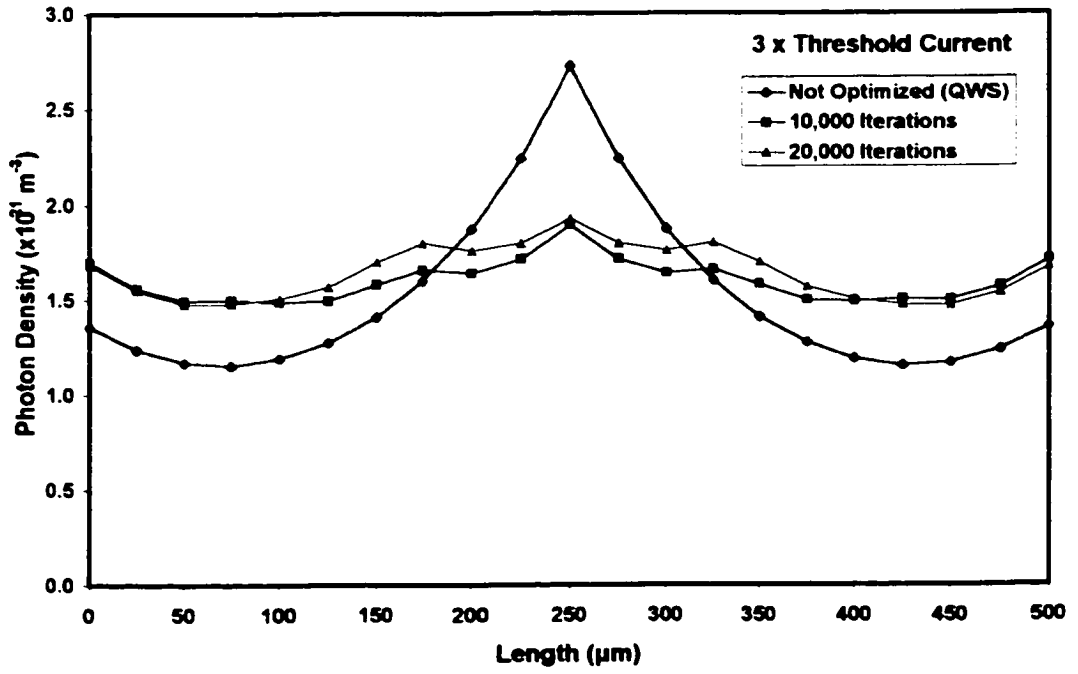

Figure C4 Photon Density (*PS* Optimization at 3 x i_{th})

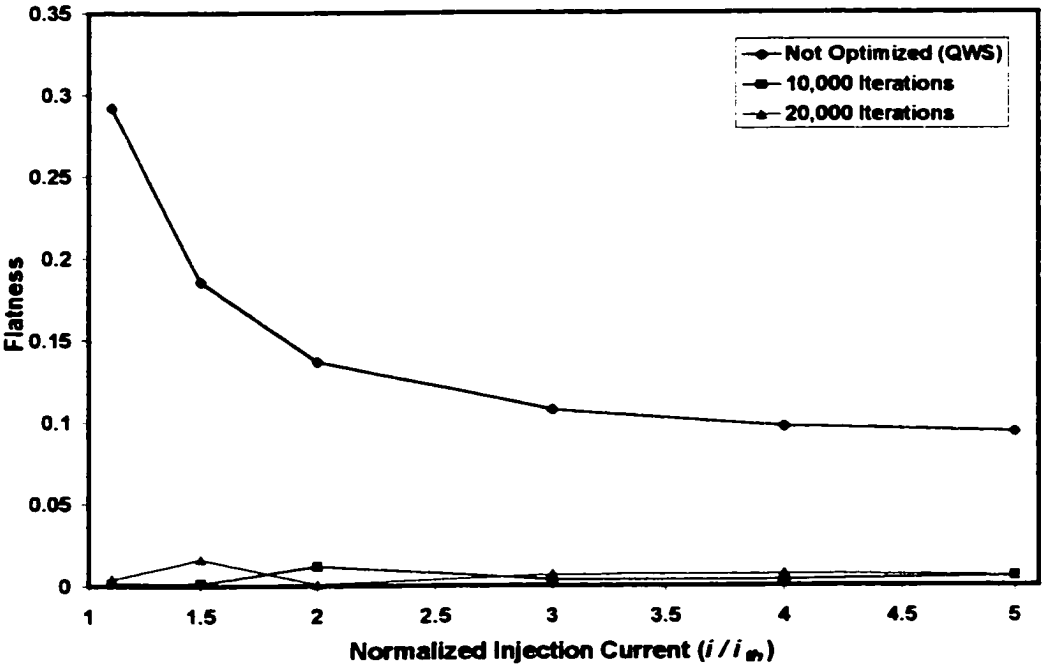

Figure C5 Field Intensity Flatness (*PS* Optimization)

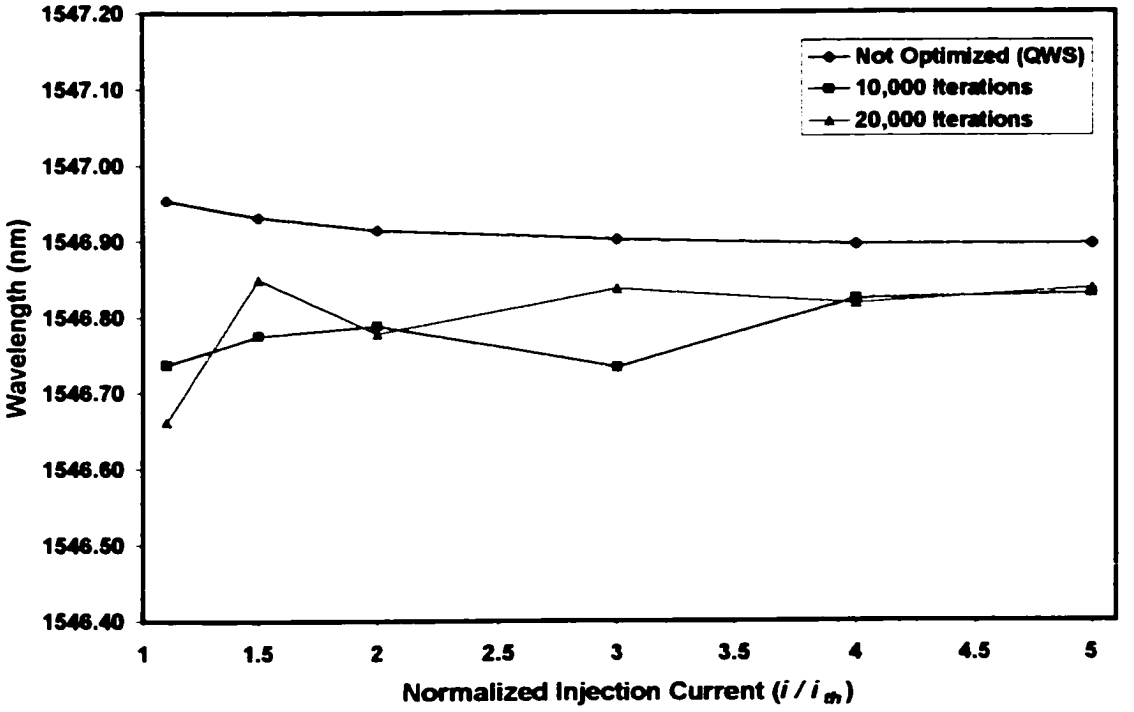

Figure C6 Wavelength (*PS* Optimization)

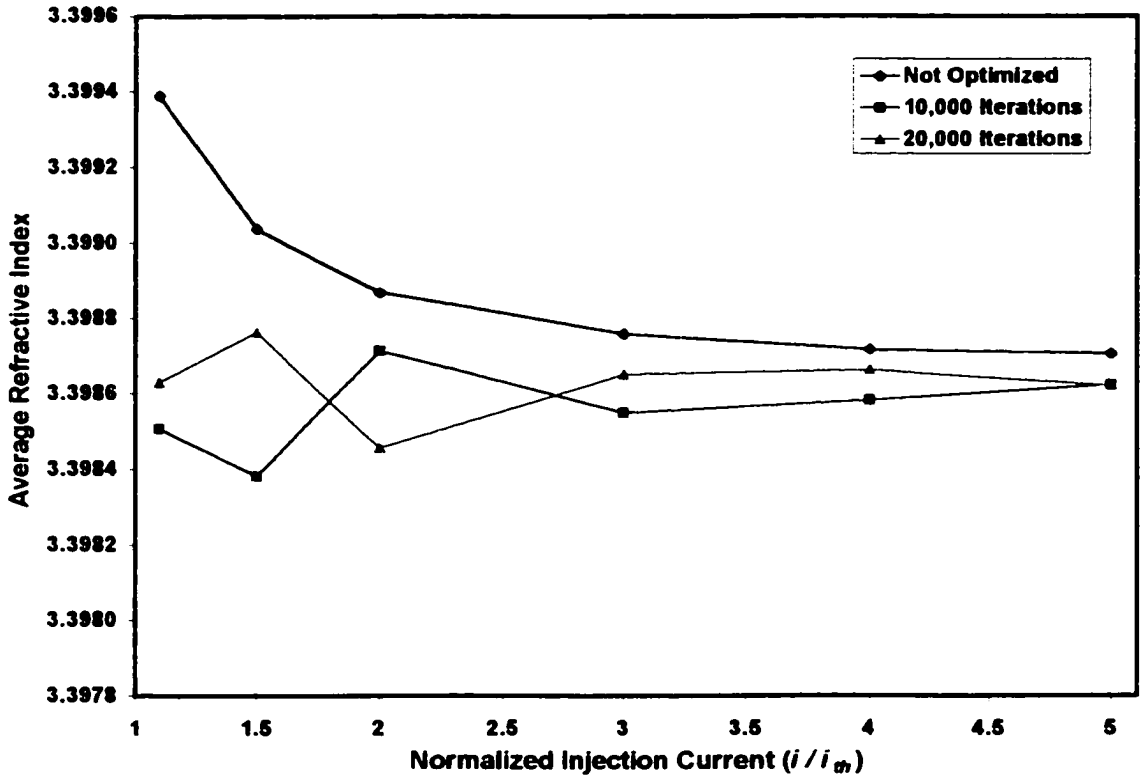

Figure C7 Average Refractive Index (*PS* Optimization)

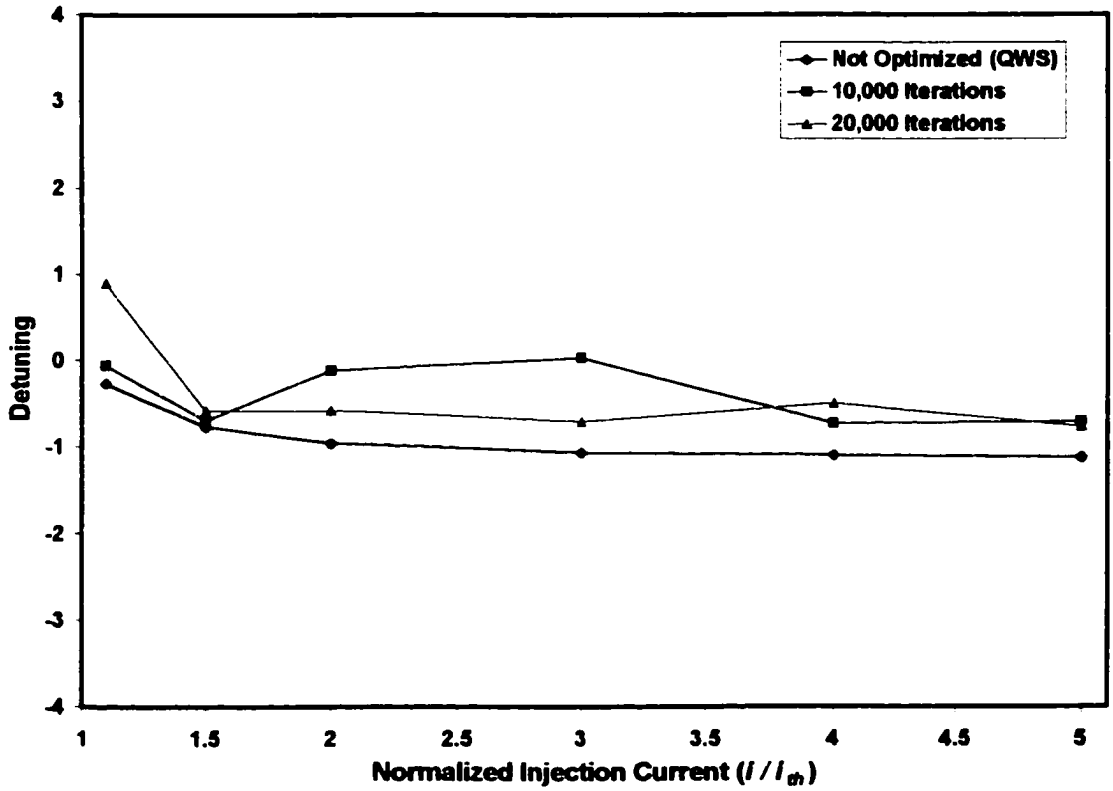

Figure C8 Average Normalized Detuning (*PS* Optimization)

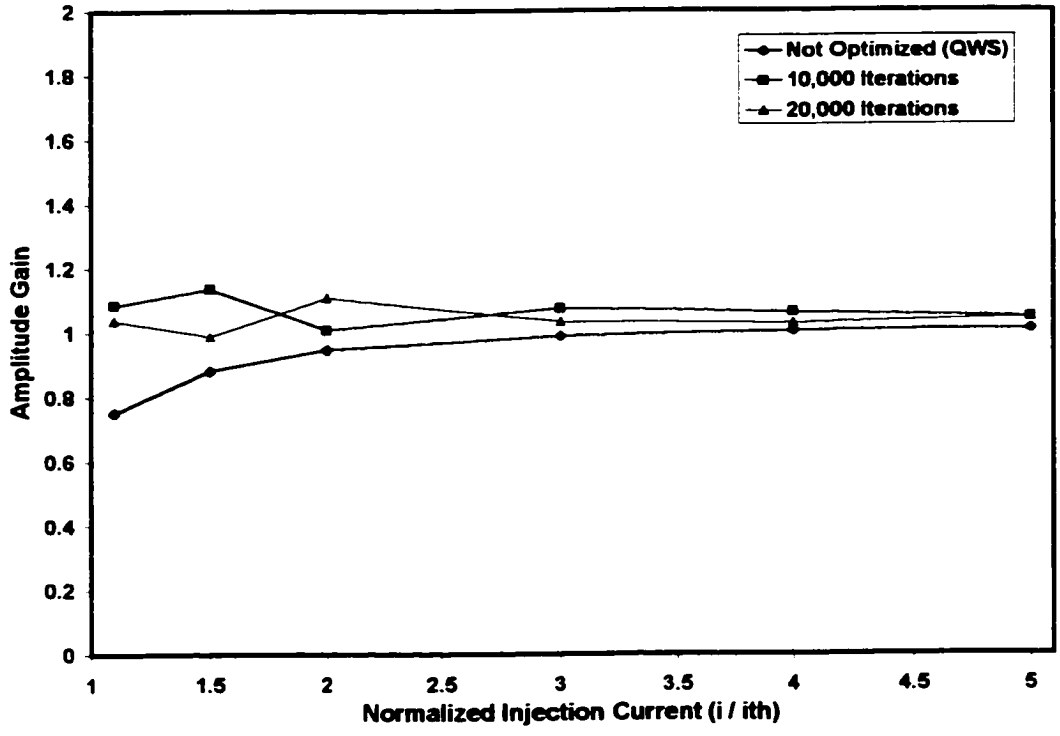

Figure C9 Average Normalized Amplitude Gain (*PS* Optimization)

APPENDIX D

COUPLING COEFFICIENT PLUS PHASE OPTIMIZATION GRAPHS

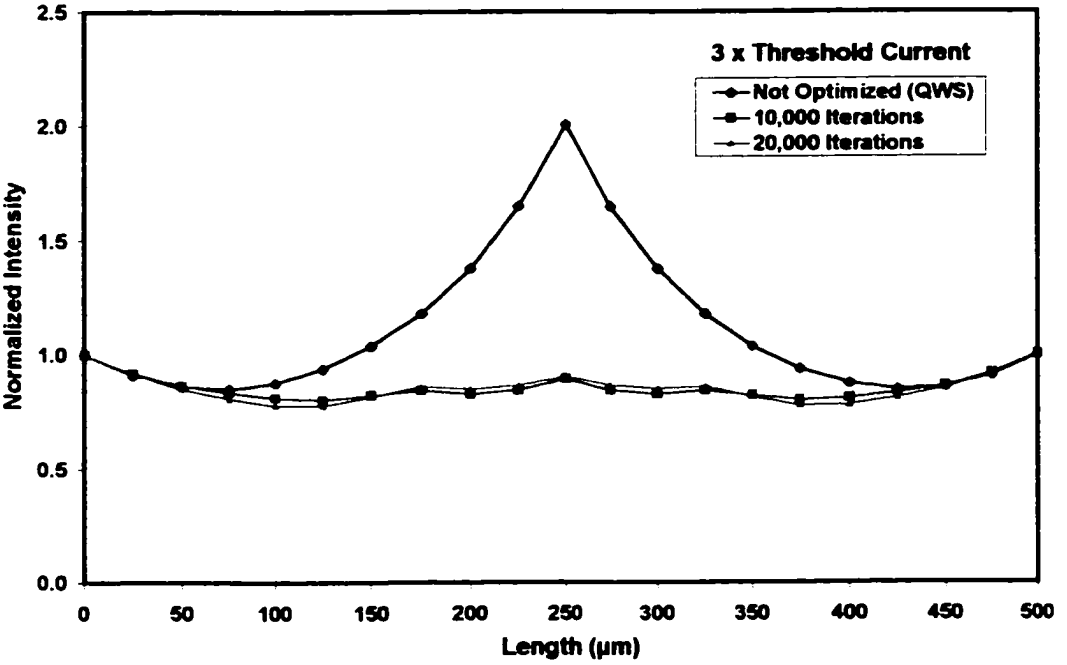

Figure D1 Field Intensity (*KL* plus *PS* Optimization at 3 x i_{th})

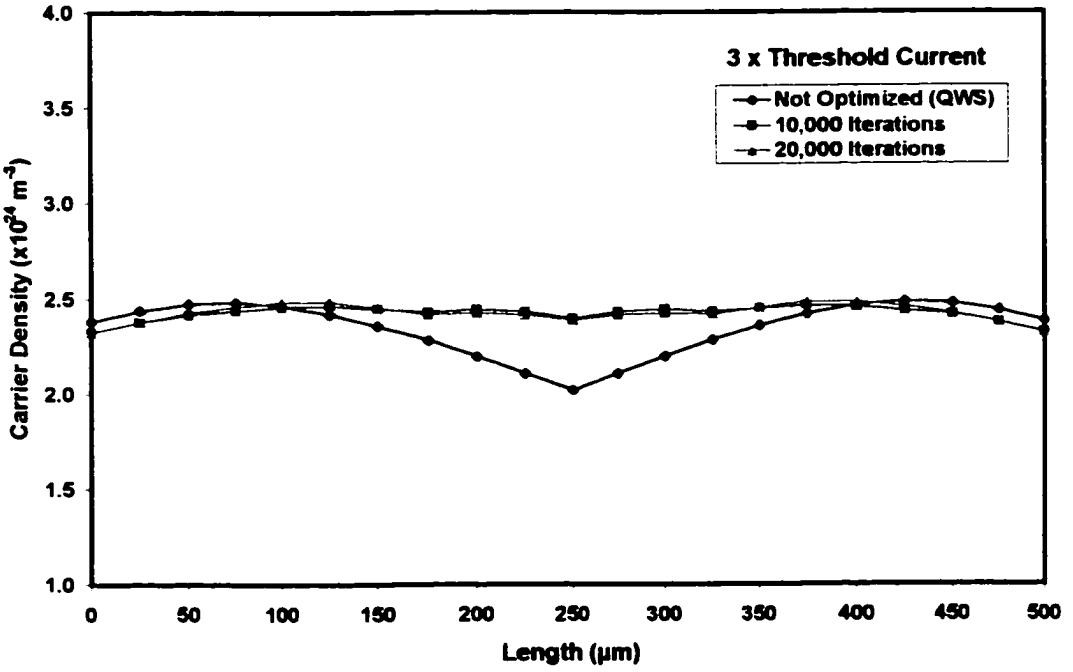

Figure D2 Carrier Density (*KL* plus *PS* Optimization at 3 x i_{th})

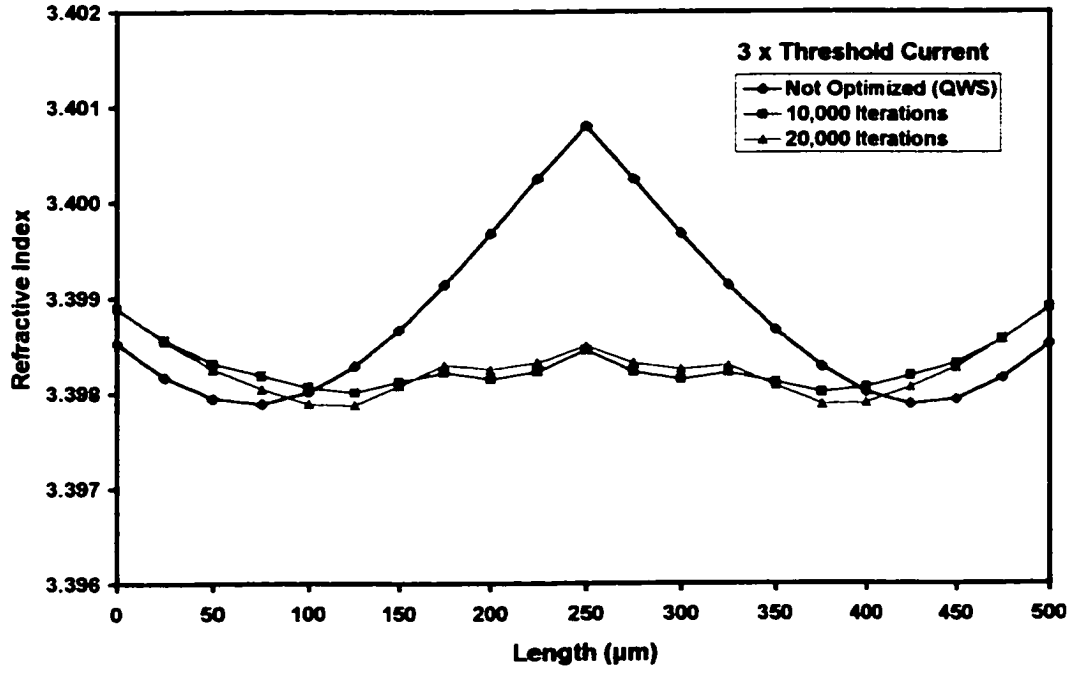

Figure D3 Refractive Index (*KL* plus *PS* Optimization at 3 x i_{th})

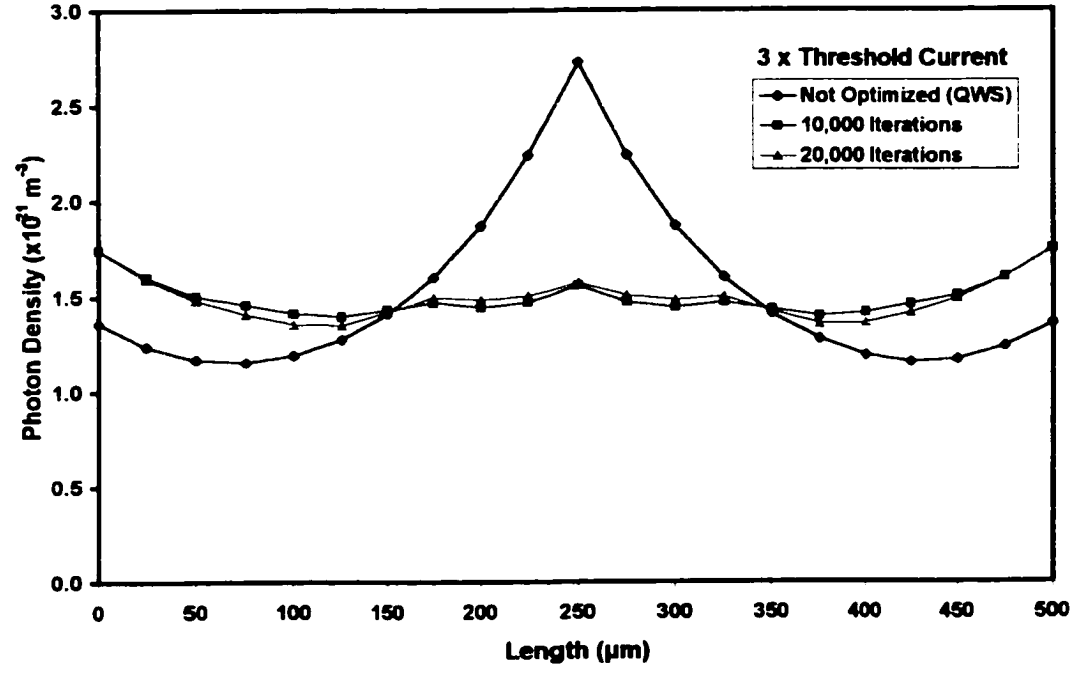

Figure D4 Photon Density (*KL* plus *PS* Optimization at 3 x i_{th})

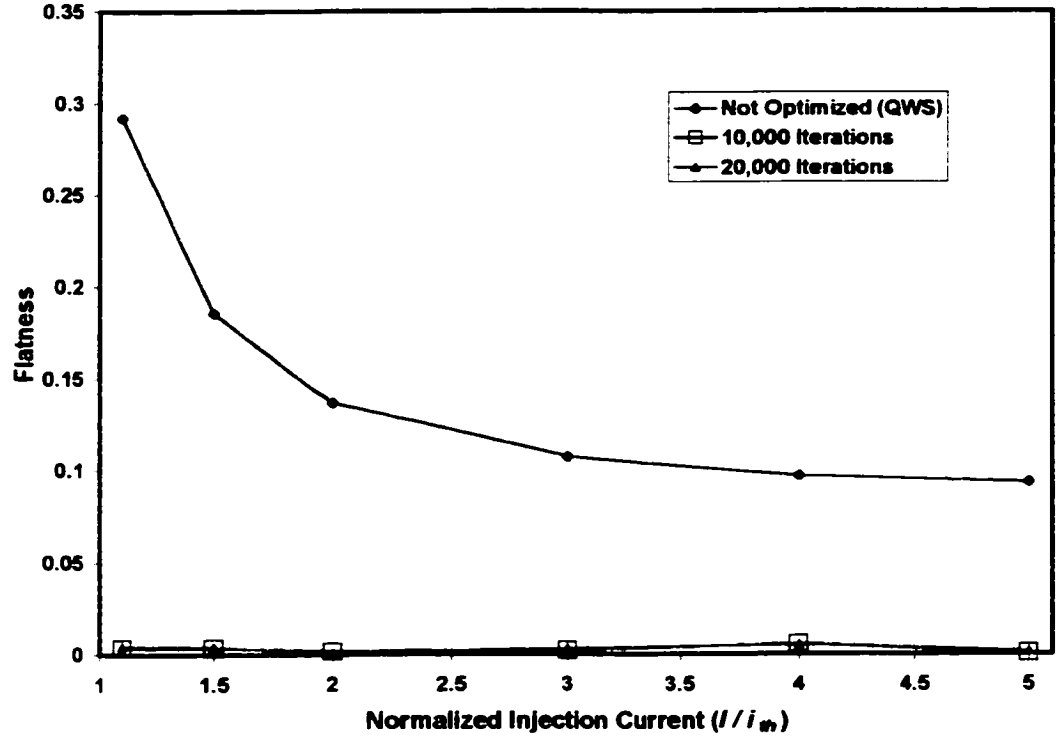

Figure D5 Field Intensity Flatness (*KL* plus *PS* Optimization)

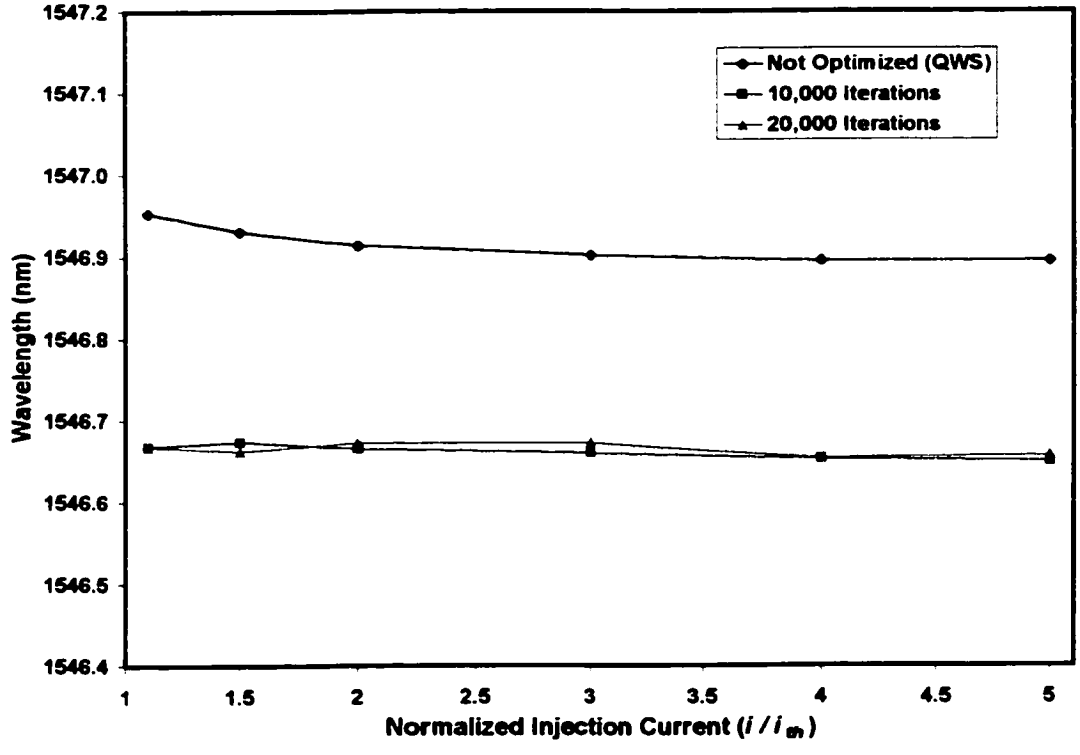

Figure D6 Wavelength (*KL* plus *PS* Optimization)

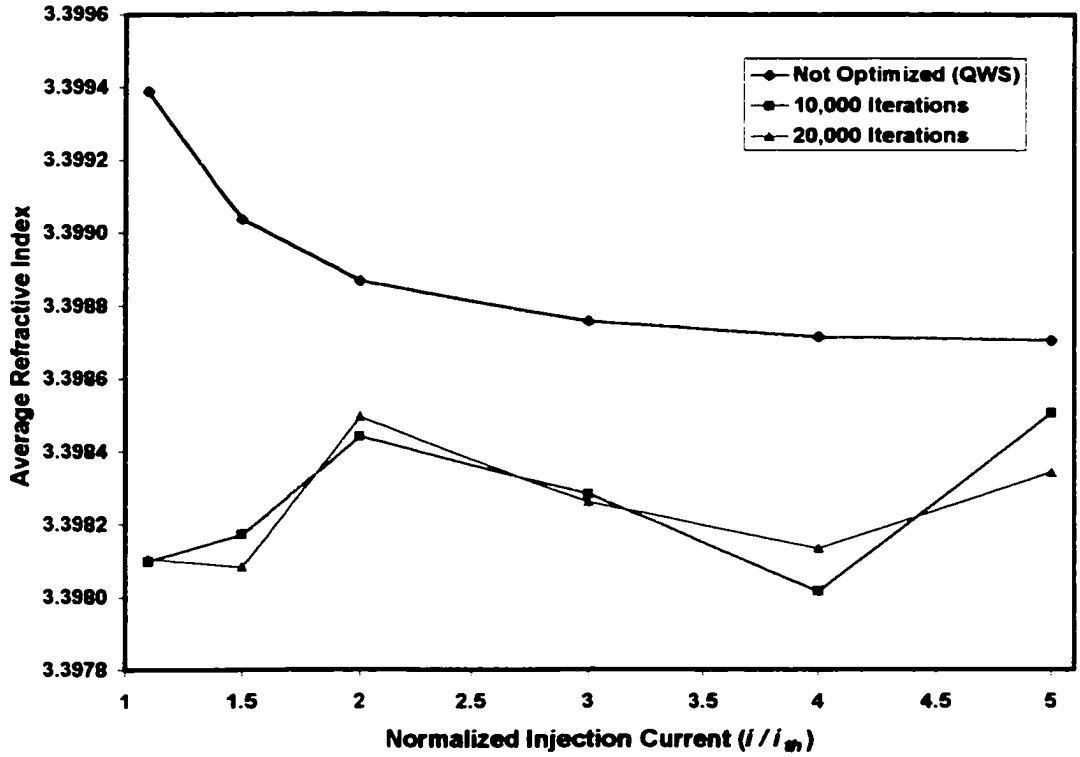

Figure D7 Average Refractive Index (*KL* plus *PS* Optimization)

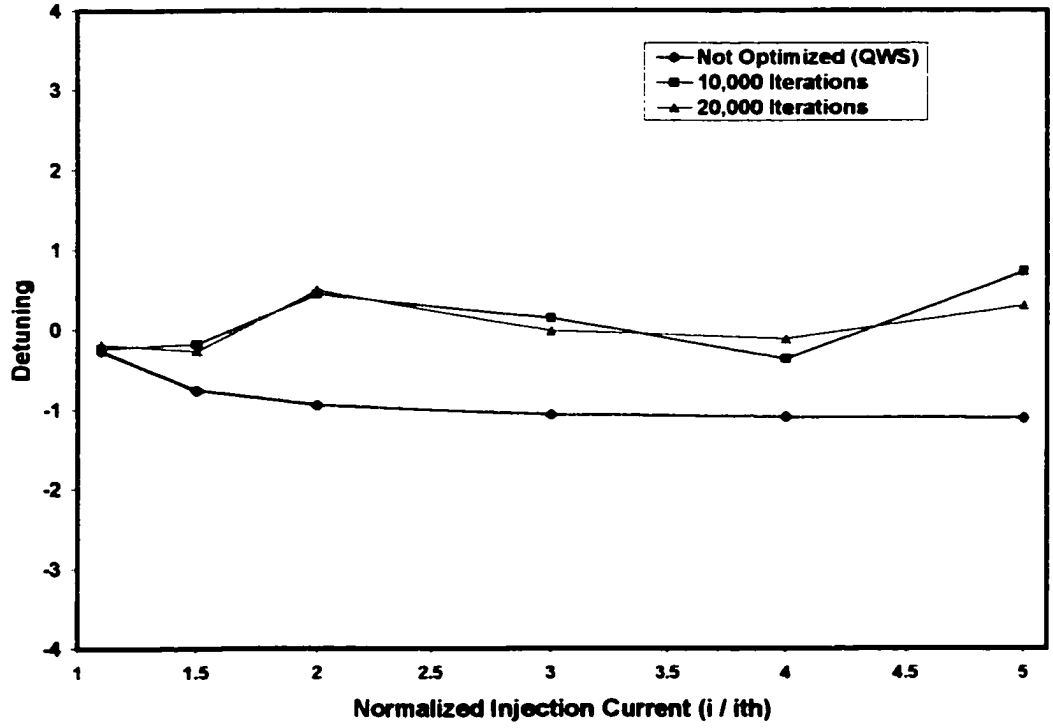

Figure D8 Average Normalized Detuning (*KL* plus *PS* Optimization)

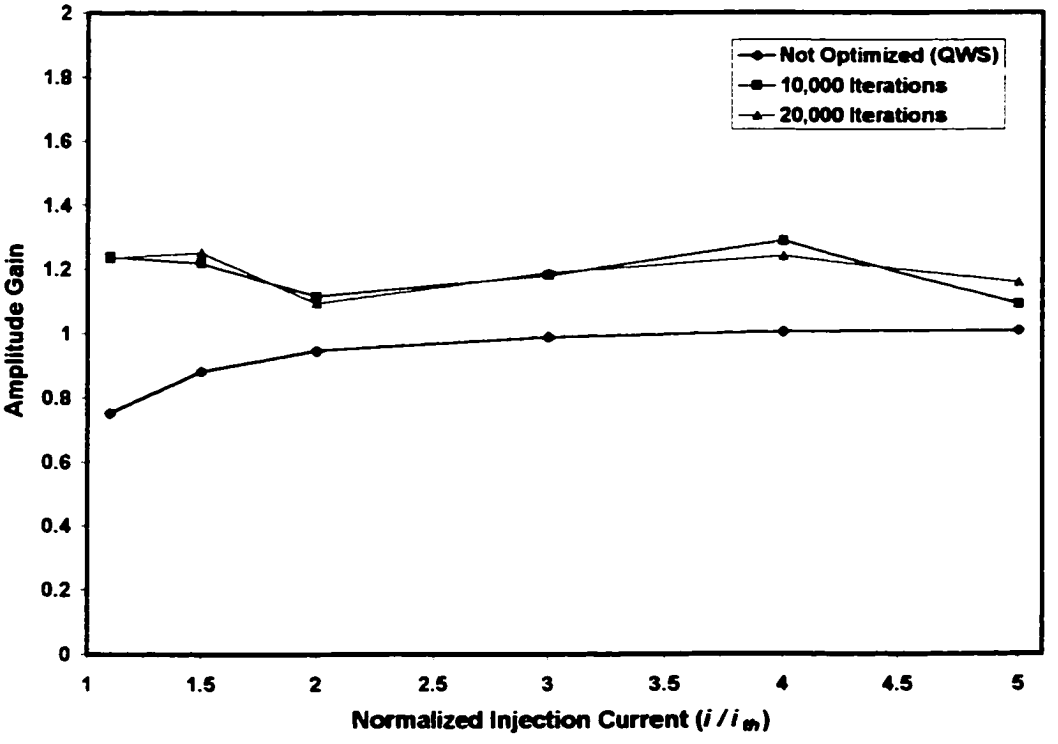

Figure D9 Average Normalized Amplitude Gain (*KL* plus *PS* Optimization)

APPENDIX E

OPTIMIZATION CODE LISTING

DFB1F.FOR

This code listing contains the subroutine USER_FCT, which is called by the LGO solver system. USER_FCT in turn calls subroutine RBC_Out, the code that defines the objective function to be minimized by the optimization process.

```
C     Program DFB1F.FOR
C     Optimizes both sectional coupling coefficients and intra-sectional
C     phase shifts to achieve maximum internal field profile flatness while
C     minimizing the right hand facet boundary condition error of a
C     6 section DFB laser.

C     SUBROUTINE USER_FCT Called From LGO



!     DFB1F.FOR ---
!     ------------------------------------------------------------------------

!     This is the function segment template, to be prepared (adapted) by LGO
!     users. The use of all included statements is (minimally) necessary.
!     Additional user statements - related to problem description, further
!     reporting options, calls, etc. - can also be included or connected.

!     Please retain an original copy of this segment for further reference
!     Save your own USERFCT.FOR file in text format

!     ------------------------------------------------------------------------

      SUBROUTINE USER_FCT(x,objf,objname,ctype,con,conname)

      implicit real*8 (a-h,o-z)
!     Please define all (real) variables and operations in double precision,
!     in order to attain higher numerical accuracy

!     The following statement is needed only in Windows DLL program versions
!      DLL_EXPORT USER_FCT

!     Notation:
!     x     - vector of decision variables (maximal dimension: maxdim)
!     objf  - scalar objective function value (to be minimized)
!             (maximization problems are standardized, multiplying objf by -1)
!     objname - (optional) name for objective function; max. 20 characters
!     ctype - vector of constraint function types (maximal dimension: maxcon)
!             for constraints of the form    con(i).eq.0    set   ctype(i)= 0
!             for constraints of the form    con(i).le.0    set   ctype(i)=-1
!             (con(i).ge.0 type constraints are standardized, multiplying the
!             constraint by -1)
!     con   - vector of constraint function values (maximal dimension: maxcon)
!     conname - vector of (optional) names for individual constraints; max. 20
!            characters for each constraint (maximal dimension: maxcon)

!     Please note that the dimension settings given below are specific to
!     your present LGO version, and they can not be modified. Please contact
!     Pinter Consulting Services, if a larger LGO configuration is needed.
      parameter(maxdim=50, maxcon=52) ! maxcon includes two extra work entries
      dimension x(maxdim), ctype(maxcon), con(maxcon), conname(maxcon)
      character*20 conname, objname
      integer*2 ctype
```

```
!     ------------------- User problem definitions begin ------------------

!     Note: for the given demonstration problem class, the unique optimal
!     solution is the zero vector.

!     Auxiliary terms
      real*8 KL1, KL2, KL3, LAMSTART, LAMC, DPS1, DPS2, DPS3,
     c RBCerror,FLATNESS,AVGALPHA,AVGLDELTA,PSTOTAL

       LAMC=1.546d0
       KL1=x(1)
       KL2=x(2)
       KL3=x(3)
       LAMSTART=(1.d-6)*(x(4)+LAMC)
       Co=(1.d5)*x(5)
       DPS1=x(6)
       DPS2=x(7)
       DPS3=x(8)


!     --- Objective function (to be minimized) ---

      call RBC_Out(KL1,KL2,KL3,LAMSTART,
     c Co,DPS1,DPS2,DPS3,RBCerror,FLATNESS,AVGLALPHA,AVGLDELTA,PSTOTAL)

       scal=1000.d0
       objf=FLATNESS+scal*RBCerror
       objname='Flatness Function'


!     --- Constraint types and functions ---

!     Note: explicit box constraint handling is done separately by LGO;
!     therefore only the additional constraints need to be declared here.

!     Boundary Condition Constraint
!     *****************************
      con(1)=scal*RBCerror
      ctype(1)=0
      conname(1)='RBC Error'


!     Constraints on AVGLALPHA
!     ************************

!     Lower
!     -----
c      con(2)=(0.6D0-AVGLALPHA)
c      ctype(2)=-1
c      conname(2)='AVGLALPHA lower boundary'


!     Upper
!     -----
c      con(3)=(AVGLALPHA-1.5D0)
c      ctype(3)=-1
c      conname(3)='AVGLALPHA upper boundary'
```

```
!      Fundamental mode constraints on AVGLDELTA
!      ******************************************

!      Lower
!      -----
       con(2)=((-1.00d0)-AVGLDELTA)
       ctype(2)=-1
       conname(2)='AVGLDELTA lower boundary'

!      Upper
!      -----
       con(3)=(AVGLDELTA-(1.00D0))
       ctype(3)=-1
       conname(3)='AVGLDELTA upper boundary'

!      -1 Mode constraints on AVGLDELTA
!      *********************************************

!      Lower
!      -----
!       con(4)=(-1.0d0-AVGLDELTA)
!       ctype(4)=-1
!       conname(4)='AVGLDELTA lower boundary'

!      Upper
!      -----
!       con(5)=(AVGLDELTA-1.0D0)
!       ctype(5)=-1
!       conname(5)='AVGLDELTA upper boundary'

!       Total Phase shift Constraint
!       ****************************
!       Lower
!       -----
c         con(6)=(0.0D0-PSTOTAL)
c         ctype(6)=-1
c         conname(6)='Minimum phase shift'

!       Upper
!       -----
c         con(7)=(PSTOTAL-180.0D0)
c         ctype(7)=-1
c         conname(7)='Maximum phase shift'

!      Mid Point Field Constraint
!      ****************************
!      con(2)=1000.0d0*(1.0d0-MPFC)
!      ctype(2)=-1
!      conname(2)='Mid point field constraint'

!      constraints can also be scaled (to objf), if deemed necessary
!      one-by-one scaling of constraints is also possible, to guarantee that the
!      order of constraints and objective function are approximately identical
!      scalc=1.d0
!      do i=1,5
!        con(i)=scalc*con(i)
!       end do
```

```
!     ---------- User problem definitions end ----------

      return
      end

      SUBROUTINE RBC_Out(KL1,KL2,KL3,LAMSTART,
     c  Co,DPS1,DPS2,DPS3,RBCerror,FLATNESS,AVGLALPHA,AVGLDELTA,PSTOTAL)
c       Glenn Isenor; December 2, 2000

c      Program searches for an above threshold
c      optimized solution for varicus injection currents.
c     An overall merit function is used that minimizes
c     RHB error as well as maximizes the field flatness.
c     Minimal RHB error is a constraint.

       implicit real*8 (a-h,o-z)

       common /C1input/ C1      ! read C1 from file, then pass it into RBC_out

C      C1               THRESHOLD CURRENT FACTOR (C1*ITH)
C      L                LENGTH OF LASER (m)
C      D                ACTIVE LAYER THICKNESS (m)
C      W                ACTIVE LAYER WIDTH (m)
C      B                BIMOLECULAR RECOMBINATION COEFFICIENT (m**3/s)
C      C                AUGER RECOMBINATION COEFFICIENT (m**6/s)
C      TAO              (TAO**-1) SPONTANEOUS EMISSION RATE (1/s)
C      V                ACTIVE LAYER VOLUMN (m**3)
C      Q                ELECTRONIC CHARGE (c)
C      RTH              RATE OF OTHER NONCOHERENT RECOMBINATIONS
C      ITH              THRESHOLD CURRENT
C      ALPHATH          AMPLITUDE THRESHOLD GAIN (1/m)
C      DELTATH          THRESHOLD DETUNING COEFFICIENT ()
C      NNTH             THRESHOLD CARRIER CONCENTRATION (1/m**3)
C      ALPHALOSS        INTERNAL CAVITY LOSS (1/m)
C      NNo              CARRIER CONCENTRATION AT TRANSPARENCY (1/m**3)
C      GAM              OPTICAL CONFINEMENT FACTOR (DIMENSIONLESS)
C      Ao               DIFFERENTIAL GAIN (m**2)
C      A1               GAIN CURVATURE
C      nTH              THRESHOLD INDEX (DIMENSIONLESS)
C      nINI             EFFECTIVE REFRACTIVE INDEX AT 0 CARRIER CONC
C      R                DIFFERENTIAL INDEX (m**3)
C      LALPHATH         NORMALIZED ALPHATH
C      LDELTATH         NORMALIZED DELTATH
C      K                COUPLING COEFFICIENT
C      G                BRAGG GRATING (m)
C      LAMTH            THRESHOLD WAVELENGTH (m)
C      LAMB             BRAGG WAVELENGTH
C      LAMo             PEAK GAIN WAVELENGTH AT 0 TRANSPARANCY
C      nG               REFRACTIVE INDEX AT 0 GAIN INJECTON CURRENT
C      A2               DIFFERENTIAL PEAK WAVELENGTH (m**3)
C      LLAM             OPERATING WAVELENGTH
C      Co               DIMENSIONLESS PARAMETER
C      LAM              WAVELENGTH GUESSES (5 PER GRID CALL)
C      MATGAIN          MATERIAL GAIN COEFFICIENT
C      epsil            NONLINEAR GAIN COEFFICIENT
C      EPSILo           FREE SPACE PERMITTIVITY
C      S                LOCAL PHOTON DENSITY
C      vg               GROUP VELOCITY AT BRAGG WAVELENGTH
C      h                PLANK'S CONSTANT
C      cLIGHT           SPEED OF LIGHT IN VACUUM
```

```
C       SECTMAX          NUMBER OF LASER SECTIONS
C       MPFC            MID POINT FIELD CONSTRAINT


        DOUBLE PRECISION ALPHATH,DELTATH,NNTH,ALPHALOSS,NNo,GAM
        DOUBLE PRECISION Ao,A1,nTH,nINI,R,LALPHATH,LDELTATH,K,G,PI
        DOUBLE PRECISION LAMTH,LAMB,nG,LAMo,A2,L,D,W,B,C,TAO,V,Q,RTH,ITH
        DOUBLE PRECISION BETAo
        DOUBLE PRECISION LAM,Co,S(5000),vg,epsil,LS,NN1
        DOUBLE PRECISION ALPHA,DELTA,MGAIN

        INTEGER SECTMAX,SECTNUM,PCOUNT,maxcount

c       COMPLEX leftER,leftES,rightER,rightES,ERend,ESend
        COMPLEX leftER,leftES,rightER,rightES
        DOUBLE PRECISION SECTINDEX(5000),SECTCONC(5000)
        DOUBLE PRECISION h,cLIGHT,EPSILo,C1,INTENSITY(5000),IES,IER
c       DOUBLE PRECISION NEWSECTINDEX(5000),MATGAIN(5000)
        DOUBLE PRECISION NEWSECTINDEX(5000),LAMSTART,FLATNESS
        DOUBLE PRECISION AVGLALPHA,AVGLDELTA,AALPHA(5000),DDELTA(5000)
       DOUBLE PRECISION FPWR
       DOUBLE PRECISION KL1,KL2,KL3,KL4,KL5,KL6,AVGKL,NLam,NCo
       DOUBLE PRECISION DPS1,DPS2,DPS3
       DOUBLE PRECISION RPS1,RPS2,RPS3,MPFC,PSTOTAL

C       Initializations (see table 6.1 Shiraz and Lo P164)
c       KL1 = 2.0D0
c       KL2 = 2.0D0
c       KL3 = 2.0D0
        KL4 = KL3
        KL5 = KL2
        KL6 = KL1

       AVGKL = 2.0d0*(KL1*850+KL2*825+KL3*825)/5000

        LALPHATH  = 0.9796D0
        LDELTATH  = 0.42D0
C       C1        = 1.1D0


        SECTMAX   = 5000

        D         = 1.2D-7
        W         = 1.5D-6
        B         = 1.0D-16
        C         = 3.0D-41
        TAO       = 4.0D-9
        Q         = 1.602D-19

        G         = 2.27039D-7
c       K         = 4.0D3
        L         = 500.0D-6
        A2        = 2.7D-32
        ALPHALOSS = 4.0D3
        NNo       = 1.5D24
        GAM       = 0.35D0
        Ao        = 2.7D-20
        A1        = 0.15D-20

        nINI      = 3.41351524D0
```

```
        R          = -1.8D-26
        PI         = 3.1415926535898D0
        nG         = 3.7D0
        vg         = 8.108108D7


C       Convert phase shift from degrees to radians
C       -------------------------------------------
        RPS1 = 2.0D0*PI*(DPS1/360.0D0)
        RPS2 = 2.0D0*PI*(DPS2/360.0D0)
        RPS3 = 2.0D0*PI*(DPS3/360.0D0)

c        When Using LGO ensure the following
c        series of statements are commented out.

c  1.1Xith
c       LAMSTART =  0.154695384303690283D-05
c       Co =  171440.469342084689

c  1.5Xith
c        LAMSTART =  0.15469305237908274 8D-05
c        Co =  408067.291920556338

c  2Xith
c        LAMSTART =  0.154691435934087471D-05
c        Co =  602960.530241662753

c  3Xith
c         LAMSTART =  0.154690071799906363D-05
c         Co =  885113.525866291136

c  4Xith
c        LAMSTART =  0.154689498330103411D-05
c        Co =  1103874.92251847917

c  5Xith
c        LAMSTART =  0.154689321319027050D-05
c        Co =  1290804.58423460647

         epsil      = 1.5E-23
         EPSILo     = 8.854E-12
         h          = 6.6256D-34
         cLIGHT     = 2.998E8

c        Number of iterations chosen to obtain a stable sol'n
c        for a given LAM, Co combination
         maxcount  = 15

         OPEN(UNIT=14,FILE='DFB1FP',STATUS='UNKNOWN')
         REWIND 14

C        Determine actual threshold alpha and delta from
C        normalized values
C        ----------------------------------------------
         ALPHATH    = LALPHATH/L
         DELTATH    = LDELTATH/L

C        **********************

C        Calculate BETAo
```

```
C       ---------------
        BETAo=PI/G

C       CALCULATE THRESHOLD CONDITIONS GIVEN (ALPHATH,DELTATH)
C       ======================================================

C       Threshold conditions (NNTH,nTH,LAMTH,LAMo,ITH)

C       Bragg Wavelength (2.4.8)
C       ------------------------
        LAMB = 2.0*nINI*G

C       Threshold Carrier Concentration (6.2.17)
C       ----------------------------------------
        NNTH = NNo+(ALPHALOSS+2.0*ALPHATH)/(GAM*Ao)

C       Threshold Index (6.2.18)
C       ------------------------
        nTH  = nINI+GAM*R*NNTH
C       PRINT*,"LAMB = ",LAMB," NNTH = ",NNTH," nTH = ",nTH
        WRITE(14,*) "LAMB = ",LAMB," NNTH = ",NNTH," nTH = ",nTH

C       Threshold Wavelength (6.2.19)
C       -----------------------------------------------------------------
        LAMTH = 2.0*PI*LAMB*(nTH+nG)/(DELTATH*LAMB+2.0*PI*nG+LAMB*PI/G)

C       Peak gain wavelength at 0 transparancy (6.2.20)
C       -----------------------------------------------
        LAMo  = LAMTH+A2*(NNTH-NNo)

        WRITE(14,*) "LAMTH = ",LAMTH,"    ","LAMo = ",LAMo

C       Active region volume
C       --------------------
        V = D*W*L

C       Calculate threshold current ITH (6.2.10,11)
C       -------------------------------------------
        RTH = NNTH/TAO+B*NNTH**2+C*NNTH**3
        ITH = RTH*Q*V

C       All threshold conditions have now been determined
C       we have (NNTH,nTH,LAMTH,LAMo,ITH)
C       ================================================================


C       Calculate the length of each matrix section (LS)
C       ------------------------------------------------
        LS=L/SECTMAX

C       Make Initial guess at (Co LAM)
C       ------------------------------

        LAM = LAMSTART
C       Co is provided in initial parameters



C       First Initialize refractive index profile to threshold value
C       ------------------------------------------------------------
```

```
        NN1=NNTH
        DO 20 SECTNUM=1,SECTMAX
           SECTINDEX(SECTNUM)=nTH

20      CONTINUE


C       START MATRIX PROPAGATION
C       ========================================================

C       On each complete propagation, the index profile RINDEX(k)
C       is saved for each subsection k. (There are M subsections)

        Do 150 i=1,maxcount

C       Set the left side Boundary Conditions
C       -------------------------------------
        leftER=(0.0,0.0)
        leftES=(1.0,0.0)

C***************************************************************
C       START OF TMM SECTION PROPAGATION DO LOOP
C       Propagates field through each matrix section (SECTMAX)

        DO 100 SECTNUM=1,SECTMAX

C       I. Calculate photon concentration at left facet
C       -----------------------------------------------
        S(SECTNUM)=((2.0*EPSILo*SECTINDEX(SECTNUM)*nG*LAM)
     c  /(h*cLIGHT))*Co**2*(leftER*CONJG(leftER)+leftES*
     c  CONJG(leftES))

C       II. Solve for Carrier Density inner left facet
C       ----------------------------------------------
        CALL CUBIC(NN1,B,C,S(SECTNUM),vg,epsil,C1,
     C  ITH,Q,V,TAO,SECTNUM,Ao,NNo,A1,A2,LAMo,LAM)

        SECTCONC(SECTNUM)=NN1

C       (store new index for next iteration)
        NEWSECTINDEX(SECTNUM)=nINI+GAM*R*SECTCONC(SECTNUM)

C       III. Solve for ALPHA and DELTA
C       ------------------------------
        MGAIN = Ao*(SECTCONC(SECTNUM)-NNo)-A1*
     C  (LAM-(LAMo-A2*(SECTCONC(SECTNUM)-NNo)))**2
        ALPHA = (GAM*MGAIN-ALPHALOSS)/2.0
        DELTA = (2.0*PI/LAM)*SECTINDEX(SECTNUM)-
     C  ((2.0*PI*nG)/(LAM*LAMB))*(LAM-LAMB)-PI/G

        AALPHA(SECTNUM) = ALPHA
        DDELTA(SECTNUM) = DELTA

C       IV. Propagate fields
C       --------------------

        IF(SECTNUM.GE.1.AND.SECTNUM.LT.833)THEN
          K=KL1/L
        ELSE IF(SECTNUM.GE.833.AND.SECTNUM.LT.1667)THEN
          K=KL2/L
```

```
          ELSE IF(SECTNUM.GE.1667.AND.SECTNUM.LT.2500)THEN
            K=KL3/L
          ELSE IF(SECTNUM.GE.2500.AND.SECTNUM.LT.3333)THEN
            K=KL4/L
          ELSE IF(SECTNUM.GE.3333.AND.SECTNUM.LT.4166)THEN
            K=KL5/L
          ELSE IF(SECTNUM.GE.4166)THEN
            K=KL6/L
          ELSE
          ENDIF


          CALL MATRIX(SECTNUM,LS,leftER,leftES,ALPHA,DELTA,K,
     C              BETAo,rightER,rightES,RPS1,RPS2,RPS3)

          INTENSITY(SECTNUM)=rightER*CONJG(rightER)+
     C             rightES*CONJG(rightES)


C         Go to next TMM section
C         ----------------------
          leftER=rightER
          leftES=rightES
c         (redefine index for next iteration)
          SECTINDEX(SECTNUM)=NEWSECTINDEX(SECTNUM)

C         END OF TMM SECTION PROPAGATION DO LOOP
C         you have transversed 1 TMM section

100       CONTINUE


C*************************************************************

C         YOU ARE NOW AT THE RIGHT HAND FACET AND HAVE
C         TRANSVERSED "SECTMAX" TMM SECTIONS

          IER=rightER*CONJG(rightER)
          IES=rightES*CONJG(rightES)


C         Test for Right Hand B.C. Error
C         ------------------------------------------

C         Select arbitrarily large starting value

              RBCerror=IES

c         Output the results
c         ------------------
c       Calculate average AVGLALPHA AND AVGLDELTA
c       i.e. normalized average ALPHA and DELTA

        AVGLALPHA = 0.0
        AVGLDELTA = 0.0
        Do 530 SECTNUM = 1,SECTMAX
            AVGLALPHA = AVGLALPHA + AALPHA(SECTNUM)
           AVGLDELTA = AVGLDELTA + DDELTA(SECTNUM)
530     CONTINUE
```

```
      AVGLALPHA = (AVGLALPHA / SECTMAX) * L
      AVGLDELTA = (AVGLDELTA / SECTMAX) * L

c     Calculate Facet Output Power

      FPWR = ((D*W)/GAM)*vg*((h*cLIGHT)/Lam)*S(5000)

      NLam = (Lam/1.0D-6) - 1.546d0
      NCo = Co/100000.0d0

c     Calculate total phase shift PSTOTAL
      PSTOTAL = 2.0D0*(RPS1+RPS2)+RPS3


C       Output ongoing results
      WRITE(14,*) "  "
      WRITE(14,*) " THRESHOLD CURENT = ",ITH
      WRITE(14,*) " INJECTION CURRENT = ",C1
      WRITE(14,*) " Wavelength = ",Lam
      WRITE(14,*) " Co = ",Co
      WRITE(14,*) " Normalized Wavelength = ",NLAM
      WRITE(14,*) " Normalized Co = ",NCo
      WRITE(14,*) " LALPHA Average = ",AVGLALPHA
      WRITE(14,*) " LDELTA Average = ",AVGLDELTA
      WRITE(14,*) " RBCerror = ",RBCerror
      WRITE(14,*) " IER = ",IER
      WRITE(14,*) " IES = ",IES
      WRITE(14,*) " Facet Power = ",FPWR
      WRITE(14,*) " KL1 = ",KL1
      WRITE(14,*) " KL2 = ",KL2
      WRITE(14,*) " KL3 = ",KL3
      WRITE(14,*) " DPS1 = ",(RPS1*360.0D0)/(2.0D0*PI)," Deg"
      WRITE(14,*) " DPS2 = ",(RPS2*360.0D0)/(2.0D0*PI)," Deg"
      WRITE(14,*) " DPS3 = ",(RPS3*360.0D0)/(2.0D0*PI)," Deg"
      WRITE(14,*) " PSTOTAL = ",(PSTOTAL*360.0D0)/
     c                          (2.0D0*PI)," Deg"

      WRITE(14,*) " Average KL = ",AVGKL


c       Calculate the flatness function value:
c     ****************************************
      IF(i.EQ.maxcount)THEN
         CALL FLAT(L,LS,SECTMAX,INTENSITY,FLATNESS)
        WRITE(14,*) " FLATNESS = ",FLATNESS
      ELSE
      ENDIF

c     Define Mid Point Field Constraint MPFC:
c     ****************************************
      MPFC = INTENSITY(2500)
      WRITE(14,*) " Mid Point Field Constraint (MPFC) = ",MPFC

        PCOUNT = 1
        WRITE(14,7) PCOUNT,INTENSITY(PCOUNT),
     C  SECTCONC(PCOUNT),SECTINDEX(PCOUNT),S(PCOUNT)
        DO 710 SECTNUM = 1,SECTMAX
         IF(PCOUNT.EQ.250)THEN
           PCOUNT=1
```

```
          WRITE(14,7) SECTNUM,INTENSITY(SECTNUM),
     C     SECTCONC(SECTNUM),SECTINDEX(SECTNUM),S(SECTNUM)
7          FORMAT(1I6,2X,4E18.10)
         ELSE
           PCOUNT=PCOUNT+1
         ENDIF
710     continue


c       Repeat this loop maxcount times with the
c       current values of Lam and Co to allow
c       index to stabilize

150     continue

c       Calculate the flatness function value:

c         CALL FLAT(L,LS,SECTMAX,INTENSITY,FLATNESS)

c         WRITE(14,*) " FLATNESS = ",FLATNESS

        WRITE(16,81) RBCerror
81      FORMAT(" RBCerror = ",e25.12)
        WRITE(16,82) FLATNESS
82      FORMAT(" FLATNESS = ",e25.12)
        WRITE(16,83) AVGKL
83      FORMAT(" Average KL =",e25.12)

        REWIND 14

c       STOP
        return
        END


C       ********************************************
C       SUBROUTINES
C       ********************************************


        SUBROUTINE MATRIX(SECTNUM,LS,leftER,leftES,ALPHA,
     C       DELTA,K,BETAo,rightER,rightES,RPS1,RPS2,RPS3)

      implicit real*8 (a-h,o-z)

        COMPLEX leftER,leftES,rightER,rightES
        DOUBLE PRECISION ALPHA,DELTA,K,BETAo
        DOUBLE PRECISION Z1,Z2,LS,theta,PI,RPS1,RPS2,RPS3
        COMPLEX RHO,gamma,T11,T12,T21,T22,E1,E2
        INTEGER SECTNUM

        PI=3.1415926535898D0

        IF(SECTNUM.EQ.833.OR.SECTNUM.EQ.4166)THEN
          theta=RPS1
c        theta=0.0
        ELSE IF(SECTNUM.EQ.1667.OR.SECTNUM.EQ.3333)THEN
          theta=RPS2
c        theta=0.0
       ELSE IF(SECTNUM.EQ.2500)THEN
```

```
c        theta=PI/2.0d0
           theta=RPS3
       ELSE
         theta=0
       END IF


c      SECTNUM starts at 1 .. for the 1st section


       Z1=(SECTNUM-1)*LS
       Z2=Z1+LS

       gamma=SQRT((cmplx(ALPHA,-DELTA))**2+K**2)
       RHO=cmplx(0.0,K)/(cmplx(ALPHA,-DELTA)+gamma)

       E1=exp(gamma*LS)
       E2=exp(-gamma*LS)

       T11=((E1-RHO**2*E2)*exp(cmplx(0.0,-BETAo*LS))*
     .  exp(cmplx(0.0,theta)))/(1.0-RHO**2)
       T12=(-RHO*(E1-E2)*exp(cmplx(0.0,-BETAo*(Z2+Z1)))*
     .  exp(cmplx(0.0,-theta)))/(1.0-RHO**2)
       T21=(RHO*(E1-E2)*exp(cmplx(0.0,BETAo*(Z2+Z1)))*
     .  exp(cmplx(0.0,theta)))/(1.0-RHO**2)
       T22=(-(RHO**2*E1-E2)*exp(cmplx(0.0,BETAo*LS))*
     .  exp(cmplx(0.0,-theta)))/(1.0-RHO**2)

c      TT=T11*T22-T12*T21

       rightER=T11*leftER+T12*leftES
       rightES=T21*leftER+T22*leftES

       RETURN
       END

c      ---------------------------------------------

       SUBROUTINE CUBIC(NN1,B,C,S,vg,epsil,C1,ITH,Q,
     c  V,TAO,SECTNUM,Ao,NNo,A1,A2,LAMo,LAM1)

      implicit real*8 (a-h,o-z)

c      Solves for section carrier concentration using
c      Bisection Method
c      LB = Lower Bound
c      UB = Upper Bound

       DOUBLE PRECISION B,C,S,vg,g,epsil,C1,ITH,Q
       DOUBLE PRECISION V,TAO,NN1,NNo,A1,A2,LAMo,LAM1
       DOUBLE PRECISION TOL,F,Ao,LB,UB,P,F1,F2,FF
      INTEGER I,MAXCOUNT,SECTNUM

       UB=3.5e24
       LB=1.0e24

       TOL=1.0E10
       MAXCOUNT = 200
       DO 20, I=1,MAXCOUNT
```

```
      P=LB+(UB-LB)/2.0


      g=Ao*(P-NNo)-A1*(LAM1-(LAMo-A2*(P-NNo)))**2
      F=P/TAO+B*P**2+C*P**3+(vg*g*S/
     C      (1.0+epsil*S))-(C1*ITH)/(Q*V)

      IF((UB-LB)/2.0.LT.TOL.OR.F.EQ.0.0)THEN
         GO TO 30
      ELSE

      F2=F

      g=Ao*(LB-NNo)-A1*
     C      (LAM1-(LAMo-A2*(LB-NNo)))**2
      F=LB/TAO+B*LB**2+C*LB**3+(vg*g*S/
     C      (1.0+epsil*S))-(C1*ITH)/(Q*V)

      F1=F

      FF=F1*F2
      END IF

      IF(FF.GT.0.0)THEN
        LB=P
      ELSE
        UB=P
      END IF


      IF(I.EQ.MAXCOUNT)THEN
         Print*,"Process failed ..Max iterations exceeded"
         Print*,"I = ",I,"SECTNUM = ",SECTNUM
         Print*,"  "
      ELSE
      END IF
20    CONTINUE

30    NN1=P

      RETURN
      END

C     ------------------------------------------


      SUBROUTINE FLAT(L,LS,SECTMAX,INTENSITY,FLATNESS)

      implicit real*8 (a-h,o-z)

c     Subroutine calculates flatness of field profile
c     return value (FLATNESS)

c     First Calculate the Average Field Intensity IAV

c     IAV = Average Intensity

      INTEGER SECTMAX,SECTNUM
      DOUBLE PRECISION L,LS,INTENSITY(SECTMAX),FLATNESS
```

```
      DOUBLE PRECISION IAV,ITOT,FSUM

      ITOT = 0.0D0

c     -------------------------
c     Test Loop

c     DO 10 SECTNUM = 1,SECTMAX
c     IF(SECTNUM.LE.2500)THEN
c       INTENSITY(SECTNUM) = 4
c     ELSE
c       INTENSITY(SECTNUM) = 2
c     ENDIF
c10   CONTINUE
c     -------------------------


      DO 20 SECTNUM = 1,SECTMAX
        ITOT = ITOT + INTENSITY(SECTNUM)
20    CONTINUE

c     Add the RHS (1st node) Normalization value 1.0
      ITOT = ITOT + 1.0D0

c     There is 1 more node than sections therefore
c     add 1 to SECTMAX to get the correct number of
c     nodes.

      IAV = ITOT/(1+SECTMAX)

c     WRITE(*,*) " IAV = ",IAV

c     Now calculate the flatness function

      FSUM = 0.0D0

      DO 30 SECTNUM = 1,SECTMAX
         FSUM = FSUM + ((INTENSITY(SECTNUM)-IAV)**2)*LS
30    CONTINUE

      FLATNESS = FSUM / L

      RETURN
      END
```

DFB1M.FOR

This program activates the LGO solver system as well as opens the various input and output files.

```
!     DFB1M.FOR ---
!     ------------------------------------------------------------------------

!     This is a program template, to be prepared (adapted) by LGO users.
!     The use of all included statements is (minimally) necessary.
!     Additional user operations - related to problem description, further
!     reporting options, additional program/system calls, etc. - can also
!     be included or connected, at corresponding points (segments) below.

!     Usage:
!     USER_MAIN: mandatory usage - calls the LGO solver system (via
!                                                  LGO_RUN_SHELL)
!     USER_FILES: mandatory usage - gives names to user I/O files units

!     Please retain an original copy of this file for further reference
!     Save your own USERMAIN.FOR file in text format

!     ------------------------------------------------------------------------

      PROGRAM USER_MAIN

      USE WINTERACTER
!     WINTER.F90 contains numerous Windows features needed (WiSK version)

      implicit real* 8 (a-h,o-z)

!     The following statement is needed (only) in Windows DLL program versions
!      DLL_IMPORT LGO_RUN_SHELL

      common /C1input/ C1    ! read C1 from file, then pass it into RBC_out
       open(123,file='C1.in',status='unknown')
       rewind(123)
       read(123,124) C1
124    format (f20.10)
!      c1=3.0d0
!      Activate LGO optimization (solver) system
       call LGO_RUN_SHELL

      stop
      end

!     ------------------------------------------------------------------------

      SUBROUTINE USER_FILES

!     This routine serves to give names to three user I/O files (units)
!     Note: the logical unit numbers 8,9,10,11,12 and 13 are fixed (mandatory)
!     They could be changed only by modifying the optimization program system
!     (the latter being provided as an object file)

      implicit real* 8 (a-h,o-z)
```

```
!     Please define all (real) variables and operations in double precision,
!     in order to attain higher numerical accuracy

!     The following statement is needed (only) in Windows DLL program versions
!      DLL_EXPORT USER_FILES

!     --- User filename definitions ---
!     Please modify the file names given below, to suit user model

      OPEN(8,FILE='DFB1.IN',STATUS='OLD')
!     This file serves for parameterizing the LGO program system.
!     Note that the input parameterization is problem-dependent;
!     please see the *.IN file, and check the comments on pm settings.

      OPEN(9,FILE='DFB1.OUT',STATUS='UNKNOWN')
!     This file serves for (optional) post-run analysis: it provides the
!     principal information describing the problem, and the process log
!     obtained during the optimization procedure.

      OPEN(10,FILE='DFB1.SUM',STATUS='UNKNOWN')
!     This file contains a brief summary of the run results.

      open(unit=16,file='DFB1_ck',status='unknown')
!     RBCerror      FLATNESS        Total KL

      return
      end
```

DFB1.IN

This code listing is the program input file, providing the range of solution variables (box constraint) plus nominal values. Solution convergence and termination criteria are also set in this file.

```
DFB1.IN FILE --- 8-variable  3-constraint
Input data to LGO program system.
NOTE TO USERS: Please retain a copy of this file for further reference;
save your own file in text format. The given structure is to be followed
exactly; keep all comment lines and the given *** input data formats.
Numerous parameters are automatically defined in the LGO object files;
the parameter values provided below can be changed by the user.

----------------- PROBLEM SIZE AND VARIABLE DEFINITIONS ----------------------
-

NUMBER OF CONSTRAINTS:  3                              *** input format: 22x, i12

NUMBER OF VARIABLES  :  8                              *** input format: 22x, i12

VARIABLE NAMES      |    LOWER BOUND    |  NOMINAL SOLUTION |    UPPER BOUND
Format: 20x         |      f20.10       |      f20.10       |      f20.10
Arbitrary nominal values can be set between the lower and upper bounds.
 KL1                        0.1                 2.0                 3.0
 KL2                        0.1                 2.0                 3.0
 KL3                        0.1                 2.0                 3.0
 LAMSTART_delt              0.00066             0.00068             0.00070
 Co                         0.5                 6.0                 10.0
 DPS1                      10.00                36.0                45.0
 DPS2                      10.00                36.0                45.0
 DPS3                      10.00                36.0                45.0

--------------- GLOBAL SEARCH PHASE (OPTIMIZATION) PARAMETERS ----------------
-

ACC_TR global search termination criterion parameter: global phase ends, if
the overall merit function value found in global search is less than ACC_TR.
The merit function is the sum of the objective function and the violated
constraints (if present). In the global search phase, the latter are added
to the objective, applying unit penalty multiplier factors (set within LGO).
      ACC_TR    = 0.01                             *** input format: 16x, f20.10

G_MAXFCT global search termination criterion parameter: global scope search
ends, if the number of merit function evaluations (approximately) attains
G_MAXFCT. For G_MAXFCT=0 local search starts from the given nominal solution.
      G_MAXFCT =10000                              *** input format: 16x, i12

MAX_NOSUC global search termination criterion parameter: global search phase
ends, if the current best solution did not improve during (at least) the last
MAXNOSUC subsequent merit function evaluations.
      MAX_NOSUC= 100000                          *** input format: 16x, i12

FCT_CUT merit function cutoff value, used only to improve visualization:
this value should be larger, than the optimum value, to be found by LGO.
The usage of some 'huge' value is safe, but may give less visual details.
```

```
      FCT_CUT   =  200.                              *** input format: 16x, f20.10

---------------- LOCAL SEARCH PHASE (OPTIMIZATION) PARAMETERS ----------------
-

FI_TOL local search termination criterion parameter: first local search phase
ends, if the merit function improvement is less, than FI_TOL.
      FI_TOL    = 1.0d-6                             *** input format: 16x, f20.10

FCT_TRG target objective function value in local search; partial stopping
criterion in second local search phase.
If unknown, then can be set to 'safe' lower bound, in order to skip criterion.
      FCT_TRG   =  1.d-6                             *** input format: 16x, f20.10

CON_TOL maximal constraint violation tolerance in local search; partial
stopping criterion in second local search phase.
      CON_TOL   =  1.d-6                             *** input format: 16x, f20.10

KT_TOL: tolerance in satisfying the Kuhn-Tucker local optimality conditions;
stopping criterion in third local search phase.
      KT_TOL    =  1.d-6                             *** input format: 16x, f20.10

------------------------------------------------------------------------------
-

NOTE TO USERS: the parameters listed above are problem-dependent - please check
your own LGO model runs and modify them, if thought necessary.
```

APPENDIX F

THRESHOLD MODES CODE LISTING

MODESOLVE.FOR

This code is used to solve for the threshold modes of a 6 section DFB laser given the sectional coupling coefficient and inter-sectional phase shift profiles.

```
C     Last change:  GI   20 Mar 2001   11:04 pm
      PROGRAM MODESOLVE

C     SUBROUTINE MODESOLVE(LALPHA,LDELTA,ERROR,LALPC,LDELC)

!     Glenn Isenor 01/01/25

!     Solves for the threshold oscillation modes of a DFB laser
!     With 6 TMM sections

!     TMAX = Number of TMM sections (max = 6)
!     SECTMAX = Number of sections Laser is divided into (5000)

!        *-*--------*-*--------*-*--------*-*--------*-*
!        I I   T1   I I    T2  I I   T3   I I  T4    I I ... etc.
!        *-*--------*-*--------*-*--------*-*--------*-*
!        P1          P2          P3          P4          P5
!                                      MIDPOINT
!                                  6 Section laser
!                                  QWS: P4 = PI/2

!     Order of matrix multiplication T1*P1=C1, T2*P2*C1=C2, etc


      implicit real*8 (a-h,o-z)
      DOUBLE PRECISION L,LSECT,BETAo
      DOUBLE PRECISION Z(6),KL(6),PS(6),K(6),PI,GPERIOD
      DOUBLE PRECISION ALPHAL,DELTAL,INCALPHAL,MAXALPHAL,MINALPHAL
      DOUBLE PRECISION INCDELTAL,MAXDELTAL,MINDELTAL,FUNCTMIN
      DOUBLE PRECISION SMALPHAL,SMDELTAL,SMFUNCTMIN
      DOUBLE COMPLEX Y(2,2)
      INTEGER SECTMAX,TNUM,TMAX,GRIDMAX,DLGRIDNUM,ALGRIDNUM
      INTEGER ZZ(6)



!     Define laser length L (meters) and # of TMM sections TMAX
!     ============================================================
      L=500.0D-6
      SECTMAX=5000
      TMAX=6

      PI=3.1415926535898D0
      GPERIOD=2.27039D-7

!     Initialize variables at an arbitrary + ive value
!     ================================================
      SMFUNCTMIN=500.0D0
      SMALPHAL=500.0D0
      SMDELTAL=500.0D0


!     Define section length ZZ IN # OF SECTIONS
```

```
!     ============================================================
!     Note that SECTMAX would represent the number of TMM sections
!     in the above threshold analysis but at threshold the number
!     of TMM sections is significantly reduced and determined by
!     the number of KL sections. Each threshold TMM section consists
!     of a number of the smaller sections. ZZ represents the size
!     of a threshold TMM section.


      OPEN(UNIT=14,FILE='MODEV1OUT',STATUS='unknown')
      REWIND 14



!     ************************************************************
!     *          START USER CONFIGURABLE PARAMETERS              *
!     ************************************************************

!     ALPHAL and DELTAL search Parameters
!     ===================================
      GRIDMAX = 100

      MINALPHAL=  0.5D0
      MAXALPHAL=  2.5D0

      MINDELTAL= -1.00D0
      MAXDELTAL=  1.00D0

c      MINDELTAL= -5.00D0
c      MAXDELTAL= -1.00D0

c      MINDELTAL=  5.00D0
c      MAXDELTAL=  7.00D0


!     Size of each KL (TMM) Section (in small laser sections)
!     =======================================================
      ZZ(1)=834
      ZZ(2)=833
      ZZ(3)=833


!     ZZ(4 TO 6) are determined from symmetry
!     Define KL values for each TMM section
!     =====================================
      KL(1) = 2.0
      KL(2) = 2.0
      KL(3) = 2.0


!     KL(4 TO 6) are determined from symmetry

!     Define PS (DEG) values between each TMM  section
!     ================================================
!     Note: Always set PS(1) = 0
      PS(1) =  0.0D0
      PS(2) = 21.36551
      PS(3) = 29.19348
      PS(4) = 31.04674
```

```
!     ************************************************************
!     *             END USER CONFIGURABLE PARAMETERS             *
!     ************************************************************

!
!     Define remaining ZZ, KL and PS parameters using symmetry
!     ========================================================

      ZZ(4)  = ZZ(3)
      ZZ(5)  = ZZ(2)
      ZZ(6)  = ZZ(1)

      KL(4)  = KL(3)
      KL(5)  = KL(2)
      KL(6)  = KL(1)

      PS(5)  = PS(3)
      PS(6)  = PS(2)

!     Calculate BETAo
!     ===============
      BETAo=PI/GPERIOD


!     Calculate Length Z(0 to L)(m) and K(SECTNUM)
!
!     ========================================================

!     Calculate LSECT - the length of each small section (m)
      LSECT=L/SECTMAX

!     Calculate all remaining TMM section distances (m) from
!     the left hand facet.
!     ========================================================

       Z(1) = ZZ(1)*LSECT

       DO 20 TNUM=2,TMAX
          Z(TNUM)=Z(TNUM-1)+ZZ(TNUM)*LSECT
!          PRINT*,"Z   ",TNUM,"   ",Z(TNUM)
20    CONTINUE
!
!     Calculate the Y matrix and determine Y22 for a search grid
!     ============================================================

      INCALPHAL=(MAXALPHAL-MINALPHAL)/GRIDMAX
      INCDELTAL=(MAXDELTAL-MINDELTAL)/GRIDMAX

      ALPHAL=MINALPHAL
      DELTAL=MINDELTAL

      DO 40 DLGRIDNUM=1,GRIDMAX+1
         DO 30 ALGRIDNUM=1,GRIDMAX+1
!              WRITE(14,*) " ALPHAL =",ALPHAL," DELTAL =",DELTAL

            CALL MATRIX(BETAo,L,LSECT,Z,ZZ,PS,KL,TMAX,ALPHAL,DELTAL,Y)

            FUNCTMIN = Y(2,2)*CONJG(Y(2,2))

            CALL SORT(ALPHAL,DELTAL,FUNCTMIN,SMALPHAL,SMDELTAL,
```

```
     c                SMFUNCTMIN)

!           WRITE(14,*) " ALPHAL =",ALPHAL," DELTAL =",DELTAL,
!     c                  " FUNCTMIN =",FUNCTMIN

            ALPHAL=ALPHAL+INCALPHAL
30        CONTINUE
          ALPHAL=MINALPHAL
          DELTAL=DELTAL+INCDELTAL
40     CONTINUE

       WRITE(14,*) " ALPHAL =",SMALPHAL," DELTAL =",SMDELTAL,
     c                " FUNCTMIN =",SMFUNCTMIN

       PRINT*, " ALPHAL =",SMALPHAL," DELTAL =",SMDELTAL,
     c                " FUNCTMIN =",SMFUNCTMIN



       STOP
       END
!      ****************************************************************
!      *                      SUBROUTINES                             *
!      ****************************************************************

       SUBROUTINE MATRIX(BETAo,L,LSECT,Z,ZZ,PS,KL,TMAX,ALPHAL,DELTAL,Y)

!      This subroutine computes the overall Y matrix

       implicit real*8 (a-h,o-z)
       DOUBLE PRECISION Z1,Z2,ZDIFF,ZSUM,L,LSECT,BETAo
       DOUBLE PRECISION Z(6),PS(6),K(6),KL(6)
       DOUBLE PRECISION THETA,PI,ALPHA,DELTA,ALPHAL,DELTAL
       INTEGER TMAX,TNUM,ZZ(6)
       DOUBLE COMPLEX RHO,GAMMA,T(2,2),Y(2,2),C(2,2),E1,E2

       PI=3.1415926535898D0


!      Initialize C Matrix  to the Identity Matrix
!      ===========================================
       C(1,1) = (1.0D0,0.0D0)
       C(1,2) = (0.0D0,0.0D0)
       C(2,1) = (0.0D0,0.0D0)
       C(2,2) = (1.0D0,0.0D0)

       T(1,1) = (0.0D0,0.0D0)
       T(1,2) = (0.0D0,0.0D0)
       T(2,1) = (0.0D0,0.0D0)
       T(2,2) = (0.0D0,0.0D0)

       Y(1,1) = (0.0D0,0.0D0)
       Y(1,2) = (0.0D0,0.0D0)
       Y(2,1) = (0.0D0,0.0D0)
       Y(2,2) = (0.0D0,0.0D0)

!      Un-normalize ALPHAL,DELTAL
!      ==========================
       ALPHA=ALPHAL/L
       DELTA=DELTAL/L
```

```
!     Un-normalize KL
!     ===============
      DO 20 TNUM=1,TMAX
         K(TNUM)=KL(TNUM)/L
 20    CONTINUE


!     Compute the Y matrix
!     ====================

      ZSUM=0.0D0

      DO 30 TNUM=1,TMAX

      GAMMA=SQRT(K(TNUM)**2+(ALPHA-DCMPLX(0.0D0,DELTA))**2)
      RHO=(DCMPLX(0.0,K(TNUM)))/(GAMMA+ALPHA-DCMPLX(0.0D0,DELTA))

!      WRITE(14,*) "GAMMA = ",GAMMA," RHO = ",RHO


!            GAMMA=SQRT((cmplx(ALPHA,-DELTA))**2+K(TNUM)**2)
!            RHO=(cmplx(0.0,K(TNUM)))/(cmplx(ALPHA,-DELTA)+GAMMA)



       ZDIFF=ZZ(TNUM)*LSECT

       ZSUM=Z(TNUM)-ZDIFF+Z(TNUM)

!        WRITE(14,*) "TNUM ",TNUM,"Z = ",Z(TNUM)," ZSUM =  ",ZSUM,
!     C   "ZDIFF = ",ZDIFF

       E1=exp(GAMMA*ZDIFF)
       E2=exp(-GAMMA*ZDIFF)
         THETA=PS(TNUM)*2.0D0*PI/360.0D0

       T(1,1)=((E1-RHO**2*E2)*exp(cmplx(0.0,-BETAo*ZDIFF))*
     .  exp(cmplx(0.0,THETA)))/(1.0-RHO**2)
       T(1,2)=(-RHO*(E1-E2)*exp(cmplx(0.0,-BETAo*(ZSUM)))*
     .  exp(cmplx(0.0,-THETA)))/(1.0-RHO**2)
       T(2,1)=(RHO*(E1-E2)*exp(cmplx(0.0,BETAo*(ZSUM)))*
     .  exp(cmplx(0.0,THETA)))/(1.0-RHO**2)
       T(2,2)=(-(RHO**2*E1-E2)*exp(cmplx(0.0,BETAo*ZDIFF))*
     .  exp(cmplx(0.0,-THETA)))/(1.0-RHO**2)



       Y(1,1)=T(1,1)*C(1,1)+T(1,2)*C(2,1)
       Y(1,2)=T(1,1)*C(1,2)+T(1,2)*C(2,2)
       Y(2,1)=T(2,1)*C(1,1)+T(2,2)*C(2,1)
       Y(2,2)=T(2,1)*C(1,2)+T(2,2)*C(2,2)

       C(1,1)=Y(1,1)
       C(1,2)=Y(1,2)
       C(2,1)=Y(2,1)
       C(2,2)=Y(2,2)
```

```
30     CONTINUE

       RETURN
       END

!      ================================================================

       SUBROUTINE SORT(ALPHAL,DELTAL,FUNCTMIN,SMALPHAL,SMDELTAL,
      c                SMFUNCTMIN)

!      This Subroutine finds the smallest "FUNCTMIN" from the grid
!      search and returns this value with the corresponding
!      ALPHAL,and DELTAL

       implicit real*8 (a-h,o-z)
       DOUBLE PRECISION ALPHAL,DELTAL,FUNCTMIN,SMALPHAL,SMDELTAL
       DOUBLE PRECISION SMFUNCTMIN

       IF (FUNCTMIN.LT.SMFUNCTMIN) THEN
          SMFUNCTMIN=FUNCTMIN
          SMALPHAL=ALPHAL
          SMDELTAL=DELTAL
       ELSE
       END IF

       RETURN
       END
```